

Supplementary Materials

1	Abbreviations	3
2	Supplementary Methods	4
3	Supplementary Results	6
3.1	Cellular Pathways essential for anti-cancer drug action and [¹⁸F]FLT accumulation	6
3.2	[¹⁸F]FLT accumulation in untreated tumors	6
3.2.1	Uptake of [¹⁸ F]FLT in proliferative tumors	6
3.2.2	Specificity in detection of tumor versus inflammation	9
3.2.3	Repeatability of measurements	9
3.2.4	Factors in DNA salvage pathway utilization determine [¹⁸ F]FLT uptake	10
3.2.5	[¹⁸ F]FLT transport into the cell might limit tracer accumulation	11
3.2.6	Endogenous thymidine as competing factor for [¹⁸ F]FLT	12
3.2.7	Hypoxia impacts [¹⁸ F]FLT accumulation	13
3.2.8	Vascularization impacts [¹⁸ F]FLT delivery	13
3.2.9	Methodological confounders of [¹⁸ F]FLT detection	13
3.3	Imaging of response to chemotherapy	14
3.3.1	Alkylating agents	14
3.3.2	Interference with topoisomerase activity	16
3.3.3	Cisplatin	17
3.3.4	Microtubule stabilizing agents	18
3.3.5	Purine and pyrimidine analogs	20
3.3.6	Antifolates	23
3.3.7	Other chemotherapeutic drugs	24
3.4	Imaging of response to targeted therapies	25
3.4.1	ErbB inhibitors	25
3.4.2	VEGF signaling inhibitors	28
3.4.3	FGFR inhibitors	28
3.4.4	c-MET / HGF inhibitors	29
3.4.5	PI3K inhibitors	30
3.4.6	mTOR inhibitors	30
3.4.7	Aurora kinase inhibitors	32
3.4.8	BRAF inhibitors	33
3.4.9	MEK inhibitors	34
3.4.10	CDK inhibitors	34
3.4.11	Multiple kinase inhibitors	35
3.4.12	HDAC inhibitors	36
3.4.13	HSP90 inhibitors	37
3.4.14	Cadherin inhibitors	38
3.4.15	Inhibition of Ca ²⁺ channels	38
3.4.16	Inhibition of arginine metabolism enzymes	38
3.4.17	Inhibition of hypoxia induced gene regulation	39

3.4.18	Specific delivery of toxic molecules.....	39
3.4.19	Targeted radionuclide therapy.....	39
3.5	Imaging of response to radiotherapy.....	40
3.6	Imaging of response to other therapy approaches	44
3.6.1	Gene therapy.....	44
3.6.2	Oncolytic virotherapy	46
3.6.3	Photodynamic therapy.....	46
3.6.4	Androgen depletion	47
3.6.5	Metformin.....	47
3.6.6	Interleukin-22.....	47
3.6.7	Immunotherapy.....	48
3.7	Imaging of response to combination therapies	48
3.7.1	Combinations of chemotherapeutic drugs.....	48
3.7.2	Combinations of targeted therapies	49
3.7.3	Combinations of chemotherapeutic and targeted agents.....	50
3.7.4	Combinations with radiotherapy	52
3.8	Summary of study designs	53
3.8.1	Experimental setup.....	53
3.8.2	PET acquisition and quantification	54
4	Supplementary Information: QuIC-ConCePT consortium participants.....	57
5	Supplementary Figures	58
6	Supplementary Tables.....	62
6.1	Supplementary Table S1: PRISMA 2009 checklist.	62
6.2	Supplementary Table S2: Quantitative data (relative changes) from the studies included in this review.....	65
6.3	Supplementary Table S3: Correlation data from the studies included in this review.	74
6.4	Supplementary Table S4: Number of studies reported on in this review sorted for major characteristics and therapy approach.	76
6.5	Supplementary Table S5: Number of studies sorted for acquisition and quantification protocols.....	77
6.6	Supplementary Table S6: Number of treatment studies and datapoints providing quantitative data.....	77
7	References.....	78

1 Abbreviations

[¹⁸F]FDG: 2-[¹⁸F]-fluoro-2-deoxy-D-glucose; [¹⁸F]FLT: 3'-deoxy-3'-[¹⁸F]fluorothymidine; [¹⁸F]FHBG: (9-[4-[¹⁸F]fluoro-3-(hydroxymethyl)butyl]guanine); 5-FU: fluorouracil; ACNU: 1-(4-amino-2-methyl-5-pyrimidinyl) methyl-3-(2-chloroethyl)-3-nitrosourea hydrochloride; ATP: adenosine triphosphate; AKT: protein kinase B; AUC: area under the normalized time activity curve; bl: baseline; BrdU: bromodeoxyuridine; CDK: cyclin-dependent kinase; CITG: cdiREStkgfp, *Escherichia coli* cytosine deaminase - internal ribosomal entry site - herpes simplex virus type 1 thymidine kinase - green fluorescent protein; CT: computed tomography; CV: coefficient of variation; DNA: deoxyribonucleic acid; *E. coli* CD: *Escherichia coli* cytosine deaminase; EGFR: epidermal growth factor receptor; ERK: extracellular signal regulated kinase; FdUrd: 2'-deoxy-5-fluorouridine; FGFR: fibroblast growth factor receptor; FRT: fractional retention; GLUT: glucose transporter; HDAC: histone deacetylase; hENT1: human equilibrative nucleoside transporter; HGF: hepatocyte growth factor; HSP: heat shock protein; HSV: herpes simplex virus; ID: injected dose; max: maximum; MEK: mitogen-activated protein kinase kinase; MET: HGF receptor; MRI: magnetic resonance imaging; mTOR: mechanistic target of rapamycin; n.d.: not determined; n.s.: not significant; NSCLC: non-small cell lung cancer; NUV: normalized uptake value; PCNA: proliferating cell nuclear antigen; PI3K: phosphatidylinositol-4,5-bisphosphate 3-kinase; PDT: photodynamic therapy; PET: positron emission tomography; PRISMA: Preferred Reporting Items for Systematic Reviews and Meta-analyses; RNA: ribonucleic acid; SCC: squamous cell carcinoma; TAC: time activity curve; TK1: thymidine kinase 1; TMZ: temozolomide; TS: thymidylate synthase; TP: thymidine phosphorylase; T/B: tumor-to-background ratio; T/M: tumor-to-muscle ratio; SUV: standardized uptake value; uPAR: urokinase plasminogen activator receptor; VEGFR: vascular endothelial growth factor receptor; vs.: versus; wk: week

2 Supplementary Methods

The search terms used in Embase.com were as follows:

Query (1): FLT: '3'fluorothymidine'/exp OR alovudine:ab,ti OR '18f flt':ab,ti OR 'flt':ab,ti OR fluorothymidin*:ab,ti OR fddt:ab,ti OR deoxythymidin*:ab,ti OR dideoxythymidin*:ab,ti OR fluorodeoxythymidin*:ab,ti OR flt:ab,ti OR flts:ab,ti AND ('positron emission tomography'/exp OR pet:ab,ti OR petscan*:ab,ti OR (emission:ab,ti AND (tomograph:ab,ti OR tomographs:ab,ti OR tomographic*:ab,ti OR tomography:ab,ti OR tomographies:ab,ti OR scan:ab,ti))) AND [1998-2014]/py

Query (2): neoplasms[mesh] OR cancer[sb] OR oncolog*[tiab] OR cancer*[tiab] OR neoplas*[tiab] OR tumour*[tiab] OR tumor[tiab] OR tumors[tiab] OR tumori*[tiab] OR carcinom*[tiab] OR melanom*[tiab] OR lymphom*[tiab] OR leukemia*[tiab] OR malignan*[tiab] OR metasta*[tiab] OR carcinogen*[tiab] OR oncogen*[tiab] OR anticarcinogen*[tiab] OR sarcoma*[tiab] OR precancerous[tiab] OR paraneoplastic[tiab] OR neuroma*[tiab] OR blastoma*[tiab] OR meningioma*[tiab] OR lymphangioma*[tiab] OR lymphangiomyoma*[tiab] OR lymphangiosarcoma*[tiab] OR "hodgkin disease"[tiab] OR plasmacytoma*[tiab] OR carcinosarcoma*[tiab] OR hepatoblastoma*[tiab] OR mesenchymoma*[tiab] OR chordoma*[tiab] OR germinoma*[tiab] OR gonadoblastoma*[tiab] OR mesonephroma*[tiab] OR teratoma*[tiab] OR teratocarcinoma*[tiab] OR nsccl[tiab]

All studies meeting the selection criteria were included, irrespective of study quality. We did not make any restriction on

- cancer type studied (mostly grown as subcutaneous xenografts in nude mice and most of them were of human origin, if not indicated otherwise)
- number of tumors analyzed
- use of [¹⁸F]FLT or [³H]FLT
- mode of data acquisition (dynamic or static PET, gamma counter measurements, or autoradiography)
- mode of data quantification (e.g. evaluation of maximum or mean tracer uptake)
- imaging time point (i.e. early or late, after changes in tumor volume already occurred)
- type and schedule of tumor therapy

The following information was extracted from each included publication:

- model system (*in vitro*, in mice, in rats, in dogs, or in rabbits)
- tumor type
- type of therapy
- numerical data of [¹⁸F]FLT accumulation
- number of objects studied
- comparison to [¹⁸F]FDG
- relation to respective *ex vivo* analyses
- PET protocol
- PET quantification mode

We did not contact authors to retrieve numerical data if not provided in the original manuscript. If applicable, we calculated percent change of [^{18}F]FLT uptake to have a more homogeneous measure of therapy induced alterations which we presented graphically in **Fig. 4**.

We sorted the data for the therapy paradigm employed. In two cases, two publications were based on the same dataset. However, the respective quantitative data were listed only once in the analysis of our systematic review.

We performed analyses to give an overview on

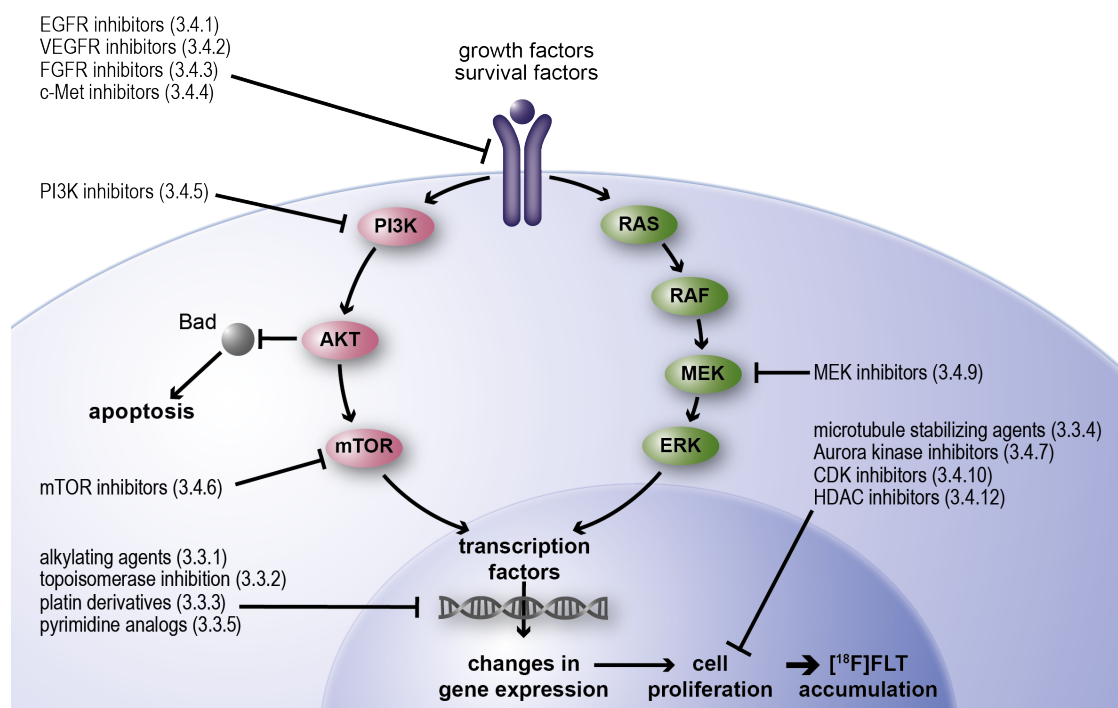
- tumor models analyzed
- PET imaging protocols pursued
- PET quantification modes employed
- how many studies showed a change of [^{18}F]FLT after tumor therapy
- how [^{18}F]FLT performed compared to [^{18}F]FDG
- how many studies related [^{18}F]FLT to *ex vivo* markers of proliferation (thereby distinguishing the description of a relation from the statistical calculation of a correlation)
- percent change of [^{18}F]FLT uptake after tumor therapy

None of these analyses was planned at the time when designing the search strategy. Hence, none was pre-specified.

3 Supplementary Results

3.1 Cellular Pathways essential for anti-cancer drug action and [¹⁸F]FLT accumulation

Supplementary Fig. S1 summarizes some of the major pathways that are of importance for cancer cell proliferation and which may serve as targets for anti-cancer therapies. Several of these treatment strategies have been evaluated in preclinical studies with the help of [¹⁸F]FLT. Results of these studies are further described and discussed in the upcoming chapters. The studies were sorted for the therapy approach pursued.



Supplementary Fig. S1: Schematic presentation of the major signal transduction pathways responsible for cancer cell proliferation. Extracellular binding of growth and survival factors to respective receptor tyrosine kinases on the cell surface mediates a range of proliferative signals. Subsequently induced signal transduction pathways involve various kinases (e.g. PI3K, MEK). Finally, gene expression is altered resulting in induction of cell proliferation and anti-apoptotic signals. Many of these steps can be targeted by chemotherapeutic or targeted anti-cancer agents, as indicated. The mechanisms of these agents are further described in the respective chapters (in brackets) in these supplementary results.

3.2 [¹⁸F]FLT accumulation in untreated tumors

3.2.1 Uptake of [¹⁸F]FLT in proliferative tumors

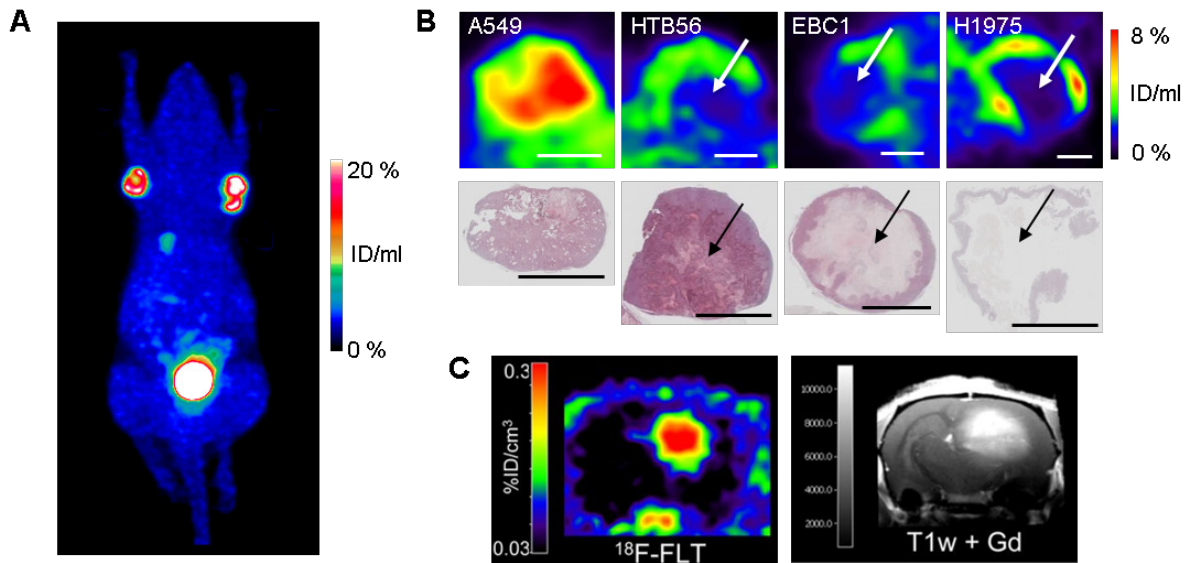
In 1998, Shields et al. were the first to demonstrate accumulation of radiolabeled [¹⁸F]FLT by PET in proliferative tissues, including bone marrow and tumors, in dogs ($n = 3$ healthy individuals, $n = 2$ with tumors) and a human ($n = 1$) [1]. Furthermore, they show that the tracer's catabolism *in vivo* is slow – in contrast to [¹¹C]thymidine, a proliferation tracer already established then. This group further explored

the kinetics of clearance from the blood and uptake into tissues in dogs and developed a three-compartment model for quantification of [¹⁸F]FLT uptake by PET [2]. Of note, biodistribution of [¹⁸F]FLT in mice was reported to vary in different strains [3].

Since the publication of these first reports, many studies have been performed that describe the detection of tumors in rodents by [¹⁸F]FLT PET. In several tumor models [¹⁸F]FLT accumulates in cancerous tissue to a higher extent than [¹⁸F]FDG, for instance in gastric cancer (NCI-N82, MKN74, *n* = 3-4) [4], leukemia (K562) [5], head and neck squamous cell carcinoma (HNSCC FaDu, *n* = 12) [6], or neuroblastoma (Kelly, *n* = 29 [7] or SK-N-SH, *n* = 18 [8]). Some studies report that uptake of [¹⁸F]FLT and [¹⁸F]FDG is comparable for example in gastrointestinal stromal tumors (GIST882) [9], or orthotopic endometrial cancer cells (called ishikawa) in the uterus (*n* = 15) [10].

On the other hand, in some other models [¹⁸F]FDG accumulation in tumor tissue is higher than that of [¹⁸F]FLT, for example in subcutaneous PC-3 prostate cancer (*n* = 6) [11]. Alberni et al. employed a transgenic mouse model that develops tumors in the mammary epithelium. These tumors are detectable on [¹⁸F]FDG PET images, whereas [¹⁸F]FLT does not accumulate (*n* = 4), despite exhibiting high Ki67 staining (44 % ± 5 %) [12]. The authors hypothesize that high serum thymidine levels or the balance of the thymidine *de novo* and salvage pathway could be the cause (see also 3.2.6 or 3.2.4). [¹⁸F]FLT also does not accumulate in papillomavirus-induced tumors in rabbits (tumor-to-muscle ratio (T/M) post-injection: 2 months: 0.8 ± 0.06, *n* = 2; 4 months: 0.75 ± 0.25, *n* = 3; 10 months: 1.0, *n* = 1) [13]. This low uptake might be related to a low tumor proliferation rate. Furthermore, rabbits were anaesthetized with ketamine which could impede [¹⁸F]FLT uptake [14] (see 3.2.9). These studies already point to a complex nature of [¹⁸F]FLT uptake, which will be further discussed in the upcoming chapters.

Intriguingly, one group reports that [¹⁸F]FLT uptake in intracranial DBT glioblastoma might be confounded by uptake in the cranium (*n* = 4) [15]. Unfortunately, the authors did not provide any images. In case of gross uptake in bones, possible *in vivo* defluorination of [¹⁸F]FLT should be considered, which might have been the case in this study. We are not aware of any studies demonstrating substantial uptake of [¹⁸F]FLT in bones of mice. Furthermore, there are numerous reports demonstrating that intracranial tumors in rodents can readily be imaged by [¹⁸F]FLT PET, for example intracranial C6 tumors in rats [16] or melanoma brain metastases from H1 cells (a cell line isolated from a human melanoma brain metastasis) at a size of 250 μm [17]. Further examples can also be found within this review and in **Supplementary Fig. S2C**.



Supplementary Fig. S2: Examples of $[^{18}\text{F}]\text{FLT}$ accumulation in subcutaneous and intracranial tumors in rodents. (A) A maximum intensity projection of a whole body PET scan (70 min - 90 min acquisition after injection of 10 MBq $[^{18}\text{F}]\text{FLT}$) of an NMRI nude mouse is displayed here. Heterogeneous $[^{18}\text{F}]\text{FLT}$ accumulation can be seen in two subcutaneous H1975 lung cancer xenografts implanted in the shoulder region. Background activity can be observed in excretory organs (bladder, gall bladder). No significant $[^{18}\text{F}]\text{FLT}$ accumulation can be noted in other organs, such as brain, heart, lung, spleen, muscle or bones. (B) Tumor $[^{18}\text{F}]\text{FLT}$ uptake might differ in various subcutaneous xenografts even if they are of the same origin as shown here for four human NSCLC xenografts. In this case, $[^{18}\text{F}]\text{FLT}$ uptake appears to be determined by different expression levels of tumor thymidine phosphorylase which alters thymidine levels and thereby affects $[^{18}\text{F}]\text{FLT}$ uptake (see 3.2.6). Note the missing $[^{18}\text{F}]\text{FLT}$ uptake in tumor parts showing histological signs of necrosis (arrows). Scale bars = 5 mm. This research was originally published in J Nucl Med [18]. (C) Also intracranial brain tumors can be visualized by $[^{18}\text{F}]\text{FLT}$ PET as shown here for a human glioma spheroid xenograft in a rat model. $[^{18}\text{F}]\text{FLT}$ uptake in brain tumors is dependent on disruption of the blood brain barrier, which is indicated by T1 weighted MRI after administration of a gadolinium-based contrast agent. This research was originally published in J Nucl Med [19].

Viel et al. employed a multi-modal imaging approach in rats, comparing angiogenic and infiltrative intracranial glioma phenotypes from two spheroids isolated from two different patients ($n = 6$ nude rats per tumor). They show that absence of $[^{18}\text{F}]\text{FLT}$ accumulation does not exclude the presence of proliferating tumor tissue. The infiltrative tumor phenotype does not accumulate this radiotracer despite a high Ki67 proliferation index. In this model uptake of $[^{18}\text{F}]\text{FLT}$ is most likely hampered by the intact blood brain barrier and possibly could also be diminished due to low cellular density suggested by diffusion weighted MRI [19] (**Supplementary Fig. S2C**)

Some studies point at a complementary nature of $[^{18}\text{F}]\text{FLT}$ and $[^{18}\text{F}]\text{FDG}$, where use of both tracers can aid in discriminating different tumor phenotypes. Wang et al. show that two colorectal cancer models of the same genetic origin isolated from the same patient differ significantly in growth rates, metastatic potential, survival rates, and $[^{18}\text{F}]\text{FDG}$ and $[^{18}\text{F}]\text{FLT}$ uptake ($[^{18}\text{F}]\text{FLT}$ T/B of SW480: 3.65 ± 0.51 vs. SW620: 2.22 ± 0.42 , $P < 0.001$, $n = 3$ per group). $[^{18}\text{F}]\text{FLT}$ uptake in the primary tumors significantly correlates with the number of metastases in lung and liver ($r = 0.763$, $P = 0.005$). However, in this study no clear relation of $[^{18}\text{F}]\text{FLT}$ accumulation with Ki67 expression can be detected, and $[^{18}\text{F}]\text{FDG}$ better predicts survival rates [20].

3.2.2 Specificity in detection of tumor versus inflammation

One of the major reasons for developing [^{18}F]FLT as an oncology PET tracer was to overcome the nonspecific accumulation of [^{18}F]FDG in inflammatory lesions. In the setting of cancer treatment inflammatory cells might be recruited to tumor tissue, resulting in a temporary rise in [^{18}F]FDG uptake. This “flare” might mask a possible treatment effect and result in a false-negative evaluation of treatment efficacy. Four reports in rats focus on identifying whether [^{18}F]FLT is indeed more specific than [^{18}F]FDG in terms of targeting tumors over inflammation.

[^{18}F]FLT is superior to [^{18}F]FDG in discriminating an *Escherichia coli* induced inflammation from a subcutaneous 9L glioma model by means of gamma counter measurements (blood corrected tumor-to-inflammation ratio: [^{18}F]FDG: 3.2 ± 1.6 , [^{18}F]FLT: 12.0, $n = 4-5$) [21] or a turpentine induced inflammation model from C6 rat gliomas (selectivity index: [^{18}F]FDG: 3.5 ± 1.2 , [^{18}F]FLT > 10.6, $n = 5$) [22,23]. Zhao et al. show similar results for another turpentine-induced inflammation model (^3H]FLT differential uptake value measured by gamma counter: KDH-8 hepatoma: 2.66 ± 0.41 , inflammation: 0.99 ± 0.13 , $P < 0.01$, $n = 5$). However, in their experiments ^3H]FLT is not able to differentiate between tumors and *Mycobacterium bovis* bacillus Calmette-Guérin induced granulomas (tumor: 2.30 ± 0.67 vs. granuloma: 1.98 ± 0.70 , $n = 7$). The authors hypothesize that ^3H]FLT accumulates in granulomatous lesions with proliferative inflammation. A detailed analysis of Ki67 proliferation index in these lesions would be required to prove this theory [24]. A recent study shows that [^{18}F]FLT accumulates in atherosclerotic lesions, presumably reflecting uptake in macrophages. Ki67 flow cytometry confirms that these macrophages are proliferative [25]. And also in patients, [^{18}F]FLT has been described to accumulate in inflammatory tissue resulting in false-positive findings. In 7 out of 10 [^{18}F]FLT positive lymph nodes in head and neck cancer patients, accumulation of the tracer appears to be the result of the accumulation of B-lymphocyte within the germinal centers [26]. And in a study with 21 patients with suspected laryngeal cancer [^{18}F]FLT provides a false-positive tumor detection in one patient having inflammatory laryngeal tissue [27]. Furthermore, [^{18}F]FLT accumulates in tuberculosis and sarcoidosis [28].

Taken together, these studies imply that [^{18}F]FLT has a higher selectivity for tumors and provides less false-negative accumulation in inflammatory tissue than [^{18}F]FDG. However, presence of activated proliferating lymphocytes might hamper this selectivity.

3.2.3 Repeatability of measurements

To be used as pharmacodynamic response biomarker for therapy evaluation it is important that uptake of a radiotracer in untreated tumors is repeatable. Two studies acquired [^{18}F]FLT PET scans 6 h apart (after repeated tracer injection) and determined the coefficient of variation (CV, calculated as the standard deviation of the first scan and second scan divided by their mean) as a statistical measure of absolute reliability. The CV of the %ID/g is $14 \% \pm 10 \%$ for rat C6 glioma xenografts. The authors state that in serial studies a change would need to be greater than twice the CV to indicate a real change at the individual subject level. Accordingly, a change in %ID/g would have to be 28 % in the C6 model ($n = 9$ mice, $n = 17$ scans) [29]. Furthermore, these authors also report, that the fasting state or dose of radiotracer injected does not affect the variability of the scans. The second study demonstrates a CV of $4.0 \% \pm 3.8 \%$ for BT474 breast cancer xenografts, implying that in these tumors a change in [^{18}F]FLT uptake would have to be at least 8 % to represent a real change ($n = 12$) [30]. In another study analysis

of [¹⁸F]FLT PET measurements acquired on two consecutive days reveals standard deviations of the percent difference of %ID/g of 20 % for A431 epidermoid carcinoma and 29 % for LLC Lewis lung tumors ($n = 10$ per group). These data indicate that in A431 tumors a change of more than 40 % in %ID/g would indicate actual changes in tumors, which corresponds to twice the percent difference. The LLC model has lower levels of [¹⁸F]FLT phosphorylation and also other static and kinetic parameters of [¹⁸F]FLT uptake show poor reproducibility. Accordingly, the authors hypothesize that [¹⁸F]FLT PET is repeatable in tumors that have a high [¹⁸F]FLT phosphorylation [31]. And also the aforementioned studies claim that uptake of [¹⁸F]FLT is repeatable with moderately low variability and it should therefore be feasible to use this tracer for detection of treatment response. As the repeatability of [¹⁸F]FLT uptake measurements differs significantly between tumor types, it is advisable to incorporate test-retest study designs in preclinical studies.

3.2.4 Factors in DNA salvage pathway utilization determine [¹⁸F]FLT uptake

As indicated in **Fig. 1**, it is widely accepted that [¹⁸F]FLT is a tracer of the thymidine salvage pathway. The key enzyme of this pathway is thymidine kinase 1 (TK1) [32]. Analysis of different cell lines (murine breast EMT6, fibrosarcoma RIF-1, sarcoma KHT; human lung A549, colorectal WiDr, and HT29) confirms that accumulation of [¹⁸F]FLT is dependent on TK1 activity during *in vitro* growth (correlation between TK1 activity and [³H]FLT uptake: $r^2 = 0.80$, $P < 0.0001$) [33]. Furthermore, knockdown of TK1 by siRNA reduces [¹⁸F]FLT uptake in cell culture experiments ([³H]FLT levels are $14 \% \pm 3 \%$ of control treatment in epidermoid A431 cells, $P < 0.001$; and $14 \% \pm 4 \%$ of control treatment in head and neck squamous cell line SCC1 cells, $P < 0.001$, $n = 3$ independent experiments) [34]. Analysis of a thymidine salvage incompetent (TK1^{-/-}) subcutaneous L5178Y mouse lymphoma model underlines the importance of TK1 for [¹⁸F]FLT uptake (area under the normalized tumor time-activity curve (TAC) in MBq/ml*min for TK1^{+/-} vs. TK1^{-/-} variant: 0.89 ± 0.02 vs. 0.79 ± 0.03 , $P = 0.043$, $n = 5$ per tumor type; correlation between [¹⁸F]FLT accumulation and TK1 protein levels: $r = 0.68$, $P = 0.046$) [35]. Keen et al. reveal a moderate correlation of [¹⁸F]FLT uptake and TK1 expression (Spearman $r = 0.592$, $P = 0.017$, $n = 20$) or Ki67 ($r = 0.655$, $P = 0.002$, $n = 20$) in a broad range of tumor xenografts (U87 glioma and colorectal Colo205, HCT116, LoVo and SW620) [36]. High uptake of [¹⁸F]FLT in three orthotopically implanted pancreatic cancer xenografts ($n = 4$ PancTul, $n = 5$ Colo357, and $n = 3$ BxPC3) is also related to high TK1 levels [37].

Seitz et al. measured pyrimidine metabolizing enzymes and [¹⁸F]FLT uptake in pancreatic cancer cell lines [38]. They confirm dependence of [¹⁸F]FLT accumulation on TK1 and show similar overexpression patterns of both TK1 and TS in cancer compared to normal pancreatic cells. On the other hand, a negative correlation between TK1 and TS activity levels ($r = -0.26$; $P < 0.0001$) can be observed in breast cancer patients as reported by Foekens et al. [39]. The dependence of [¹⁸F]FLT accumulation on the DNA salvage pathway and hence TK1 expression is also demonstrated by McKinley and coworkers [40]. In their experiments [¹⁸F]FLT accumulation is not correlated with proliferation markers such as Ki67 or PCNA, but with TK1 (Spearman $r = 0.36$, $P < 0.05$) in a range of tumor models (colorectal cancer cell lines DiFi, HCT116, Colo205, SW620, HT-29, and Lim2405, and the breast cancer cell line BT474). Furthermore, they manipulated the balance of *de novo* and salvage DNA synthesis in HCT116 tumors. Subsequent [¹⁸F]FLT PET analysis of respective xenografts underlines the importance of the DNA

salvage pathway for the uptake of this tracer (%ID/g: HCT116: 8.56 ± 1.17 , HCT116 $p21^{-/-}$: 6.91 ± 1.07 , $P = 0.005$) [40]. These data illustrate that reliance on *de novo* pathway utilization by tumors results in underestimation of proliferation by [^{18}F]FLT PET. Specifically, the tracer does not enable the distinction between moderately proliferative tumors that rely largely on thymidine salvage from highly proliferative tumors that are more dependent on the *de novo* pathway.

The interplay between *de novo* and salvage pathways is complex and the balance can be disrupted by TS-inhibiting agents [39,41] such as 5-FU, antifolates [42] or topoisomerase inhibitors [43]. This needs to be considered when using [^{18}F]FLT for assessment of tumor response (see also 3.3.5 and 3.3.6).

The role of ATP levels as a cofactor for TK1 activity is illustrated in a study analyzing [^{18}F]FLT kinetics in glioma patients [44]. Preclinical studies underline the importance of ATP for [^{18}F]FLT uptake in murine radiation-induced fibrosarcoma (RIF-1) *in vivo* [45], or C6 rat glioma cells *in vitro* [46].

Some studies report a mismatch between changes in TK1 levels and [^{18}F]FLT uptake, as observed in MDA-MB-231 breast cancer cells treated *in vitro* with different agents [47] (% change of TK1 levels / [^{18}F]FLT uptake 72 h after incubation with 5-FU: $443 \pm 58 / 46 \pm 32$, doxorubicin: $473 \pm 348 / 273 \pm 209$, paclitaxel: $52 \pm 32 / 166 \pm 18$). The authors attribute these discrepancies to unchanged TK1 activity when cells accumulate in G₁ phase. The other potential confounding factor identified in this study is expression and activity of the mitochondrial isoform of thymidine kinase TK2. However, other reports indicate that [^{18}F]FLT is a far better substrate for TK1 than for TK2 [48,49]. Furthermore, in proliferating cells TK1 levels are much higher than TK2 levels [50], pointing at a predominant role of TK1 over TK2 for uptake of [^{18}F]FLT in tumor cells.

[^{18}F]FLT retention has been assigned primarily to alteration of the strict transcriptionally regulated S-phase expression of TK1. This, however, does not explain how anticancer agents acting primarily through G₂/M arrest, such as taxanes, affect [^{18}F]FLT uptake. An alternative mechanism of [^{18}F]FLT cellular retention involving post-translational modifications of TK1 during mitosis is proposed by Sala et al. [51]. They demonstrate the presence of at least two phosphorylated residues on TK1 that are responsible for modulating the activity of the enzyme. They show that [^{18}F]FLT cellular retention following G₂/M arresting drug treatment reflects TK1 phosphorylation and not expression of total protein. In conclusion, although TK1 remains the major determinant of [^{18}F]FLT tumor uptake, there are other factors confounding direct correlation between [^{18}F]FLT and cellular proliferation, such as TK1 activity (phosphorylation status), its substrate availability (ATP levels), activity of *de novo* DNA synthesis pathway (TK1-TS relationship) and possibly mitochondrial TK2 activity.

3.2.5 [^{18}F]FLT transport into the cell might limit tracer accumulation

Other factors that could confound accumulation of [^{18}F]FLT include the transport of the tracer into cells. In sarcomatoid mesothelioma (211H) showing high TK1 activity *in vitro* Tsuji et al. observe a low *in vivo* [^{18}F]FLT uptake when compared to epitheloid mesothelioma (H226, $n = 3-6$ per tumor). Also Ki67 staining is not related to [^{18}F]FLT accumulation in these models. Hence, the authors conclude that other factors, like expression of nucleoside transporters may confound accumulation of [^{18}F]FLT [52]. And indeed, overexpression of human nucleoside transporters in *Xenopus laevis* oocytes or respective inhibition in different cell types *in vitro* (lung carcinoma A549, breast adenocarcinoma MCF-7, glioblastoma U251, and pancreatic carcinoma MIA PaCa-2 and Capan-2) underpin the importance of

nucleoside transporters, especially the human equilibrative nucleoside transporter 1 (hENT1), for [³H]FLT uptake. In five of the six cell lines there is a strong correlation between [¹⁸F]FLT uptake and binding sites for the hENT1 inhibitor extracellular nitrobenzylmercaptapurine ribonucleoside ($r^2 = 0.98$, $P = 0.0011$ [53]. In the lung cancer cell line A549 reduction of hENT1 levels by 55 % using shRNA reduces accumulation of [³H]FLT *in vitro* (0.68-fold reduction, $P < 0.05$, $n = 3$ different experiments in triplicate) and of [¹⁸F]FLT *in vivo* (SUV_{max}: 0.82 ± 0.15 vs. 0.53 ± 0.12 ; $P < 0.01$, $n = 5$), whereas TK1 is unaltered [54]. Furthermore, analysis of the spatial relation of [¹⁸F]FLT uptake by means of autoradiography and immunohistochemistry reveals high tracer uptake in proliferating tumor regions which show higher hENT1 levels than non-proliferating tumor regions [55]. Moreover, redistribution of hENT1 has been shown to be involved in temporal increase of [¹⁸F]FLT retention after 5-FU therapy which is further discussed in 3.3.5 [56].

3.2.6 Endogenous thymidine as competing factor for [¹⁸F]FLT

According to Zhang et al. the concentration of thymidine in the plasma is about 200x higher than the concentration of [¹⁸F]FLT [57]. Endogenous thymidine levels can affect [¹⁸F]FLT uptake by two different mechanisms. Thymidine present in the blood competes with [¹⁸F]FLT for the transporters at the cell surface and tracer delivery into the cell as shown in **Fig. 1**. Competition of [¹⁸F]FLT with endogenous thymidine present inside the tumor cell could be reflective of the less-studied nucleotide turnover process linked to tumor metabolic activity [58].

Plasma levels of thymidine in rodents are 10-300 fold higher than those in humans [59,60]. This difference should be considered when translating findings from preclinical models to humans. Tseng et al. note a weak correlation of serum thymidine and uptake of [¹⁸F]FLT in C6 rat glioma xenografts ($R^2 = 0.40$, $n = 6$) [29]. The lack of [¹⁸F]FLT correlation with proliferation as assessed by growth rate, Ki67 expression or TK1 staining in a range of different tumor xenografts (breast MDA-MB-231 and MX1, colorectal Colo2015, HT29, LS174T and HCT116, lymphoma Raji, and prostate PC3) is attributed to competition of [¹⁸F]FLT with endogenous thymidine by Zhang et al. [57]. They demonstrate an inverse relation of tumor thymidine levels and tracer uptake. Furthermore, infusion of thymidine by an osmotic pump reduces [¹⁸F]FLT uptake in HCT116 colorectal xenografts [57]. Some treatments might induce thymidine changes in plasma [61] and tumor. Therefore, consideration should be given to this factor when using [¹⁸F]FLT to assess treatment response.

Given the fact that thymidine is a substrate for catabolism by thymidine phosphorylase (TP), van Waarde et al. manipulated [¹⁸F]FLT tumor uptake by infusion of exogenous thymidine phosphorylase into rats bearing C6 rat glioma xenografts [22]. Although the change in [¹⁸F]FLT tumor uptake after TP treatment does not reach statistical significance, there is a profound increase of tracer accumulation in the bone marrow [22].

Schelhaas et al. analyzed TP and tumor thymidine levels in four different non-small cell lung cancer (NSCLC) xenografts (A549, EBC1, HTB56, H1975) having varying baseline uptake of [¹⁸F]FLT (**Supplementary Fig. S2B**). They demonstrate that tumors with high TP expression possess low levels of thymidine and increased [¹⁸F]FLT accumulation (thymidine vs. [¹⁸F]FLT: $r = -0.682$, $P < 0.005$, $n = 27$) [18]. Furthermore, *in vitro* experiments reveal a significant correlation of cellular TP activity and the ratio of [³H]FLT over [³H]thymidine uptake in a range of cell lines (A431 cervical squamous cell carcinoma,

HT29 colon adenocarcinoma, ACHN renal adenocarcinoma, SKOV3 ovarian adenocarcinoma, and A549 and HOP92 lung adenocarcinoma, $r = 0.94$, $P < 0.01$). No relation of [^{18}F]FLT uptake to TK1 or ENT1 activity is apparent in this study. Moreover, TP immunohistochemistry score is related to [^{18}F]FLT uptake in the samples from 85 lung cancer patients [62].

These observations indicate that in certain tumors [^{18}F]FLT uptake does not reflect TK1 activity or proliferation but TP activity linked to nucleotide turnover processes.

3.2.7 Hypoxia impacts [^{18}F]FLT accumulation

Autoradiography in combination with immunohistochemistry is frequently applied to shed light on the spatial relation of tracer uptake with cellular and molecular determinants. Li et al. [63] studied [^{18}F]FDG and [^{18}F]FLT distribution in subcutaneous A549 and HTB177 lung cancer xenografts as well as samples from patients with lung cancer. [^{18}F]FDG accumulates in hypoxic zones as identified by *ex vivo* pimonidazole staining, while [^{18}F]FLT is detectable in proliferative cancer regions as identified by Ki67 staining. The authors hypothesize that a combination of [^{18}F]FLT and [^{18}F]FDG would give a more accurate presentation of total viable tumor tissue than either tracer alone [63]. Another study using A549 and HTB177 lung tumors grown in mice confirms that hypoxic cancer cells with a low proliferation rate exhibit high [^{18}F]FDG uptake but low [^{18}F]FLT accumulation, whereas well-oxygenated cancer cells with a high proliferation rate accumulate high levels of [^{18}F]FLT but relatively low [^{18}F]FDG ($n = 5$ subcutaneous and $n = 3$ peritoneal tumors per cell line) [64]. However, a direct comparison of the spatial distribution of radioactive tracers visualizing hypoxia with [^{18}F]FLT shows strong correlation ($R^2 = 0.83$) in subcutaneous 9L rat gliosarcomas ($n = 5$ per group [65]). Hence, the relation between glucose uptake, proliferation and hypoxia appears to be inconsistent between studies and tumor models. The authors speculate that this could be related to the fact that hypoxia might develop in different tumors through mechanisms unrelated to oxygen supply [65].

3.2.8 Vascularization impacts [^{18}F]FLT delivery

Bruns et al. show that treatment with C225, an anti-EGFR antibody, leads to a reduction in microvessel density in pancreatic cancer xenografts, which might directly impact tracer delivery [66]. This finding not only holds true for EGFR-targeting therapies, but also for VEGFR-targeting therapies [67]. For instance, Viel et al. show that after bevacizumab treatment the number of vessels are reduced in a rat glioma model [68]. Differences in vasculature might contribute to variances in tracer and drug delivery [69]. Tumor vascularization might be addressed by multimodality imaging [70] and should be taken into account as a confounding factor.

3.2.9 Methodological confounders of [^{18}F]FLT detection

Experimental design and technological limitations can influence tumor uptake of [^{18}F]FLT. For example oxygen breathing of mice which are awake during the tracer uptake period can lead to acidosis and consequently reduced cell proliferation and [^{18}F]FLT uptake as demonstrated for CT26 colon tumors ($n = 12-13$) as well as arthritic ankles [71]. Furthermore, also the choice of anesthesia can affect tracer accumulation. Fuchs et al. recommend the use of isoflurane for [^{18}F]FLT PET imaging, since it yields stable tracer uptake and is easy to handle. The group observes that [^{18}F]FLT accumulation in

subcutaneous CT26 tumors is significantly reduced in ketamine / xylazine-anesthetized mice (4.4 ± 0.9 %ID/ml) compared to medetomidine / midazolam- (7.0 ± 1.5 %ID/ml) or isoflurane-anesthetized mice (6.4 ± 1.5 %ID/ml). Furthermore, mice that are awake during tracer uptake period tend to have lower [^{18}F]FLT uptake in tumors [14].

Mouse body temperature has been shown to be an important factor that can influence tracer uptake and must be carefully regulated and reported. C6 rat glioma xenografts in mice at 24 °C accumulate less activity than respective tumors in mice at 35 °C (%ID/g 24 °C: $3.8 \% \pm 0.6 \%$, 35 °C $7.9 \% \pm 3.6 \%$, $P = 0.04$, $n = 3$), probably because of decreased blood flow and declined body functions at lower temperature, which would reduce tracer delivery and cell proliferation [29].

Caretti et al. describe an aspect that could especially confound the imaging of brain lesions. They used an HRRT PET scanner for the detection of E98 brain tumors in the mouse. Even though the tracer is readily detectable in subcutaneous tumors ($n = 4$), intracranial lesions ($n = 6$) are not visible which the authors attribute to the limited spatial resolution of the scanner (2.3 mm - 2.7 mm) [72]. However, also an undisrupted blood-brain barrier could possibly explain a missing [^{18}F]FLT accumulation in this experimental setup. In clinical studies in glioma patients it has been shown that [^{18}F]FLT uptake in brain tumors depends on the blood brain barrier status [73]. Preclinical studies in glioblastoma models confirm this finding [19].

A different study raises the issue that also the limited spatial resolution of autoradiography might explain inconsistencies in [^{18}F]FLT signal intensities. In a head and neck squamous cell carcinoma model (FaDu) BrdU staining and [^{18}F]FLT accumulation are spatially related. However, a second model (SQ20B) shows a highly dispersed pattern of cellular proliferation, that cannot be spatially resolved by [^{18}F]FLT autoradiography [74].

Obviously, drug-induced reduction in [^{18}F]FLT uptake cannot be detected unless a tumor model with sufficient baseline [^{18}F]FLT uptake is chosen. Keen et al. suggest that for treatment response studies a lower SUV_{mean} cut-off limit of 0.3 is used [36]. [^{18}F]FLT uptake might be hampered by the fact that a specific cell primarily depends on the thymidine *de novo* and not the salvage pathway, as described above (3.2.4). Also, in some studies described in this review, poor performance of [^{18}F]FLT uptake as an imaging biomarker might be attributed to low baseline tracer accumulation [75–77].

3.3 Imaging of response to chemotherapy

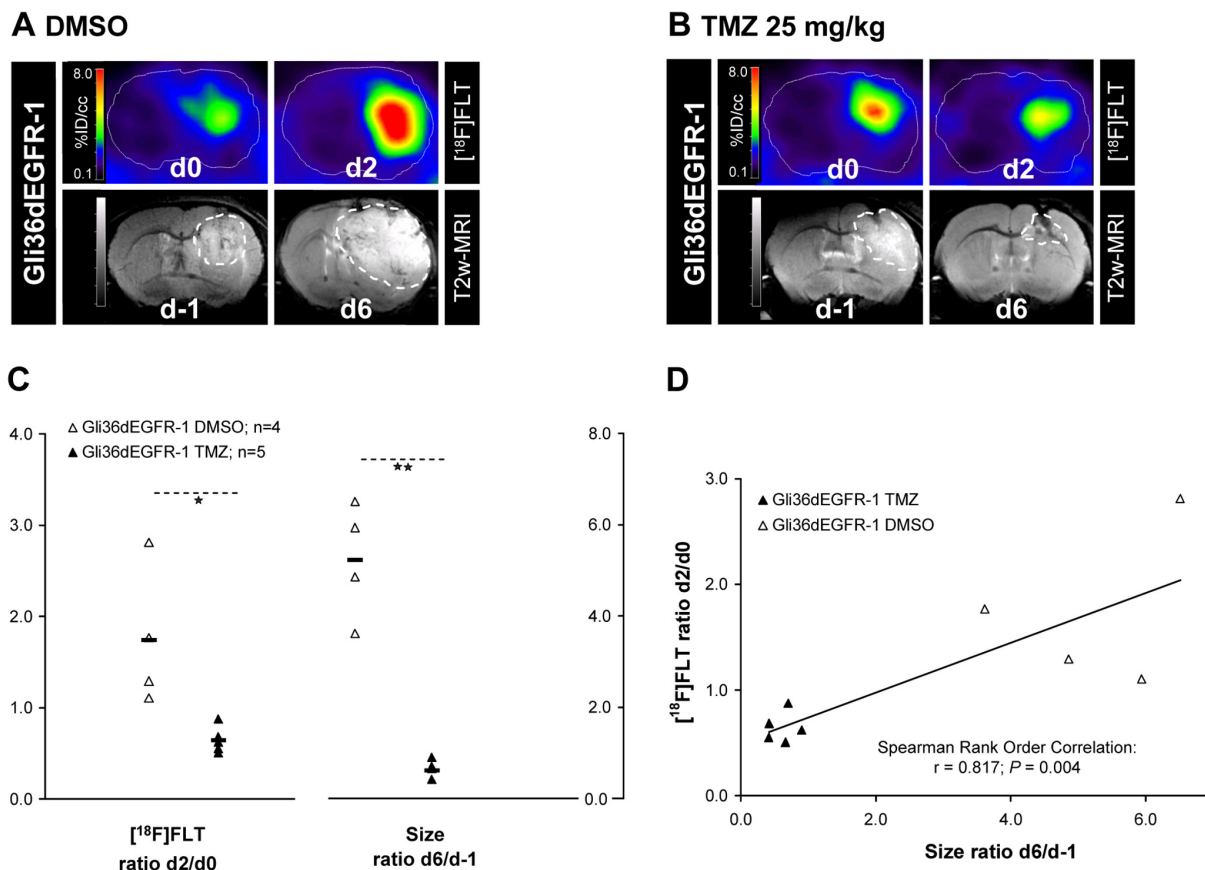
In the next chapters we evaluate whether [^{18}F]FLT PET is capable to detect tumor response to classical anti-proliferative chemotherapeutic agents. These agents act on rapidly dividing cells and exert cytotoxic or cytostatic effects. We categorized the respective studies depending on the mode of action of the chemotherapeutic agent.

3.3.1 Alkylating agents

Alkylating agents add an alkyl group ($\text{C}_n\text{H}_{2n+1}$) to the DNA at several locations (**Supplementary Fig. S1**). Hence, the cell's mismatch repair system is activated, which leads to DNA strand breaks. If these are not repaired, the cell undergoes apoptosis.

1-(4-amino-2-methyl-5-pyrimidinyl) methyl-3-(2-chloroethyl)-3-nitrosourea hydrochloride (ACNU) is an alkylating agent adding a methyl group to DNA [78]. An *in vitro* study of ACNU treated rat C6 glioma cells reveals a time-dependency of [³H]FLT uptake. [³H]FLT accumulation is increased to 120 % -140 % of control after ACNU treatment for 3 h - 6 h, which might result from transient induction of TK1 activity. After 24 h, [³H]FLT uptake decreases to 60 % - 40 % in a dose-dependent manner. Puzzlingly, this effect can be observed in both, sensitive and resistant clones, indicating that in this experimental setup [³H]FLT is not predictive for drug response as measured by cell growth arrest. On contrary [³H]FDG is decreased in the sensitive cell line but unchanged in the resistant clone after 24 h [79].

However, [¹⁸F]FLT predicts the tumor response to other alkylating agents. Daily administration of temozolomide (TMZ) leads to a reduction of Ki67 ($P < 0.01$) and an increase in cleaved caspase-3 on d2 ($P < 0.01$) in subcutaneous and intracranial Gli36 glioma xenografts, whereas TK1 is unaltered. At the same time, [¹⁸F]FLT decreases in subcutaneous tumors relative to control (relative change of [¹⁸F]FLT T/B (d2/d0): vehicle group: 1.42 ± 0.30 , $n = 9$; TMZ group: 0.99 ± 0.15 , $n = 8$). The change in [¹⁸F]FLT uptake correlates with the change in tumor size on d7, and hence therapy response ($r = 0.759$, $P < 0.0001$). Respective intracranial gliomas show a similar change in [¹⁸F]FLT uptake (relative change (d2 vs. d0) of [¹⁸F]FLT T/B: vehicle group: $+70 \% \pm 80 \%$, $n = 4$; TMZ group: $-40 \% \pm 10 \%$, $n = 5$, $P = 0.015$; Spearman correlation of change in size (d6 vs. d-1) vs. change of [¹⁸F]FLT T/B ratio (d2 vs. d0): $r = 0.827$, $P = 0.0039$) (Supplementary Fig. S3 [80]).



Supplementary Fig. S3: [¹⁸F]FLT can visualize response to chemotherapeutic treatment in tumor xenografts and predict changes in tumor volume at later time points. Intracranial Gli36dEGFR gliomas were treated by daily administration of temozolomide (TMZ, B) or vehicle (A). (C) [¹⁸F]FLT is markedly reduced in the tumors 2 d after onset of therapy. (D) Changes in tracer uptake at that time

point significantly correlate with changes in tumor volume on d7, as determined by T2 weighted MRI. *: $P < 0.05$; **: $P < 0.01$. Taken from [80].

Two days after administration of cyclophosphamide [^{18}F]FLT uptake is significantly reduced in DoHH2 follicular lymphoma (%ID/g: control: 5.4; treated group: 3.9 ± 2.0 , $P = 0.0005$), consistent with decreased Ki67 staining (control: $83.6 \% \pm 3.2 \%$, cyclophosphamide: $39.9 \% \pm 9 \%$, $P = 0.0001$, $n = 10$ per group) [81]. Another group employed Granta-519 lymphoma xenografts to show a reduction of [^{18}F]FLT already on d1 lasting for up to 2 weeks after a single dose of cyclophosphamide ([^{18}F]FLT PET performed on d1, d2, d4, d7, d9, d11, d14, change of SUV_{mean} on d2: -26.1% , on d7: -18.8% , $n = 5$). This is accompanied by an increase in apoptotic or necrotic tumor fraction as shown by immunohistochemistry, whereas Ki67 is unaltered. In this model imaging with [^{18}F]FDG is confounded by the invasion of inflammatory cells at later time points [82].

3.3.2 Interference with topoisomerase activity

Topoisomerases are responsible for unwinding DNA strands, a critical step in DNA replication and transcription (**Supplementary Fig. S1**). Examples of topoisomerase inhibitors used in the clinic are irinotecan and doxorubicin. When given in weekly intervals to colorectal HCT116 tumor bearing mice irinotecan reduces [^{18}F]FLT uptake 1 d after each drug administration up to three weeks (SUV_{max} as percentage from baseline, vehicle vs. irinotecan treated group: d1: 96 ± 5 vs. 61 ± 4 , d8: 86 ± 4 vs. 63 ± 5 and d15: 84 ± 5 vs. 60 ± 4 , $P < 0.012$ for all time points, $n = 6$). On d5 after the first treatment, tracer uptake is not affected (89 ± 2 vs. 79 ± 8 , $n = 4$). Based on the half-life of irinotecan the drug is no longer present at significant levels 5 d after administration, explaining the unchanged [^{18}F]FLT uptake at that time point. All other measurements were performed 1 d after irinotecan, implying that early after drug administration tumor proliferation is indeed affected. The authors show that on d15 also proliferation as measured by immunohistochemical staining is significantly reduced (Ki67: 10 % inhibition vs. vehicle, $P < 0.05$; phosphorylated histone H3: 25 % inhibition), which is in line with reduced [^{18}F]FLT uptake. Interestingly, in this experimental setup [^{18}F]FDG uptake increases after each treatment for an unknown reason [83].

Intercalation of specific chemotherapeutic agents into the DNA interferes with the binding of topoisomerase II. Doxorubicin is the most commonly used intercalating agent. *In vitro* uptake assays reveal that [^{18}F]FLT is reduced 24 h upon doxorubicin treatment of C6 rat glioma cells ($1.3 \% \pm 0.2 \%$ of control, $P < 0.0001$), which is consistent with reduced S-phase fraction (baseline: $43 \% \pm 1 \%$, 24 h: $14 \% \pm 3 \%$, $P < 0.0001$), TK1 activity ($P < 0.0002$) and ATP ($60 \% \pm 2 \%$ of control, $P < 0.01$) [46]. In an *in vivo* malignant lymphoma model (SUDHL-4 diffuse large B-cell lymphoma) application of a single dose of doxorubicin leads to a reduction in [^{18}F]FLT uptake as well as Ki67 expression as early as one day after therapy, and this effect is sustained on d5 and d9 (median T/B compared to before treatment: d1: 76 %, $P = 0.048$, $n = 6$; d5: 47 %, $P = 0.068$, $n = 4$; d9: 77 %, $n = 2$) [84]. In the same model it was also shown that decrease in [^{18}F]FLT uptake and Ki67 staining on d2 occur in a dose-dependent manner (mean T/B compared to before treatment: 25 μg : 69 %, $P = 0.02$, $n = 6$; 50 μg : 73 %, $P = 0.037$, $n = 6$; 100 μg : 57 %, $P = 0.008$, $n = 3$; 200 μg : 42 %, $P = 0.001$, $n = 3$; inverse correlation between reduction in T/B and dose of doxorubicin: $r = -0.54$, $P = 0.021$). This dose-dependent decrease can also be observed *in vitro*. In this model, uptake of [^{18}F]FDG increases and varies between different groups,

presumably reflecting non-specific glucose metabolism of inflammatory cells as confirmed by histology [85].

Also in a subcutaneous lung cancer model (H460) [¹⁸F]FLT uptake is decreased when imaging is performed 2 d after the last dose of doxorubicin (applied three times in 2 d intervals, T/M untreated: 5.5 ± 0.5, doxorubicin: 3.8 ± 0.9, *P* < 0.05, *n* = 4 per group). In this experimental setup, [¹⁸F]FDG uptake is reduced in a comparable manner [86].

PEGylated liposomal doxorubicin (doxisome) administered to HepG2 hepatoma-bearing mice leads to a significant reduction in tumor growth as early as d5 after therapy initiation. [¹⁸F]FLT accumulation on d7 and d14 is reduced upon therapy (T/M: d0: 12.55 ± 0.76, d7: 3.81 ± 0.31, d14: 2.58 ± 0.41, *P* < 0.01), while the control group remains steady (d0: 12.55 ± 0.76, d7: 13.64 ± 0.56, d14: 13.76 ± 0.75, *n* ≥ 5 per group) which is consistent with reduced Ki67 staining on d15 in the treated group (relative staining intensity: control: 0.89 ± 0.04, treated: 0.44 ± 0.05). Earlier time points, i.e. before changes in tumor volume become apparent, were not investigated in this study [87]. Another group used this drug in a head and neck squamous cancer model (UM-SCC-22B cells) and investigated its effects 48 h after application of two doses. Reduction in [¹⁸F]FLT as well as Ki67 are significant (T/M, d0: 3.32 ± 0.24, d2: 2.65 ± 0.13, *P* < 0.05), whereas reduction of [¹⁸F]FLT after the first dose is only marginal (*P* > 0.05, *n* = 6 per group). Also, [¹⁸F]FDG is significantly reduced after two doses. Hence, both tracers appear to be suitable to predict therapy response in this model [88]. In a study using another liposome-encapsulated dosage form of doxorubicin, Lipo-DOX, in C26 colorectal cancers [¹⁸F]FLT is superior to [¹⁸F]FDG for early detection of response, also when analyzing different tumor sizes ([¹⁸F]FLT %ID/g: 10⁵ cells inoculated: d0: 1.62 ± 0.11, d1: 1.23 ± 0.03; 10⁶ cells inoculated: d0: 2.04 ± 0.13, d1: 1.34 ± 0.03, *n* = 5) [89].

Taken together, drugs inhibiting topoisomerase activity and thus tumor growth, induce a reduction of [¹⁸F]FLT uptake which can be determined by PET. In some models, this decrease is already detectable as early as 1 d after drug administration. However, one *in vitro* study challenges this conclusion. In MDA-MB-231 breast cancer cells, doxorubicin induces a decrease of the number of cells in S-phase, as also reported for C6 rat glioma cells [46]. In MDA-MB-231 cells this is accompanied by accumulation of cells in G₂/M-phase as shown by flow cytometry. In these cells, TK1 levels increase by more than a factor of three after 24 h of doxorubicin treatment, which is in accordance to other studies describing an upregulation of TK1 activity in G₂/M-phase [90]. Here, this increase in TK1 activity can be noted for a sustained period of time and it is accompanied by a massive increase in [¹⁸F]FLT uptake (+173 % ± 109 % at 72 h) [47]. These data imply that the effect of intercalating agents on the cell cycle might be complicated and possibly dependent on the cell type investigated. Hence, additional studies are needed to further elucidate the impact of this drug class on [¹⁸F]FLT uptake.

3.3.3 Cisplatin

Platinum complexes bind to DNA and crosslink it, which leads to the induction of cell death. *In vitro* experiments reveal a decrease in [¹⁸F]FLT accumulation in C6 rat glioma cells 24 h after cisplatin administration (decrease to 49 % ± 4 % of control, *P* < 0.0001), but not after 4 h, which is consistent with the number of cells in S-phase fraction (decrease to 63 % ± 5 % after 24 h, *P* < 0.0005) [46]. When

applied *in vitro* in three different doses in esophageal squamous cell carcinoma cells (OSC-1) [¹⁸F]FLT uptake decreases 24 h and 72 h after drug washout [91].

In vivo [¹⁸F]FLT PET appears to also be useful in monitoring response to cisplatin therapy. Leyton et al. used this drug in a murine fibrosarcoma model (RIF-1). After 24 h and 48 h tracer uptake is significantly decreased (normalized uptake value (NUV₆₀), normalized to heart, control: 1.02 ± 0.12 ; 24 h: 0.76 ± 0.08 , $P = 0.03$; 48 h: 0.51 ± 0.08 , $P = 0.03$, $n = 4$ per group) which significantly correlates with the PCNA labeling index (NUV₆₀ versus PCNA: $r = 0.89$, $P = 0.001$). Also TK1 and hexokinase expression are reduced after therapy. Even though [¹⁸F]FDG is reduced as well, [¹⁸F]FLT appears to be superior for early imaging of drug-induced changes *in vivo* in this model as it allows differentiation between cytostatic and cytotoxic response to cisplatin [92].

In another study, ovarian cancer samples isolated from the same patient were characterized as either being sensitive (PEO1) or resistant (PEO4) to platinum-based chemotherapy. 4 d chemotherapy with cisplatin induces a decrease in [¹⁸F]FLT accumulation in sensitive xenografts (NUV₆₀ of vehicle group: 1.2 ± 0.1 , cisplatin group: 1.0 ± 0.0 , $P < 0.05$), whereas tracer uptake in resistant PEO4 is unaltered. The PI3K/AKT pathway is specifically deregulated in clinically acquired platinum-resistant ovarian tumors [93]. And indeed, inhibition of AKT by API-2 makes PEO4 cells sensitive to cisplatin therapy as demonstrated by *in vitro* experiments and *in vivo* [¹⁸F]FLT uptake (NUV₆₀ vehicle group: 1.3 ± 0.0 , cisplatin group: 1.2 ± 0.1 , cisplatin + API-2 group: 1.0 ± 0.1 , $P < 0.0005$, $n = 6$ per group). Reduced [¹⁸F]FLT uptake is in accordance with reduced TK1 and Ki67 expression. In these ovarian cancer models also [¹⁸F]FDG is able to show the differences of the various therapeutic approaches in the two cell lines [94].

In summary, these studies suggest that changes in [¹⁸F]FLT truly reflect changes in tumor growth after platinum therapy.

3.3.4 Microtubule stabilizing agents

Microtubules play a key role for the chromosome separation during mitosis. Targeting these cytoskeletal components is an attractive approach to interfere with the cell cycle of cancer cells. Many microtubule targeting agents such as docetaxel belong to the family of taxanes, originating from the yew tree.

Weekly docetaxel therapy in a prostate cancer model (22Rv1) leads to a significant decrease of [¹⁸F]FLT on d14 (T/M ratios: vehicle-treated group: pre: 5.34 ± 2.16 , post: 3.79 ± 1.28 ; docetaxel-treated group: pre: 8.72 ± 3.67 , post: 2.82 ± 0.53 , $P < 0.05$, $n = 6$ per group). This decrease is accompanied by decreased proliferation activity as assessed by immunohistochemical staining of PCNA (vehicle group: $9.82 \% \pm 3.12 \%$, docetaxel group: $3.49 \% \pm 0.53 \%$, $P < 0.05$). [¹⁸F]FDG is unchanged upon treatment. *In vitro* assays show similar results (% uptake/ 10^5 cells after 24 h: standard medium: 1.24 ± 0.53 ; 10 nM docetaxel: 0.24 ± 0.04 , $P < 0.001$; 100 nM: 0.44 ± 0.14 , $P < 0.05$) [95]. Furthermore, in an orthotopic lung cancer model docetaxel induces a reduction of [¹⁸F]FLT accumulation (change in normalized uptake value relative to right lung: d3: -57.5% , $P = 0.149$; d7: -82.7% , $P < 0.05$; d14: -96.6% , $P < 0.01$, $n = 4$). Differences in tumor volume as determined by CT are not significant before d14 (94.2 % reduction, $P < 0.001$). Ki67 staining is significantly reduced already on d3, and this reduction is even further pronounced on d7 [96].

Also growth of colorectal HCT116 xenografts is effectively inhibited by docetaxel (reaching significance after 5 d). In this model, [¹⁸F]FLT measured on d2, d5 and d7 increases over time, irrespective of treatment (%ID_{mean}/ml: vehicle: baseline: 3.56 ± 1.79, d7: 4.80 ± 1.24; docetaxel: baseline: 3.34 ± 1.18, d2: 3.23 ± 1.15, d7: 5.16 ± 0.85, *P* = 0.005 vs. baseline, *P* = 0.003 vs. d2, *n* = 8 per group). [¹⁸F]FLT results are not in line with reduced Ki67 expression (vehicle: 91 % ± 5 %, docetaxel: 59 % ± 14 %). More detailed data analysis using cluster allocation based on co-registered diffusion weighted MR imaging and histogram analysis also does not lead to a closer agreement between imaging parameters and histological findings. The authors suggest that preferential use of the thymidine *de novo* pathway could explain why [¹⁸F]FLT does not reflect proliferation in this setting. [¹⁸F]FDG PET uptake is unchanged upon docetaxel therapy, suggesting unaltered glucose metabolism which is inconsistent with the reduced GLUT1 or GLUT3 staining in immunohistochemistry [97].

Cao et al. evaluated the effect of an RGD peptide-paclitaxel conjugate in an orthotopic breast cancer model (MDA-MB-435). They specifically targeted the drug to receptors involved in tumor angiogenesis. Anti-tumor effectivity in terms of impact on growth is higher than the combination of untargeted paclitaxel with RGD. Histology on d10 reveals increased cell death and reduced microvessel density, which is accompanied by decreased [¹⁸F]FDG accumulation as assessed by PET. In this experimental setup, [¹⁸F]FLT correctly identifies the missing impact of the drug on tumor proliferation as indicated by unaltered Ki67 staining (*n* = 3 per group) [98]. Also in *in vitro* experiments in breast cancer cells (MDA-MB-231) paclitaxel does not cause a decrease of [¹⁸F]FLT uptake. Direcks et al. report that half maximal inhibitory concentrations of paclitaxel induce a G₂/M accumulation, whereas [¹⁸F]FLT uptake even increases (+66 % ± 18 % at 72 h) [47].

A significant decrease of 22 % (*P* = 0.002) in [¹⁸F]FLT uptake already after 24 h can be observed in RIF-1 murine sarcoma bearing mice treated with patupilone, a potent microtubule stabilizer. Ki67 expression is decreased by 14 % and significantly correlates with [¹⁸F]FLT uptake (*R* = 0.65, *P* = 0.02). Further experiments reveal that a significant reduction of [¹⁸F]FLT on d2, d3, and d6 upon patupilone therapy is paralleled by a reduction in Ki67 labeling (*n* = 5 per group per time point) [99].

In vitro analysis of SW620 colon and KB-V1 cervical tumor cells treated with JAC106, a colchicine-like anti-tubulin agent, shows a mitotic arrest starting at 18 h (increased fraction of cells in G₂/M-phase as assessed by flow cytometry). At the same time point a dose-dependent increase of [¹⁸F]FLT uptake can be noted (%/10⁵ cells: e.g. SW620: controls: 4.25 ± 0.64, 10 nM JAC106: 9.50 ± 2.59, *P* < 0.05; KB-V1: controls: 8.44 ± 1.14, 10 nM JAC106: 17.90 ± 5.97, *P* < 0.05) as well as an increase in TK1 activity (*P* < 0.05 with 100 nM JAC106). 3 d after *in vivo* treatment with 30 mg/kg JAC106 uptake of [¹⁸F]FLT is decreased (SUV relative to baseline: SW620: 77.9 % ± 22.4 %, *P* = 0.059, *n* = 5; KB-V1: 43.2 % ± 14.0 %, *P* < 0.01, *n* = 6), which is in line with reduced Ki67 staining (vehicle vs. JAC106: SW620: 80.04 % ± 1.92 % vs. 28.11 % ± 6.25 %, *P* < 0.001; KB-V1: 88.82 % ± 1.83 % vs. 12.87 % ± 13.82 %, *P* < 0.001) and TK1 activity (SW620: *P* < 0.05; KB-V1: *P* < 0.001). The fraction of cells in G₀/G₁ is increased. Hence, there appears to be a discrepancy between the *in vitro* and *in vivo* results, which might be explained by the time point. Directly after administration of anti-tubulin agents a mitotic arrest might occur (accumulation of cells in G₂/M-phase) which is accompanied by an increase in TK1 activity resulting in an increase in [¹⁸F]FLT. At later time points the fraction of cells in G₀/G₁ increases and a reduced amount of [¹⁸F]FLT is taken up by the cells [100]. It would be interesting to

study the temporal relationship by measuring the *in vivo* uptake of [¹⁸F]FLT at earlier time points than 3 d. Also in the other previously mentioned studies tracer uptake was mostly investigated at late time points.

In another study, vincristine, a tubulin binding protein, was applied over two consecutive days to mice bearing intraperitoneal Rh30 rhabdomyosarcoma. [¹⁸F]FLT uptake is decreased 2 weeks after therapy (%ID/ml: baseline: 3.64 ± 0.9, 2 weeks: 1.32 ± 0.52, *P* = 0.002). Even though still significantly reduced (*P* = 0.045), [¹⁸F]FLT uptake after 4 weeks suggests recovery of the proliferation (%ID/ml: 1.91 ± 0.81). Tumor volumes are reduced only after 4 weeks (MR measurements in *n* = 4 animals) and also Ki67 is reduced (one representative example shown). In this study [¹⁸F]FDG is unchanged [101].

3.3.5 Purine and pyrimidine analogs

Purines and pyrimidines are the building blocks of DNA. Hence, they are essential for proliferating cells, which makes their synthesis and metabolism pathways attractive targets for anti-cancer therapies (see also **Supplementary Fig. S1**). Development of these therapies has mainly focused on nucleoside analogs such as fluorouracil (5-FU) and related pro-drugs, and folate antagonists (see 3.3.6).

The main action of the pyrimidine analog 5-FU is via the inhibition of thymidylate synthase (TS). It is mediated by its metabolite 5-fluoro-dUMP (dFdUMP), which builds a complex with the enzyme and 5,10-methylene-tetrahydrofolate. Its metabolites can also be incorporated into DNA (via 5-fluoro-2'-deoxyuridine 5'-triphosphate, FdUTP) or RNA (via 5-fluorouridine 5'-triphosphate, FUTP) leading to other cytotoxic events including DNA strand breakage and decrease in protein synthesis [102]. As described above the balance of the two different thymidine pathways is of importance for [¹⁸F]FLT accumulation (see 3.2.4 and **Fig. 1**). It is therefore probable that blockade of the *de novo* thymidine synthesis pathway enhances salvage pathway utilization and expression of nucleoside transporters promoting enhanced cellular uptake of exogenous thymidine and its analogs like [¹⁸F]FLT. This hypothesis is supported by the following studies.

Van Waarde et al. show that in C6 rat glioma cells in culture [¹⁸F]FLT uptake significantly correlates with the number of cells in S-phase after 5-FU administration (*r* = 0.99, *P* < 0.0001). [¹⁸F]FLT accumulation is increased at early time points before a decrease can be noticed after 24 h [46]. Dittmann et al. examine the effect of short time exposure to 5-FU on [¹⁸F]FLT uptake in esophageal squamous cell carcinoma (OSC-1) *in vitro*. After 4 h treatment and 24 h recovery cells are arrested in S-phase and [¹⁸F]FLT uptake (normalized to cell number) is increased in a dose dependent manner. This effect is still apparent after 72 h [91]. On the other hand Direcks et al. observe a decrease of [¹⁸F]FLT uptake in MDA-MB-231 breast cancer cells after 72 h of 5-FU treatment (-54 % ± 32 %), whereas tracer uptake is unchanged at earlier time points. This is inconsistent with the increased TK1 protein levels and the mildly increased TK1 activities measured. Conversely, the cells accumulate in G₁-phase, where TK1 activity should be low [47]. This is not in accordance with the observations of Dittmann et al. (S-phase accumulation) [91] or Mirjolet et al. (G₁/S-phase accumulation) [103]. These inconsistent results may indicate that the effect of 5-FU on [¹⁸F]FLT uptake is depending on the cell line.

Lee et al. have analyzed a variety of tumor cell lines (epidermoid A431, colon HT29, HCT116 and HCT8, mammary MDA-MB-231 and MCF7, lung Calu6 and A549, and cervical HeLa) and show that 5-FU increases [¹⁸F]FLT uptake *in vitro*. In most cell lines this effect is dose-dependent ($P < 0.05$; average [¹⁸F]FLT uptake increase after 24 h in A431, HT29, HeLa, MDA-MB-231, and Calu6 cells at 10 μ M: 2.46-fold and at 100 μ M: 3.54 ± 0.60 -fold). A time-dependency was shown in a subset of cell lines (A431, HT29, HCT8). 5-FU induces TK1 expression in most cell lines (except HCT8). However, no analysis of the cell cycle has been performed [104]. With regards to the effect of 5-FU on MDA-MB-231 breast cancer cells *in vitro* there appears to be a discrepancy. Lee et al. show that this drug induces an increase of [¹⁸F]FLT already after incubation for 24 h with a starting dose as low as 2 μ M, whereas Direcks et al [47] could not observe any changes with 5 μ M after 24 h and even a decrease after 72 h. Dissimilarities of various cell clones or culture conditions in different labs may explain these differences.

Also Plotnik et al. attribute enhanced [¹⁸F]FLT uptake to increased TK1 activity 1 h after 5-FU of A549 lung tumor cells [105]. Other experiments performed by Lee et al. show that silencing of TK1 results in abolition of [¹⁸F]FLT uptake increase *in vitro* (cells transduced with lentivirus encoding TK1 scrambled shRNA vs. specific shRNA in A431: 2.33-fold vs. 0.50-fold; and in HT29: 2.64-fold vs. 1.46-fold, $n = 4$). The authors hypothesize that the inhibition of TS by 5-FU not only leads to an upregulation of TK1, but also that 5-FU activates checkpoint kinase 1 leading to subsequent transcriptional activation of TK1 [104].

Along this line, *in vivo* experiments reveal an increase of [¹⁸F]FLT and TK1 activity 24 h after 5-FU administration in colorectal HT29 tumors (SUV_{mean} baseline vs. 24 h: saline-treated group: 0.93 ± 0.12 vs. 0.87 ± 0.12 , 5-FU-treated group: 0.88 ± 0.13 vs. 2.26 ± 0.42 , $P < 0.05$, $n = 8$ per group; relative change of TK1 activity: saline-treated group: 1.00 ± 0.15 , 5-FU-treated group: 1.49 ± 0.11 , $P < 0.05$) [104]. A different study, also employing an HT29 tumor model, reports a dose-dependent significant increase of [¹⁸F]FLT 24 h after 5-FU treatment (saline: $n = 7$, 16.7 mg/kg 5-FU: $n = 6$, 50 mg/kg 5-FU: $n = 6$). Static as well as dynamic PET imaging parameters were calculated - however, exact numbers are not provided. Furthermore, a significant correlation of SUV_{mean} with TK1 activity is apparent ($\rho = 0.890$, $P < 0.001$) [106].

Barthel et al. [45] employed gamma counter measurements of excised RIF-1 murine fibrosarcoma xenografts to show that [¹⁸F]FLT uptake is decreased significantly 24 h and 48 h after 5-FU administration (decrease by $52.2 \% \pm 7.6 \%$ and $72.9 \% \pm 9.9 \%$, respectively, $P < 0.001$, $n = 8-12$ mice per group). This decrease is more pronounced than that of [¹⁸F]FDG and correlates with PCNA labeling index ($r = 0.71$, $P = 0.031$) as well as tumor volume changes ($r = 0.585$, $P = 0.001$). Interestingly, TK1 expression is not in line with [¹⁸F]FLT uptake ($-12.8 \% \pm 0.8 \%$ after 24 h, $+41.3 \% \pm 2.6 \%$ after 48 h). However, it is likely that the enzymatic activity of TK1 is related to tracer uptake, since concentrations of the cofactor ATP decrease in parallel with [¹⁸F]FLT (μ g/mg ATP: pretreatment: 32.8 ± 1.0 , 24 h: 27.0 ± 1.0 , and 48 h: 21.5 ± 0.6). *In vivo* PET imaging data 48 h after treatment are in agreement with *ex vivo* results (fractional retention of [¹⁸F]FLT: control: 1.09 ± 0.01 , 5-FU: 0.80 ± 0.06 , $P = 0.026$, $n = 3$ per group) [45]. In the same model the group also demonstrates elevated [¹⁸F]FLT in tumors one to two hours after 5-FU administration (NUV₆₀: vehicle: 1.08 ± 0.03 ($n = 8$) vs. 5-FU: 1.93 ± 0.11 ($n = 5$), $P = 0.0016$), but unchanged TK1 levels. They attribute the increased [¹⁸F]FLT to an increase in type-1 ENT binding sites per cell, as determined by whole-cell assays (number of type-1 ENT-binding sites per

cell in untreated cells: 49,110 vs. cells treated with 10 g/ml 5-FU for 2 h: 73,142, $P = 0.03$) [56]. Hence, this study provides an alternative mechanism for the [^{18}F]FLT flare effect.

2'-deoxy-5-fluorouridine (FdUrd) is a metabolite of 5-FU, which has also been reported to block endogenous thymidine synthesis. Application of non-toxic concentrations of this drug significantly increases [^{18}F]FLT uptake (3.2- to 7.8-fold compared with controls, $P < 0.05$) in a range of xenografts already after a few hours (Ramos Burkitt lymphomas: 5.5-fold after 1 h, 4.4-fold after 3 h; MDA-MB-231 breast adenocarcinomas: 4.7-fold after 2 h; SKBR3 breast cancer: 3.2-fold after 2 h; LS 174T colon adenocarcinomas: 4.3-fold after 2 h; and WiDr colon adenocarcinomas: 5.8-fold after 2 h; $n = 23$ mice in total, measured by gamma counter) [107].

In summary, these data demonstrate that [^{18}F]FLT imaging results after 5-FU treatment critically depend on the imaging time point which appears to vary between cell lines. It should be noted that the effect of 5-FU treatment on [^{18}F]FLT uptake was studied employing two very distinct treatment schedules *in vitro* (continuous drug exposure [46,47,104] and short drug exposure followed by recovery [56,91]). This challenges the direct comparison of some of the studies. However, most studies show that a transient increase due to TS inhibition at early time points (within hours or days) is followed by a later reduction of tracer uptake due to decreased proliferation. Furthermore, some studies indicate that there is a difference with regards to the underlying mechanism between early and very early effects of the TS inhibition [56]. Therefore, [^{18}F]FLT PET imaging of treatment response should be performed with caution at early time points.

Gemcitabine (2',2'-difluorodeoxycytidine) is another antimetabolite which exerts its cytotoxic activity by being incorporated into DNA and thereby inhibiting DNA polymerase [108]. Furthermore, it has been supposed to exert part of its action through TS inhibition [109,110]. When applied *in vitro* in esophageal squamous cell carcinoma (OSC-1) a medium gemcitabine dose induces an increased uptake of [^{18}F]FLT after 4 h of drug treatment followed by 24 h recovery [91] while at 72 h of recovery time the highest dose causes enhanced [^{18}F]FLT uptake. Hence, gemcitabine appears also to cause a flare effect similar to that observed for 5-FU, which might confound tumor response assessment results.

Paproski et al. show that gemcitabine and [^{18}F]FLT share the same nucleoside transporter (hENT1). In five of the six pancreatic cancer cell lines used in the study (Capan-2, AsPC-1, BxPC-3, PL45, MIA PaCa-2, and PANC-1) a correlation can be observed between gemcitabine toxicity and [^{18}F]FLT uptake. Therefore, use of [^{18}F]FLT-PET is suggested for prediction of gemcitabine transport capacity and sensitivity in pancreatic patients [111].

GS-9219 is a pro-drug of PMEG (9-(2-phosphonylmethoxyethyl)guanine), a purine analog. It exerts a cytotoxic effect in proliferating cells due to inhibition of nuclear DNA polymerases, resulting in inhibition of DNA synthesis or repair [112]. Measured late after GS-9219 treatment, [^{18}F]FLT decreases significantly in non-Hodgkin lymphomas in dogs responding to this treatment (mean maximum body mass SUV pre-treatment: 9.8 (2.6-22.3); d5 (± 1 d): 3.5 (1.1-7.9), $P = 0.016$; 3 weeks following completion of five cycles: 2.4 (1.5-3.4), $P < 0.031$, $n = 7$ dogs responding to treatment). Analysis of three lymph node samples revealed that Ki67 labeling index changes correspond to decreased [^{18}F]FLT uptake. Furthermore, increased uptake in two dogs precedes relapse of disease [113,114]. Thus, change in

[¹⁸F]FLT accumulation is a putative biomarker for imaging the response of non-Hodgkin lymphomas in dogs treated with GS-9219.

3.3.6 Antifolates

Several antifolate drugs have been developed which inhibit the pivotal enzymes involved in thymidylate synthesis, TS and/or dihydrofolate reductase, including methotrexate, pemetrexed, BGC 9331 and the more tumor-specific BGC 945.

Pemetrexed inhibits several enzymes involved in purine and pyrimidine synthesis, including TS. This inhibition of the *de novo* thymidine synthesis pathway probably causes the cells to compensate for the thymidine shortage by increasing uptake of thymidine and respective analogs (see also 3.2.4). Saito et al. used fluorescently labelled MSTO211H mesothelioma cells (DsRed or TurboRFP) to perform fluorescence and radioactive imaging to visualize cell and tumor growth in response to pemetrexed treatment *in vitro* and *in vivo*. Growth of these tumors is significantly impaired on d10 of pemetrexed therapy. *In vitro* [³H]FLT uptake peaks after 12 h to an 8- to 10-fold increase. *In vivo*, increased uptake of [³H]FLT can be observed in a time-dependent manner as determined by liquid scintillation counting (%ID/g: DsRed: 0 h: 1.97 ± 0.39, 1 h: 6.43 ± 3.33*, 12 h: 4.00 ± 0.91*, 24 h: 5.36 ± 1.47*, 48 h: 2.23 ± 0.17; TurboRFP: 0 h: 2.09 ± 0.55, 1 h: 4.69 ± 1.59*, 12h: 2.38 ± 0.94, 24 h: 5.57 ± 1.77*, 48 h: 1.85 ± 0.19; * *P* < 0.01 vs. control, *n* = 3-5 per group) [115].

Methotrexate is another folate antimetabolite. Its antifolate activity is mainly due to dihydrofolate reductase inhibition. When applied *in vitro* in human esophageal squamous carcinoma cells (OSC-1) in culture it induces an increase of [¹⁸F]FLT uptake after 4 h of drug exposure and 24 h recovery time which is more profound at higher doses. Enhanced uptake is still notable after 72 h recovery with the highest dose employed [91].

To conclude 3.3.5 and 3.3.6, the studies employing agents inhibiting TS indicate that it is essential to know the exact mechanism of a therapeutic drug and its interference with the thymidine metabolism pathways to understand [¹⁸F]FLT imaging results. With this respect, antimetabolites are similar to purine and pyrimidine analogs: these drugs interfere with the balance between the thymidine *de novo* and salvage pathway resulting in subsequently increased [¹⁸F]FLT uptake in the first days after treatment start. Therefore, early assessment of anti-proliferative response to therapy by [¹⁸F]FLT PET remains challenging. Nevertheless when imaging is performed at later time points [¹⁸F]FLT PET shows promise as response marker, as described by Barthel et al. [45]. Interestingly, the early increase in tracer uptake after 5-FU administration prompted studies to investigate whether this effect could be exploited to improve PET imaging sensitivity using nontoxic doses of the 5-FU metabolite FdUrd [107].

It will be interesting to see how these findings can be translated to the clinical situation. There are a few studies investigating [¹⁸F]FLT uptake after chemotherapy with TS targeting antimetabolites or gemcitabine. The combination of 5-FU, epirubicin and cyclophosphamide leads to reduction in [¹⁸F]FLT uptake after 1 week in responsive breast cancer patients [116]. Challapalli et al. studied [¹⁸F]FLT uptake in pancreatic cancer patients receiving gemcitabine treatment. They did not investigate the relationship between baseline uptake and response but found that 3 weeks after the first cycle of chemotherapy an increase in SUV_{60max} predicts progressive disease [117]. Employing the 5-FU prodrug capecitabine,

however, Kenny et al. noted an [^{18}F]FLT flare effect. The drug induces an increase in [^{18}F]FLT retention variables in breast cancer patients 1 h after drug administration [118]. Interestingly, Hong et al. found that a large [^{18}F]FLT flare is associated with poor treatment response in patients with colorectal cancer. The authors hypothesize, that these tumors can compensate for TS inhibition by upregulation of the thymidine salvage pathway which is accompanied by increased [^{18}F]FLT uptake [119]. However, a pilot study in non-small cell lung cancer patients shows that changes in [^{18}F]FLT accumulation are variable 4 h after pemetrexed therapy and are not associated with tumor response, time to progression or overall survival [120]. Hence, further studies are needed to investigate the role of the [^{18}F]FLT flare effect and its usefulness in prediction of treatment outcomes.

3.3.7 Other chemotherapeutic drugs

Munk et al. employed the experimental chemotherapeutic agent TP202377 in a sensitive A2780 ovary cancer cell line as well as its resistant clone A2780/Top216 and the naturally resistant colon cancer cell line SW620. The exact mechanism of action of TP202377 is unknown. However, the anti-cancer effect is somehow linked to the mTOR pathway (see also 3.4.6) and it might be related to depletion of intracellular amino acids. It was shown that TP202377 inhibits protein and DNA synthesis and induces apoptosis. It demonstrates potent anti-cancer activity in several tumor cell lines and mouse models of human cancer. Growth inhibition of the sensitive model can be detected 6 d after intravenous administration of a single dose of the agent. Already after 6 h [^{18}F]FLT uptake is significantly reduced. Uptake is still reduced on d1, but not on d6, probably reflecting re-proliferation of the tumors (SUV_{mean} of sensitive A2780 at baseline: 1.51 ± 0.07 , 6 h: 0.78 ± 0.03 (-46 % \pm 3 %, $P < 0.001$), d1: 0.79 ± 0.04 (-46 % \pm 3 %, $P < 0.001$), d6: 1.67 ± 0.12 , $n = 8-16$ tumors per group). Ki67 expression parallels [^{18}F]FLT uptake (compared to baseline: 6 h: -40 % \pm 2 %, $P < 0.001$, d1: -65 % \pm 3 %, $P < 0.001$). [^{18}F]FLT uptake is unchanged in the resistant tumor models, indicating that [^{18}F]FLT PET can distinguish between resistant and responsive tumors [121].

Ursolic acid is a pentacyclic triterpene compound, a natural product found in medicinal herbs. Ursolic acid exerts anti-tumor effects by inhibiting the activities of DNA polymerase and DNA topoisomerase. In subcutaneously growing H22 hepatocellular carcinoma xenografts ursolic acid treatment reduces the proliferation of tumor cells as analyzed by flow cytometry, as well as [^{18}F]FLT uptake as determined by visual examination of PET images (no quantification of tracer uptake was performed) [122].

The nicotinamide phosphoribosyltransferase inhibitor APO866 inhibits biosynthesis of cellular nicotinamide adenine dinucleotide, which leads to ATP depletion and apoptosis. Cancer cells have a high nicotinamide adenine dinucleotide turnover compared with normal cells. Since ATP is a cofactor for TK1, APO866 is likely to influence [^{18}F]FLT uptake. And indeed, after treatment [^{18}F]FLT is significantly reduced in A2780 ovary cancer xenografts in mice (SUV_{mean} baseline: 1.28 ± 0.03 , 24 h: $0.98 \pm 0.03^*$, 48 h: $0.90 \pm 0.03^*$, d7: $0.96 \pm 0.07^*$, $*P < 0.001$, $n = 10$). [^{18}F]FLT uptake significantly correlates with Ki67 staining ($r^2 = 0.75$, $P < 0.001$). [^{18}F]FDG is not altered before d7 of therapy. At this time point a significant difference in tumor growth can already be observed [123].

Mitotane is an agent exerting a cytotoxic effect on adrenocortical cancers. The exact mechanism of action is not known. *In vitro* incubation of H295R adrenocortical cancer cells with mitotane leads to a reduction in [¹⁸F]FLT uptake (% of control: control: 100 ± 7; 5 μM: 90 ± 3; 15 μM: 51 ± 4, *P* < 0.001), which is in line with reduced cell growth [124].

3.4 Imaging of response to targeted therapies

Since conventional chemotherapeutic agents exert their cytotoxic effects on all proliferating tissues, side effects can be severe. Therefore, efforts have been made to develop better-targeted therapies. There is a range of cellular pathways that are specifically deregulated in cancer cells leading to a neoplastic phenotype characterized by the “hallmarks of cancer” [125]. Among these are (i) sustaining proliferative signaling, (ii) evading growth suppressors, (iii) resisting cell death, (iv) enabling replicative immortality, (v) inducing angiogenesis, and (vi) activating invasion and metastasis. Many therapies targeting the pathways involved in the regulation of the cancerous phenotype are based on monoclonal antibodies (name ending with -mab). Also small molecule inhibitors are frequently employed (name ending with -nib). In the following we will describe preclinical studies using [¹⁸F]FLT for the visualization of tumor response to molecular-targeted therapies.

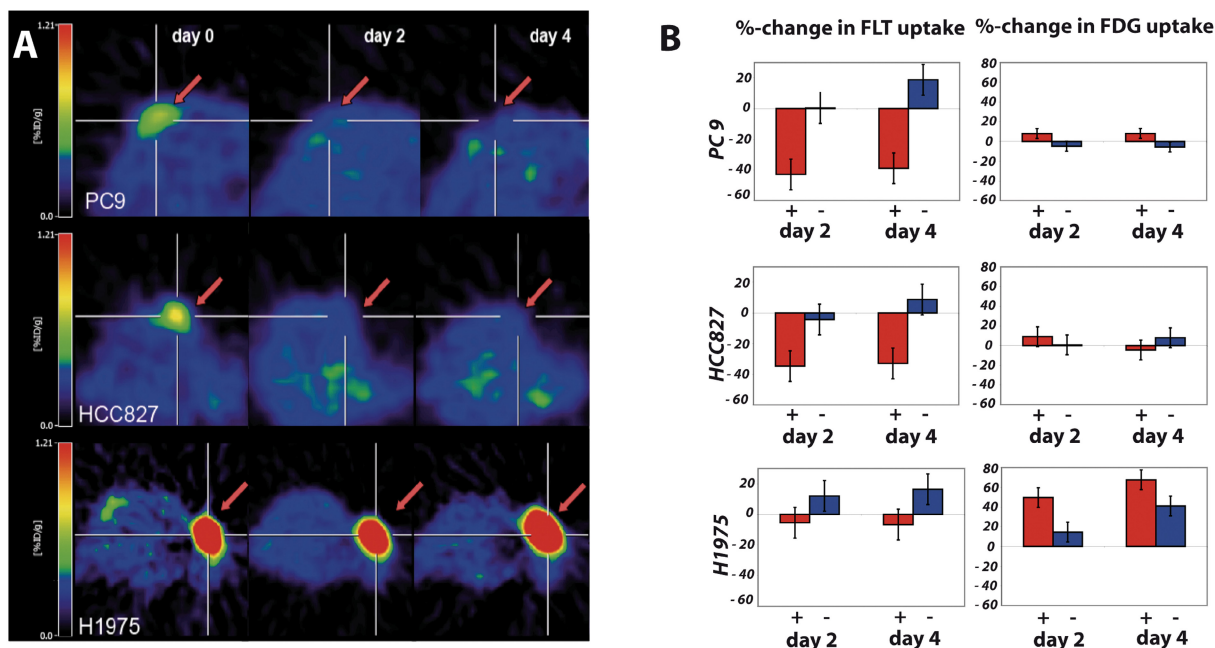
3.4.1 ErbB inhibitors

ErbB proteins are a group of receptor tyrosine kinases. The epidermal growth factor receptor (EGFR), also known as ErbB1 or Her1, is involved in many cellular processes such as signal transduction, proliferation, angiogenesis, metastasis, and evasion of apoptosis (**Supplementary Fig. S1**). Cetuximab is a chimeric monoclonal antibody targeting EGFR. When administered in a single dose (1 mg/mouse) in H1975 lung carcinoma xenograft-bearing mice, tumor [¹⁸F]FLT uptake is significantly reduced on d3 compared to control treatment (*ex vivo* uptake in %ID/g x kg as determined by gamma counter measurements: control: 0.098 ± 0.005, *n* = 5, cetuximab: 0.029 ± 0.010, *n* = 4, *P* < 0.001; *in vivo* uptake in SUV_{max} as determined by PET: before treatment: 0.41 ± 0.17, 3 d after cetuximab: 0.24 ± 0.15, *P* < 0.01, *n* = 4), consistent with altered expression of Ki67 (control: 12.8 % ± 4.0 %, cetuximab: 5.0 % ± 1.5 %, *P* = 0.01). Hence, [¹⁸F]FLT is able to visualize treatment response before tumor volume (determined by caliper) is notably changed on d8 [126]. In contrast, [¹⁸F]FLT uptake is not affected by cetuximab treatment in a sensitive (DiFi, *P* = 0.425) and in an insensitive (HCT116, *P* = 0.110) colorectal cancer model. This is in line with unaltered Ki67 staining, and hence unchanged [¹⁸F]FLT retention represents a true negative finding. However, in the sensitive model, treatment effects can be demonstrated by optical imaging of EGF uptake and annexin V accumulation [127]. Hence, proliferation is not a suitable target for pharmacodynamic monitoring of some anti-cancer therapies. Combination of different imaging approaches, delivering multiple pharmacologically relevant physiological readouts, might provide complementary information on treatment effects and/or response.

In a different study this group applied the same therapeutic regimen in the same tumor model, yielding a significantly reduced [¹⁸F]FLT uptake (*P* = 0.0012), which is in line with reduced TK1 levels (experimental details: 3 doses of 40 mg/kg cetuximab in 3 d intervals, imaging performed on d 7, DiFi xenografts in athymic nude mice from Harlan laboratories). [¹⁸F]FLT is unchanged with a lower dose of

20 mg/kg. Here, Ki67 is reduced at both doses. Hence, [¹⁸F]FLT appears to be decoupled from proliferation determined pathologically, reflecting only changes in TK1 levels. The authors hypothesize that this apparent disconnection reflects early activation of pro-survival pathways in the tumor and [¹⁸F]FLT PET might be used for predicting resistance to targeted therapies. The effect of the applied doses of cetuximab on tumor growth was not stated [128]. Thus, results of the two studies reported by this group appear to be inconsistent, even though the authors state that the two studies are in agreement. A few differences in [¹⁸F]FLT PET imaging protocols between these two studies are apparent (image acquisition 60 min - 80 min [127] vs. 40 min - 60 min [128] and quantification of tracer uptake as T_{mean}/M vs. %ID/g), which might affect results. Standardization of protocols is important for comparative studies. Consequently, due to the contradictory results, the two above mentioned publications should be treated with caution and generalization of the findings to other cancer models might be misleading.

Erlotinib is a small molecule inhibitor of EGFR. HCC827 NSCLC xenografts are sensitive towards erlotinib and [¹⁸F]FLT is significantly reduced after therapy (SUV_{max} d0 vs. d3: 50 mg/kg erlotinib: 1.48 ± 0.07 vs. 1.03 ± 0.03 , $P < 0.05$, 100 mg/kg erlotinib: 1.37 ± 0.27 vs. 0.83 ± 0.17 , $P < 0.05$, effect still visible after 6 d and 9 d, at least $n \geq 4$). Conversely, no significant changes of [¹⁸F]FLT uptake can be noted in the erlotinib insensitive model H1993. Changes in [¹⁸F]FLT are in agreement with changes in Ki67 immunohistochemistry. The latter is significantly reduced in HCC827 cells after low- ($P < 0.01$) and high-dose ($P < 0.01$) treatment with erlotinib and unchanged in H1993 xenografts [129]. A study of Ullrich et al. demonstrates similar results. They show that in two sensitive lung cancer models erlotinib induces a decrease in [¹⁸F]FLT uptake after 2 d and 4 d of treatment (change in [¹⁸F]FLT uptake on d2: HCC827: -34.6 %, $n = 7$, PC9: -43 %, $P = 0.04$, $n = 8$). They demonstrate specificity through unchanged [¹⁸F]FLT in an erlotinib resistant model (H1975: -5.4 % $P = 0.12$, $n = 8$). [¹⁸F]FLT uptake correlates with Ki67 labeling ($r = 0.87$, $P < 0.001$). Interestingly, [¹⁸F]FDG uptake is unaffected in both models in this study (**Supplementary Fig. S4**) [130]. Zennetti et al. demonstrate that drug dose-dependent differences in erlotinib sensitivity of various NSCLC xenografts can be imaged by [¹⁸F]FLT PET on d3. In addition, changes in [¹⁸F]FLT uptake are paralleled by respective changes in Ki67 staining (changes of T_{max}/B : sensitive HCC827: 50 mg/kg: -28 % \pm 4 %, 150 mg/kg: -45 % \pm 3 % $P < 0.01$, Ki67 reduced, $P < 0.01$; resistant H1975 (T790M mutation): 50 mg/kg: +33 % \pm 10 %, 150 mg/kg: +27 % \pm 15 %, Ki67 unchanged; resistant H1650: 50 mg/kg: -23 % \pm 16 %, 150 mg/kg: -49 % \pm 5%, $P < 0.01$, Ki67 reduced, $P < 0.05$, the authors state that resistance is mainly due to an impaired apoptotic program rather than a lack of growth arrest, $n \geq 4$ per group) [131].



Supplementary Fig. S4: [¹⁸F]FLT can visualize differences between erlotinib responsive and resistant tumors. Subcutaneous NSCLC xenografts were treated by daily injections of erlotinib or vehicle. (A) Representative [¹⁸F]FLT PET images of mice bearing either sensitive PC9, or HCC827 or resistant H1975 NSCLC subcutaneous xenografts. Images were acquired at baseline, and 2 d or 4 d after therapy initiation. (B) Relative changes (%ID_{max}/g corrected for mediastinum uptake relative to baseline) of [¹⁸F]FLT or [¹⁸F]FDG uptake. Red: erlotinib, blue: vehicle. Taken from [130].

Another study applied erlotinib in A431 and cetuximab in SCC1 squamous cell carcinoma xenograft models. Both treatments impair growth of the tumors. [¹⁸F]FLT is significantly reduced on d3 of erlotinib (median Δ SUV: placebo: +1 %, $n = 5$, erlotinib: -20 %, $n = 5$, $P = 0.005$), and d6 of cetuximab (placebo: -16 %, $n = 3$, cetuximab: -62 %, $n = 4$, $P = 0.05$). In both cases, suppression of [¹⁸F]FLT uptake is paralleled by reduced tumor TK1 kinase activity (counts per minute/ μ g: A431: placebo: 420 ± 18 , erlotinib: 83 ± 44 , $P = 0.002$; SCC1: placebo: 162 ± 22 , cetuximab: 30 ± 4 , $P < 0.001$) [34]. Trastuzumab is a monoclonal antibody targeting HER2, another member of the ErbB family of tyrosine kinases. It was applied in two different mouse models of HER2-overexpressing breast cancer: murine MMTV/HER2 and human BT474. MMTV/HER2 xenografts are only partly responding (16 out of 30 tumors regressed in growth) and [¹⁸F]FLT uptake is only modest and rather unchanged upon trastuzumab. The authors hypothesize that a preferential use of the thymidine *de novo* pathway can explain low uptake of [¹⁸F]FLT in these tumor cells. Therefore, this tumor model was not considered for further studies. Subsequent experiments reveal that [¹⁸F]FDG is not affected upon trastuzumab treatment in BT474 tumors (responsive in terms of change in tumor volume). However, [¹⁸F]FLT is reduced after 1 week treatment ($P = 0.0154$), which is accompanied by reduced Ki67 staining ($P < 0.001$). Therefore, in this model [¹⁸F]FLT can monitor treatment response to trastuzumab [77].

In conclusion, the majority of the above mentioned studies report that [¹⁸F]FLT uptake is reduced in sensitive xenografts after ErbB-targeting therapies, presumably reflecting decreased proliferation. Results of a pilot study in patients with KRAS wildtype rectal cancers treated with cetuximab confirm that changes in [¹⁸F]FLT uptake has the potential to be a good imaging biomarker to monitor treatment

response [132]. However, one should keep in mind, that ErbB-targeting therapies also affect vascularization and hence delivery of the tracer, as already discussed in 3.2.8. Therefore, the choice of imaging time point after tracer injection plays an important role.

3.4.2 VEGF signaling inhibitors

Bevacizumab (avastin[®]) is a recombinant monoclonal antibody that inhibits vascular endothelial growth factor 1 (VEGF-1) (**Supplementary Fig. S1**) and hence blocks angiogenesis. Viel et al. used intracranial glioblastoma spheroids in rats to study the effect of bevacizumab (weekly administration of the drugs started after 3 wk, post-treatment imaging performed after 6 wk). By additional MRI parameters they demonstrate the effect of this drug on the tumor microvasculature (vessel size and density, blood volume). Proliferation of the tumors is also affected as shown by decreased [¹⁸F]FLT accumulation ([¹⁸F]FLT T/B ratio: vehicle control: 5.96 ± 0.87 , treated: 4.61 ± 0.36 , $P < 0.05$, $n = 4$ per group) and Ki67 labeling index (vehicle control: 0.53 ± 0.09 , treated: 0.39 ± 0.08 , $P < 0.01$; correlation of [¹⁸F]FLT T/B ratio and Ki67: $r = 0.95$, $P = 0.004$) [68].

After treatment with bevacizumab on d0 and d2 H460 large cell lung cancer xenografts take up less [¹⁸F]FLT (quantitative data provided in correlation graphs only, $n = 3$ per group). This study also shows that the emitted Cerenkov light significantly correlates with tracer signals obtained by PET [133].

The VEGFR-2 tyrosine kinase inhibitor ZD4190 effectively delays growth of an orthotopic mammary carcinoma (treatment on d0, d1 and d2). [¹⁸F]FLT uptake is significantly reduced early after treatment (d1: $-8.1 \% \pm 2.9 \%$, $P < 0.05$; d3: $-21.0 \% \pm 8.5 \%$, $P < 0.01$, $n = 8$ per group) which is accompanied by reduced Ki67 staining (d1: $-45 \% \pm 6 \%$, $P < 0.01$; d3: $-30 \% \pm 3 \%$, $P < 0.01$). The proliferative activity of the tumors recovers on d7 as demonstrated by [¹⁸F]FLT PET and Ki67 immunohistochemistry. In this experimental setup [¹⁸F]FDG fails to monitor treatment response consistent with unaltered GLUT-1 staining [134].

In summary, inhibition of VEGF signaling results in significant reduction of [¹⁸F]FLT accumulation in sensitive tumor models. However, it cannot be ruled out that tracer delivery is affected by VEGF targeting drugs (see 3.2.8). Therefore, dynamic studies with kinetic modelling might be employed to address this question.

3.4.3 FGFR inhibitors

The basic-fibroblast growth factor (FGF-2) is a mitogen (**Supplementary Fig. S1**) and acts as survival factor in many experimental models. PD173074 has high affinity and selectivity for FGF receptors (FGFRs) and was shown to effectively inhibit FGF-driven neoangiogenesis *in vivo* [135]. In a study performed by Pardo et al. PD173074 inhibits tumor growth in two different small cell lung cancer xenograft models. The group performed [¹⁸F]FLT PET imaging in one of these models (H69) and observed a reduction in tracer uptake after 1 week and 2 weeks. However, quantitative numbers or information on statistical significance are not provided, so that it is hard to evaluate the authors' conclusion that [¹⁸F]FLT could provide early *in vivo* evidence of response to PD173074 in the clinical situation [136].

3.4.4 c-MET / HGF inhibitors

Overactivation of c-MET, the receptor for hepatocyte growth factor (HGF), results in increased growth and formation of new blood vessels. Mitra et al. analyzed the efficacy of the anti-HGF antibody ficlatuzumab in an orthotopic luciferase-expressing U87 glioma model in the mouse. Since [¹⁸F]FLT shows a better tumor-to-background ratio than [¹⁸F]FDG it was selected for imaging of treatment efficacy. Both [¹⁸F]FLT and bioluminescence are reduced at various time points after ficlatuzumab treatment and are predictive for therapy response determined by MRI volume measurements (ID_{max}/g ratio (lesion / background brain), imaging always performed 2 d after drug administration which was performed in 3 d intervals; control: baseline: 1.14 ± 0.2, d5: n.d., d8: 1.35 ± 0.3, d11: 2.44 ± 0.8, *n* = 8; low dose: baseline: 2.58 ± 0.8, d5: 1.46 ± 0.4, d8: 1.38 ± 0.2, d11: 1.34 ± 0.4, all *P* < 0.0001 relative to baseline, *n* = 7; high dose: baseline: 2.10 ± 0.8, d5: 1.59 ± 1.1, d8: 1.39 ± 0.6, d11: 1.47 ± 0.5, all *P* = 0.2581 relative to baseline, probably not significant due to high variability of the data, *n* = 8) [137]. Rilotumumab is a monoclonal antibody that binds and neutralizes HGF. [¹⁸F]FDG and [¹⁸F]FLT are both effective in demonstrating the treatment response of a U87-MG glioma model (tumor volumes are significantly reduced on d7 upon treatment). [¹⁸F]FDG is already reduced on d2 (*P* = 0.020, maximum reduction on d4: - 41 %) whereas [¹⁸F]FLT is significantly reduced on d4 (*P* = 0.005, maximum reduction on d7: -64 %, control: +30 %, *n* = 6 mice per group) [138]. Both radiotracers were also applied in a study employing two different responsive tumor models treated with the adenosine triphosphate-competitive c-MET kinase inhibitor crizotinib (PF-2341066). [¹⁸F]FDG uptake is reduced on d13 in the c-MET amplified GTL-16 gastric cancer model and unchanged in the U87 glioma model. [¹⁸F]FLT accumulation is already reduced at d4 and d7 in both models. GTL-16 treatment with 12.5 mg/kg or 50 mg/kg crizotinib results in reduced [¹⁸F]FLT uptake on d4 and d7 (*P* < 0.05, *n* = 6-7) and [¹⁸F]FLT uptake in U87 treated with 50 mg/kg crizotinib is decreased by 53 % (*P* < 0.001, *n* = 7-8) on d8. Therefore, [¹⁸F]FLT appears to be a better predictor of response to crizotinib treatment than [¹⁸F]FDG [139]. Also in lung cancer models alteration in [¹⁸F]FLT uptake appears to be a suitable imaging biomarker to monitor response to crizotinib. H1993 NSCLC cells have a high level of MET amplification and therapy with this drug does not only cause tumor growth inhibition but also a reduction in [¹⁸F]FLT uptake in respective xenografts (H1993: SUV_{max} baseline vs. d3: 50 mg/kg crizotinib: 2.80 ± 0.43 vs. 2.03 ± 0.24, *P* < 0.05, 100 mg/kg crizotinib: 2.96 ± 0.07 vs. 1.76 ± 0.18, *P* < 0.01, *n* ≥ 4). This reduction in tracer uptake is also observable on d 6 and d 9. On the other hand, HCC827 cells (MET expression but no gene amplification) are resistant to crizotinib. Treatment with this agent does not result in significant changes in [¹⁸F]FLT at any of the time points investigated. Results are consistent with Ki67 staining. The proliferation rate of H1993 tumors is significantly reduced after low- (*P* = 0.01) and high-dose (*P* < 0.01) treatment with crizotinib, whereas it is unchanged in the resistant HCC827 model [129].

BAY 853474 is a small molecule c-MET inhibitor, which was applied in Hs746T gastric cancer xenograft bearing mice. Tumor [¹⁸F]FLT is markedly reduced upon treatment (%ID/ml in mice treated with 10 mg/kg BAY 853474: baseline: 2.06 ± 0.67, d2: 1.23 ± 0.21, *P* < 0.05, d4: no tumor uptake detectable, *n* = 5 per group). Immunohistochemistry reveals that there are indeed no Ki67 positive nuclei detectable with doses as low as 3 mg/kg or 1 mg/kg on d4, explaining why there is no [¹⁸F]FLT uptake. [¹⁸F]FDG is reduced in a similar manner which is accompanied by decreased expression of GLUT1 [140].

3.4.5 PI3K inhibitors

Phosphatidylinositol-4,5-bisphosphate 3-kinases (PI3Ks) are involved in a range of cellular pathways, including cell growth, proliferation and survival (**Supplementary Fig. S1**). It acts upstream of mTOR (see 3.4.6). GDC-0941 is a pan-class I PI3K inhibitor. Human U87 glioma tumors are sensitive to this drug as demonstrated by growth inhibition. 18 h after treatment [¹⁸F]FLT uptake is significantly reduced (NUV_{max} baseline vs. 18 h: control: 2.17 ± 0.39 vs. 2.02 ± 0.09 , $n = 5$, treatment: 2.17 ± 0.38 vs. 1.59 ± 0.29 , $n = 6$, $P < 0.01$). TK1 expression levels are also decreased (1.00 ± 0.28 vs. 0.27 ± 0.16 , $P < 0.01$). Response of human HCT116 colorectal tumors is more variable and no significant growth inhibition can be detected. This is consistent with unaltered [¹⁸F]FLT uptake and TK1 expression after 18 h (NUV_{max} baseline vs. 18 h: control: 2.30 ± 0.81 vs. 2.78 ± 0.34 , $n = 4$, treatment: 2.36 ± 0.78 vs. 2.38 ± 0.49 , $n = 5$; TK1 expression: 0.95 ± 0.18 vs. 0.80 ± 0.11). Interestingly, a significant correlation of change in NUV_{max} (18 h/baseline) in all U87 and HCT116 tumors with tumor growth inhibition (measured by caliper over 8 d) is apparent ($R^2 = 0.3193$, $P < 0.05$). To further validate that PI3K inhibition resulting in growth arrest also leads to a reduction in [¹⁸F]FLT uptake, the authors employed an HT29 colorectal cancer model that expresses an inducible dominant-negative isoform of the p85 α regulatory subunit of PI3K ($\Delta p85\alpha$). 3 d after induction, [¹⁸F]FLT is significantly reduced (SUV_{max} at baseline vs. 18 h: control: 4.56 ± 0.36 vs. 4.01 ± 0.44 , induced: 4.15 ± 0.42 vs. 2.24 ± 0.30 , $P < 0.05$). Also liver metastases of HCT116 show reduced [¹⁸F]FLT accumulation 18 h after GDC-0941 (NUV_{max} 2.76 ± 0.16 vs. 1.99 ± 0.13 , $P < 0.05$, $n = 3$), which is in line with reduced tumor burden [141]. Furthermore, Nguyen et al. show that PI3K inhibition induced by LY294002 after insulin stimulation in HCT116 cells grown in culture causes a decrease in cellular [¹⁸F]FLT retention [142]. Hence, [¹⁸F]FLT uptake may offer a suitable biomarker for monitoring treatment response to PI3K inhibition.

3.4.6 mTOR inhibitors

The mechanistic target of rapamycin (mTOR, also known as mammalian target of rapamycin) signaling pathway is essential for proliferation and angiogenesis (**Supplementary Fig. S1**) and is often upregulated in cancer. Hence, agents targeting this kinase hold great promise in anti-cancer therapy. Several mTOR inhibitors were developed which can be classified into two categories: rapalogs (rapamycin and its analogs) and ATP-competitive inhibitors of mTOR. Rapamycin and rapalogs such as temsirolimus and everolimus are allosteric, irreversible inhibitors of Raptor-bound mTOR (mTORC1). They can also inhibit the activity of mTOR in complex with rictor (mTORC2) but only after prolonged exposure. ATP-competitive inhibitors of mTOR inhibit both, mTORC1 and mTORC2, and have also shown inhibitory activity against PI3K.

Everolimus has shown promising results in some but not all neuroendocrine tumors. Johnbeck et al. demonstrate that [¹⁸F]FLT is suitable for early prediction of therapy response in an H727 lung carcinoid neuroendocrine tumor model. Uptake of this tracer on d1 correlates with tumor growth on d7 ($r^2 = 0.63$, $P = 0.019$) and tracer uptake on d3 correlates with tumor growth on d7 ($r^2 = 0.87$, $P < 0.001$) and d10 ($r^2 = 0.58$, $P = 0.027$). For [¹⁸F]FDG such a correlation can only be seen on d3. Interestingly, differences in [¹⁸F]FLT uptake in the control vs. the everolimus treated group are not significant before d10 (change in SUV_{mean} relative to baseline, control vs. everolimus: d3: $112 \% \pm 3 \%^*$ vs. $116 \% \pm 4 \%^*$, d10: $116 \% \pm 4 \%^*$ vs. $91 \% \pm 6 \%^\#$. $*P < 0.05$ relative to baseline, $^\#P = 0.010$ everolimus vs. control group on

the same day, $n = 8$ per group) [143]. Likewise, in everolimus sensitive SUDHL-1 lymphoma [^{18}F]FLT is superior to [^{18}F]FDG in detection of early therapy response on d5 after treatment initiation (change in [^{18}F]FLT T/B on d5 ($n = 12$) relative to control treatment ($n = 7$): $P = 0.01$, [^{18}F]FDG is unchanged). Ki67 staining is significantly reduced as well (control: 57.1 %, everolimus: 20.3 %, $P < 0.0001$). The authors also demonstrate similar effects in everolimus treated Karpas299 lymphomas (change in [^{18}F]FLT T/B on d2 after everolimus relative to baseline: control: $154 \% \pm 35.5 \%$, $n = 7$, everolimus: $92 \% \pm 37 \%$, $n = 8$, $P = 0.001$; Ki67: control: $59.9 \% \pm 5.6 \%$, everolimus: $37.1 \% \pm 2.3 \%$, $P = 0.02$) [144]. Another study also demonstrates the usefulness of [^{18}F]FLT in monitoring response to everolimus therapy. After treatment uptake of this radiotracer is significantly reduced in ovarian SKOV3 xenografts before a significant difference in tumor volume can be detected on d7 (SUV_{mean} relative to baseline: d2: $-33\% \pm 12 \%$, $P = 0.003$; d7: $-66 \% \pm 8 \%$, $P < 0.001$; significant changes relative to vehicle: d2: $P = 0.0008$, d7: $P = 0.01$; similar results were obtained for SUV_{max}, $n = 7$ per group). Also BrdU incorporation is diminished (relative to vehicle: d2: -65% , not significant; d7: -41% $P = 0.02$) [145].

Honer et al. show that both, [^{18}F]FDG and [^{18}F]FLT uptake, are decreased in lung H596 xenografts treated with everolimus (SUV reduction on d2: -20% , $P < 0.01$, similar reduction on d7, $n = 10$ per group; correlation of Ki67 and [^{18}F]FLT: $r = 0.6$, $P = 0.04$). In HCT116 colorectal tumors, which were characterized as being resistant by *in vitro* assays, [^{18}F]FLT uptake is unaffected by everolimus treatment. However, both of these tumors are responsive with respect to tumor growth inhibition *in vivo*. The authors hypothesize, that in HCT116 tumors the anti-tumor activity of everolimus can be attributed to the anti-angiogenic properties of the drug. They tested the hypothesis that [^{18}F]FDG is not affected by drugs targeting angiogenesis in a well-vascularized orthotopic rat mammary tumor model treated with PTK/ZK (vatalanib, a pan VEGFR inhibitor) or NVP-AAL881 (a dual RAF and VEGFR-2 inhibitor). Hence, the authors conclude that monitoring the pharmacodynamic efficacy of drugs with anti-angiogenic properties by [^{18}F]FDG or [^{18}F]FLT PET should be treated with caution since changes in tracer uptake might not be related to tumor growth inhibition [146]. On the other hand, this review includes a range of studies that successfully demonstrate that changes in [^{18}F]FLT reflect anti-proliferative responses to treatment with anti-angiogenic drugs (e.g. see 3.4.2).

In Granta-519 leukemia-bearing mice temsirolimus induces a reduction of tumor [^{18}F]FDG accumulation on d2, which again increases on d4, d7 and d9. The authors attribute this increase in [^{18}F]FDG to the presence of inflammatory cells. In this study [^{18}F]FLT is also reduced at early time points (d2: -31%) followed by an increase which peaks at d7 ($+12 \%$), and a later decline (-13% on d9 and -11% on d11) followed by a further increase (d14: $+11 \%$; $n = 5$). Because of the timing the authors could exclude that inflammatory cells are the reason for this increase. They hypothesize that cells might have regained their proliferative capacity, which is supported by expression analysis of cyclin D1 (dropped from d1 until d4 and returned to baseline at d7). This report does not provide information on the statistical significance of the [^{18}F]FLT findings. Also the tumor response in terms of growth inhibition is not mentioned. Hence, it is not clear whether the analyzed tumors are sensitive to temsirolimus treatment at all. The authors conclude that timing of response assessment is crucial because of temporary metabolic changes induced by the treatment [82].

Rapamycin itself induces growth inhibition in U87 glioma xenografts, which is accompanied by a reduction of both, [^{18}F]FDG and [^{18}F]FLT, on d2 (reduction of tumor/mediastinum ratio of [^{18}F]FLT

relative to baseline: $-52 \% \pm 7 \% P < 0.01$, $n = 6$ mice per group). In resistant LN-229 gliomas tracer uptake is unaffected ($P = 0.2$ for $[^{18}\text{F}]\text{FLT}$). TK1 expression and Ki67 staining are markedly reduced in U87 tumors but not in LN-229 xenografts (no quantification performed), underlining the capability of $[^{18}\text{F}]\text{FLT}$ for rapamycin response prediction in glioma models [147].

Top216 is an inhibitor of the mTOR pathway, which inhibits protein, RNA, and DNA synthesis and induces apoptosis by a largely undefined mechanism. After application in A2780 ovarian cancer xenograft-bearing mice, $[^{18}\text{F}]\text{FLT}$ within the tumor is reduced relative to baseline ($\text{SUV}_{\text{mean}} = 1.09 \pm 0.03$) already after 2 h (0.53 ± 0.02 , -52% , $P < 0.001$), 6 h (0.56 ± 0.06 , -49% , $P = 0.002$) and 1 d (0.58 ± 0.03 , -47% , $P < 0.001$, $n = 5-10$ per group). Interestingly, tracer uptake in the control group correlates with subsequent tumor volume changes (SUV_{mean} baseline vs. tumor volume ratio d5/baseline: $r^2 = 0.61$, $P = 0.04$). $[^{18}\text{F}]\text{FDG}$ accumulation is reduced at 6 h and 1 d but the decrease is less pronounced. Uptake of $[^{18}\text{F}]\text{FLT}$ on d5 ($\text{SUV}_{\text{mean}} = 1.33 \pm 0.08$) is undistinguishable from baseline, suggesting that tumor cells regained their proliferative capacity. This is supported by Ki67 expression, which is reduced only after 6 h (-31% , $P = 0.01$) and 1 d (-71% , $P < 0.001$) after drug administration, but not on d5, three days after the last dose of Top216. Furthermore, the authors note a significant reduction of TK1 on d1 (-56% , $P < 0.001$) [148].

AZD8055 inhibits both mTOR complexes (mTORC1 and mTORC2) which affect different downstream molecules. As early as one hour after drug administration $[^{18}\text{F}]\text{FDG}$ as well as the mTOR biomarkers pAKT and pS6 are reduced in the sensitive human U87 glioma model. After 4 d of treatment, a persisting reduction of these biomarkers can be observed, including Ki67 (Ki67: vehicle: $84.9 \% \pm 1.6 \%$, treatment: $70.8 \% \pm 1.71 \%$, $P < 0.001$). In this model $[^{18}\text{F}]\text{FLT}$ does not show such clear results. *In vivo* tracer uptake as determined by PET is significantly reduced upon treatment (SUV_{max} on d4: vehicle: 0.84 ± 0.05 , $n = 11$, AZD8055: 0.55 ± 0.05 , $n = 9$, $P = 0.0003$; correlation between SUV_{max} and Ki67: $r = 0.63$, $P < 0.05$). However, *ex vivo* gamma counter measurements fail to reveal a significant difference ($\% \text{ID/g}$ vehicle: 2.90 ± 0.13 , $n = 10$, AZD8055: 2.41 ± 0.33 , $n = 9$, $P > 0.05$). Possibly mTOR inhibition by AZD8055 has only little impact on factors that are of importance for $[^{18}\text{F}]\text{FLT}$ accumulation. Analysis of e.g. TK1 expression could further elucidate this issue. Therefore, $[^{18}\text{F}]\text{FLT}$ appears to be less suitable for AZD8055 therapy follow up than $[^{18}\text{F}]\text{FDG}$ [149]. However, the authors mention a difference in overall proliferation and treatment response between the two cohorts enrolled in the respective $[^{18}\text{F}]\text{FDG}$ and $[^{18}\text{F}]\text{FLT}$ studies which challenges the direct comparison.

3.4.7 Aurora kinase inhibitors

Aurora kinases play a key role in mitosis (**Supplementary Fig. S1**) and are frequently upregulated in cancers. In human colorectal HCT116 cancer xenografts the multi-targeted Aurora B kinase inhibitor TAK-901 inhibits growth by 60 % on d12. $[^{18}\text{F}]\text{FLT}$ in vehicle-treated animals is stable, whereas tracer uptake in TAK-901-treated tumors is significantly reduced at all time points tested (change of SUV_{max} after treatment with 30 mg/kg relative to baseline: d4: -46% , d9: -26% , d11: -51% , d15: -25% , $P < 0.001$). $[^{18}\text{F}]\text{FLT}$ uptake returns towards baseline levels by the commencement of the next treatment cycle (d9 and d15), which is consistent with release of Aurora B kinase suppression. $[^{18}\text{F}]\text{FLT}$

accumulation parallels BrdU incorporation determined by immunohistochemistry (significant reduction on d4 and d11, $P < 0.05$). In this model, [^{18}F]FDG uptake and GLUT1 staining are not affected [150]. Another study employed the Aurora B kinase inhibitor AZD1152 which reduces the growth of two colorectal cancer models (HCT116 and SW620). Again, GLUT1 staining and [^{18}F]FDG uptake are unchanged in both models. [^{18}F]FLT uptake is only reduced in HCT116 tumors (significant reduction relative to vehicle group on d8, d15, d22, $P < 0.05$). On d37 (about 2 wk after the last treatment) a remarkable increase in [^{18}F]FLT can be noted ($P < 0.05$ relative to control), suggesting recovery of the proliferative activity in the tumors consistent with an increase in tumor volume (determined by caliper). Ki67 staining is in line with [^{18}F]FLT uptake (but no quantification was reported). No alterations in [^{18}F]FLT accumulation are detectable in SW620 xenografts. However, [^{18}F]FLT uptake in these cells is generally low, which the authors attribute to a potential dependence of this cell line on the thymidine *de novo* pathway based on TK1 expression studies. In conclusion, the authors suggest that [^{18}F]FLT uptake is most suitable as a biomarker for anti-proliferative therapy response in thymidine salvage-dependent tumors [76].

HCT116 was also used as a sensitive model in a study employing the Aurora A kinase inhibitor alisertib (MLN8237). Uptake of [^{18}F]FLT is reduced before the growth inhibitory effect is observable. Retardation in tumor growth are significant on d14 ($P = 0.003$) and d21 ($P = 0.0014$), whereas tracer uptake is significantly reduced on d7 ($P = 0.0014$), d14 ($P = 0.007$) and d21 (change of tracer uptake in a 27 mm³ volume-of-interest relative to baseline: -51 %, $P = 0.001$, $n = 8$ per group) [151].

CCT129202 is an inhibitor of Aurora A and B kinases. It is effective in a wide range of tumor cells and it exerts an anti-proliferative effect in HCT116 colorectal xenografts demonstrated by growth inhibition. Accumulation of [^{18}F]FLT is reduced as measured by dynamic PET (significant reduction in mean NUV₆₀ (normalized to heart), FRT (fractional retention), and AUC (area under the normalized time activity curve) on d7 ($P < 0.02$), although not on d2). [^{18}F]FLT reduction is associated with reduced TK1 protein levels [152].

3.4.8 BRAF inhibitors

The V600E mutation in BRAF is a commonly observed mutation and results in constitutive activation of BRAF and associated downstream effectors within the mitogen-activated protein kinase pathway. PLX4720 is a potent and selective inhibitor of ^{V600E}BRAF. *In vivo* PLX4720 reduces [^{18}F]FLT uptake in Lim2405 colorectal cancer cells expressing ^{V600E}BRAF (%ID/g on d4: vehicle group: 14.9 ± 1.5 , $n = 5$, PLX4720-treated group: 9.9 ± 1.4 , $n = 5$, $P = 0.0079$). This is in line with reduced TK1 (58.8 % vs. 34.3 %, $P = 0.0041$) and Ki67 expression (89.5 % vs. 77.4 %, $P < 0.0001$). In this model [^{18}F]FDG is unchanged. On the other hand, PLX4720 does not induce a reduction in HT29 xenograft volume, even though these tumors also express ^{V600E}BRAF. This is in accordance with unchanged [^{18}F]FLT uptake (%ID/g on d4: vehicle group: 2.21 ± 0.06 , PLX4720 group: 1.97 ± 0.14 , $n = 5$ per group) as well as unaltered TK1 protein expression and unaltered Ki67 immunoreactivity. Matrix-assisted laser desorption / ionization analyses reveals that PLX4720 cannot be detected in HT29 xenografts in treated mice, whereas PLX4720 is readily detectable in treated Lim2405 tumors, indicating that differences in vasculature or stroma may contribute to response differences after drug exposure. Therefore, [^{18}F]FLT faithfully reflects tumor proliferation in both models [69].

PLX3603 (RO5212054, RG7256) is a novel, orally available, small-molecule inhibitor of ^{V600E}BRAF. It inhibits growth of subcutaneous A375 melanoma when administered orally twice daily. This treatment effect is in line with reduced [¹⁸F]FDG uptake on d1, d3 and d7 as determined by *ex vivo* gamma counter and *in vivo* PET measurements. On the other hand, [¹⁸F]FLT is unchanged, which is probably due to low baseline [¹⁸F]FLT uptake ($n = 3$). The authors hypothesize that [¹⁸F]FLT uptake could be hampered by high plasma thymidine levels or preferential usage of the thymidine *de novo* pathway [153].

3.4.9 MEK inhibitors

MEK is a key component of the RAS/RAF/MEK/ERK pathway (**Supplementary Fig. S1**). MEK inhibitors have been found to be effective in BRAF- and RAS-mutated tumors [154]. Leyton et al. applied the mitogenic extracellular kinase 1/2 (MEK1/2) inhibitor PD0325901 in two different cancer models. After daily drug administration [¹⁸F]FLT accumulation is significantly reduced (NUV₆₀ vehicle vs. PD0325901: melanoma SKMEL-28 (harboring ^{V600E}BRAF mutation): d1: 1.52 ± 0.32 vs. 0.72 ± 0.23 , $P = 0.045$, d10: 1.38 ± 0.26 vs. 0.93 ± 0.1 , $P = 0.03$; colorectal HCT116 (harboring mutated K-RAS): 1.70 ± 0.35 vs. 0.93 ± 0.19 , $P = 0.03$, d10: 1.73 ± 0.08 vs. 0.91 ± 0.1 , $P = 0.03$, $n = 4$ per group; similar results were obtained for NUV_{max}, AUC and FRT). NUV₆₀ (and also AUC and FRT) of all tumors significantly correlates with Ki67 labeling index ($r = 0.630$, $P = 0.001$) and TK1 expression ($r = 0.518$, $P = 0.002$) [155]. Studying the effect of PD0325901 in a sensitive and an insensitive model, another group demonstrates that drug-induced growth inhibition can be followed by [¹⁸F]FLT PET. The same sensitive model as investigated by Leyton et al. (SKMEL-28) shows a mean 43 % decline in [¹⁸F]FLT uptake after one week of treatment, whereas uptake in vehicle control tumors increases by 32 %. [¹⁸F]FLT uptake in treated tumors remains stable during week 2 and week 3, whereas uptake increases in vehicle-treated tumors, consistent with an increase in tumor volume (determined by caliper). In this model, changes in [¹⁸F]FDG are only modest and delayed in comparison to [¹⁸F]FLT. BT-474 breast cancer cells harboring wildtype BRAF are resistant to MEK1/2 inhibition and consistently, [¹⁸F]FLT is not changed in these tumors following PD0325901. Unfortunately, the level of significance of these findings was not reported [156].

These studies suggest that change in [¹⁸F]FLT uptake has potential as biomarker for the detection of response to MEK inhibitor therapy.

3.4.10 CDK inhibitors

Cyclin dependent kinases (CDKs) are key players in the regulation of the cell cycle (**Supplementary Fig. S1**). [¹⁸F]FLT uptake was analyzed in MDA-MB-231 mammary carcinoma xenografts at different time points after treatment with the CDK4 inhibitor PD-0332991 on two consecutive days. A strong reduction is apparent on d1 after the last drug dose, which is still observable after 2 d. Tracer uptake returns to baseline levels on d3. This is highly consistent with staining of pRb, TK1, BrdU and Ki67 and indicates that tumor cells return to a proliferative state. Results are shown in bar charts, and unfortunately neither exact values nor statistical significance are provided [57].

3.4.11 Multiple kinase inhibitors

Nielson et al. show that targeting of various EGFRs by a pan-HER antibody is more effective in tumor growth inhibition than therapy with antibodies against single EGFRs in a subcutaneous BxPC-3 pancreatic adenocarcinomas model. 2 d after initiation of therapy, [^{18}F]FLT uptake is significantly decreased in the pan-HER treated group (%ID_{max} baseline vs. d2: vehicle: 21.2 ± 1.4 vs. 24.3 ± 1.5 , $P \leq 0.01$; EGFR: 21.3 ± 1.1 vs. 21.0 ± 1.4 ; HER2: 21.5 ± 1.2 vs. 26.3 ± 1.7 , $P \leq 0.01$; HER3: 21.9 ± 1.7 vs. 23.0 ± 2.1 ; pan-HER: 27.5 ± 2.2 vs. 21.8 ± 1.4 , $P \leq 0.01$, $n = 8$ mice per group) and a positive relation of [^{18}F]FLT uptake and growth is observable ([^{18}F]FLT ratio (d2/baseline) vs. tumor volume ratio (d23/baseline): $r = 0.53$, $P < 0.01$). Immunohistochemistry shows that reduction in [^{18}F]FLT is paralleled by down-regulation of the proliferation markers Ki67 and TK1 after 1 dose of the pan-HER antibody ($P \leq 0.05$). Three doses of pan-HER do not further down-regulate these proliferation markers. Gene expression analysis shows a trend for reduction of Ki67 and TK1. [^{18}F]FDG imaging on d1 of therapy shows comparable results [157]. It should be pointed out, that baseline [^{18}F]FLT accumulation in the pan-HER group is substantially higher than the vehicle group (difference does not reach statistical significance). Hence, the authors conclude that it is pivotal to determine baseline uptake for each mouse and that relative changes in tracer uptake may be misleading in this study.

Sorafenib is a small molecule inhibitor of several kinases including VEGFR and Raf kinases (**Supplementary Fig. S1**). In an A673 sarcoma model both [^{18}F]FDG and [^{18}F]FLT are reduced upon sorafenib therapy on d5 / d6 after start of treatment ([^{18}F]FLT %ID/g d5 relative to baseline: control: $+134 \% \pm 70 \%$, $n = 5$, sorafenib: $-46 \% \pm 29\%$, $n = 15$, $P = 0.003$; sorafenib mean %ID/g: pre: 12.9 ± 5.8 , post: 5.7 ± 1.4). Ki67 staining is significantly decreased in treated tumors (control: 42% , range $12 \% - 61 \%$, treated: 22% , range $7 \% - 47 \%$, $P = 0.029$), and caspase-3 is increased (control: $6 \% \pm 2 \%$, treated: $12 \% \pm 5 \%$, $P = 0.04$). [^{18}F]FLT is more predictive for very early response monitoring on d1 (%ID/g: pre: 14.2 ± 4.8 , post: 7.6 ± 0.8 , change of $-43 \% \pm 14 \%$, $P = 0.04$, $n = 7$) than [^{18}F]FDG (no significant change) [158]. In a contradictory study in A498 renal cell carcinoma bearing mice treated with sorafenib [^3H]FLT uptake is increased on d3 and d7 as assessed by autoradiography (%ID/g*kg control vs. sorafenib on d3: 0.74 ± 0.15 vs. 1.96 ± 0.54 , $P < 0.01$; d7: 0.80 ± 0.21 vs. 2.04 ± 0.42 , $P < 0.01$, $n = 5$ per group). Ki67 and tumor volumes are unaltered [159]. The authors attribute the increased uptake of [^3H]FLT to an upregulation of TK1 due to the inhibitory effect of sorafenib on TS [160]. It is not clear why the results of these two studies are different. In both studies the drug has been administered daily with different routes of administration (intraperitoneal vs. oral) and drug dosages (30 mg/kg vs. 80 mg/kg). One possible explanation could be that the cancer models differ with respect to the activities of thymidine salvage and *de novo* pathways.

Axitinib is a multiple receptor tyrosine kinase inhibitor with antiangiogenic properties, which inhibits growth of U87-MG glioma and MDA-MB-231 mammary carcinoma xenografts. In both tumor types [^{18}F]FDG is reduced on d10. [^{18}F]FLT, however, visualizes treatment response at earlier time points (i.e. d3 for the U87-MG and d7 for MDA-MB-231; mean %ID/g vehicle vs. axitinib: U87-MG: d0: 2.82 ± 0.69 vs. 3.02 ± 1.18 , d1: 4.3 ± 0.14 vs. 3.47 ± 1.23 , d3: 4.9 ± 0.68 vs. $3.37 \pm 0.84^*$, d7: 4.14 ± 0.56 vs. $2.65 \pm 0.60^{**}$, d10: 4.68 ± 0.89 vs. $3.34 \pm 0.60^*$, $n = 7$; MDA-MB-231: d0: 2.90 ± 0.46 vs. 3.37 ± 0.33 , d1: 3.08 ± 0.53 vs. 3.28 ± 0.29 , d3: 2.89 ± 0.83 vs. 2.54 ± 0.24 , d7: 3.29 ± 0.53 vs. $1.99 \pm 0.68^{**}$, d10:

3.30 ± 0.55 vs. 1.84 ± 0.50**, $n = 4$; * $P < 0.05$, ** $P < 0.01$). In both models Ki67 staining is significantly reduced on d10 ($P < 0.05$ for MDA-MB-231, $P < 0.01$ for U87-MG) [161].

The dual mTOR/PI3K inhibitor BEZ235 induces inhibition of growth and [^{18}F]FLT uptake in NCI-N87 gastric cancer xenografts. On d2 of therapy, [^{18}F]FLT uptake is reduced by ~20 % relative to control ($P < 0.05$, $n = 4$ animals per group with two tumors each). No change of Ki67 staining is apparent, and TK1 is decreased. In drug-resistant MKN45 and MKN28 gastric cancer xenografts BEZ235 treatment fails to reduce tumor [^{18}F]FLT uptake [162]. Contrarily McKinley et al., show that BEZ235 treatment (40mg/kg daily for three days) of Colo205 tumors *in vivo* causes a reduction in Ki67 index but TK1 and [^{18}F]FLT rest unchanged [128].

The effect of the dual PI3K/mTOR inhibitor NVP-BGT226 (BGT226) was demonstrated in large cell lymphomas by growth inhibition and a reduction of [^{18}F]FLT and [^{18}F]FDG uptake and Ki67 staining in sensitive SU-DHL-1 xenografts (mean T/B change of [^{18}F]FLT d7 relative to baseline: control: 152 % ± 42.6 %, $n = 7$, BGT226: 87 % ± 20.8 %, $n = 10$, $P = 0.0007$; Ki67: control: 64 % ± 20.3 %, treated: 14 % ± 7.5, $P = 0.002$). Uptake of both radiotracers is unaltered in BGT226 resistant Karpas299 xenografts (mean T/B change of [^{18}F]FLT: control: 98 % ± 21 %, $n = 3$, treated: 127 % ± 22 %, $n = 5$, $P = 0.2$) [163].

Sunitinib, a small molecule inhibitor of platelet derived growth factor receptor and VEGFR, reduces [^{18}F]FLT accumulation in subcutaneous U87 glioma (T/M: d0: 2.98 ± 0.33; d3: 2.23 ± 0.36, $P < 0.001$; d7: 1.96 ± 0.35, $P < 0.001$; uptake in control group remained stable around 3.0, $n = 10$ mice in imaging group), which returns to baseline on d13 (6 d after treatment termination, T/M = 3.09 ± 0.29) implying recovery of tumor proliferation. Microvessel density and Ki67 are also significantly reduced and correlate with [^{18}F]FLT uptake (Ki67: d3: $P < 0.05$, d7: $P < 0.01$, d10: $P < 0.05$; Ki67 vs. [^{18}F]FLT T/B: $r = 0.794$). This study demonstrates the importance of [^{18}F]FLT uptake parameter choice for quantification. A significant difference between sorafenib and control treated tumors can already be detected on d3 when tracer accumulation is expressed as tumor-to-muscle ratio (see above) while determination of e.g. %ID_{max}/g does not show significant differences before d7 [164].

When intracranial U87-MG gliomas in rats are treated with sunitinib a significant reduction in [^{18}F]FLT is detectable (treatment start on d6, %ID/g of vehicle vs. sunitinib treated gliomas: d6: 0.06 ± 0.01 vs. 0.06 ± 0.00, d9: 0.06 ± 0.00 vs. 0.08 ± 0.01, d13: 0.11 ± 0.01 vs. 0.06 ± 0.01, d16: 0.21 ± 0.07 vs. 0.06 ± 0.01, d20: 0.32 ± 0.06 vs. 0.13 ± 0.02, d22: 0.48 ± 0.04 vs. 0.19 ± 0.02, $P < 0.05$ from d13 onward, $n = 6$ per group, volume differences are significantly different from d16 onward) which is accompanied by reduced Ki67 staining on d22 ($P < 0.01$). In this model, [^{18}F]FDG is also reduced upon treatment, but to a lesser extent and at a later time point [165].

3.4.12 HDAC inhibitors

Histone acetylation and deacetylation is a critical step for the regulation of gene expression. Belinostat is a histone deacetylase (HDAC) inhibitor with anti-tumor effects in several tumors. In A2780 ovarian cancer xenografts it induces a slight growth inhibition, which is significant on d6 (volume relative to baseline, control: 419 % ± 39 %, belinostat: 282 % ± 30 %, $P = 0.029$, $n = 5-7$ tumors per group). There is no difference in [^{18}F]FLT uptake between treatment and control groups at any time point investigated

(d3, d6, d10) neither for SUV_{mean} nor for SUV_{max} . [^{18}F]FLT SUV_{max} remains stable during treatment whereas in the control group uptake steadily increases over time and it is significantly increased on d10 compared to baseline ($+30\% \pm 9\%$; $P = 0.048$). Interestingly, there is a correlation between tumor volume ratio d10/baseline and [^{18}F]FLT SUV_{mean} on d3 ($r^2 = 0.67$, $P = 0.02$) or d6 ($r^2 = 0.51$, $P = 0.07$). On d10 unaltered Ki67 expression is in line with unchanged [^{18}F]FLT suggesting that the imaging results reflect a true negative finding. It is interesting to note that TK1 gene expression is higher in the treatment compared to the control group (d10: 1.40 ± 0.09 vs. 1.00 ± 0.07 ; $P = 0.006$), which could possibly be explained by TS inhibition induced by belinostat [166]. In this case, however, TS inhibition is not associated with increased [^{18}F]FLT accumulation. On the other hand in this model SUV_{mean} of [^{18}F]FDG shows differences between control and treated group on d6 and d10, and hence better reflects growth inhibition by belinostat [167].

C1A inhibits HDAC6 and thereby affects tumor growth as shown for several cancer cell lines *in vitro* and HCT116 colorectal tumors *in vivo*. After drug administration reduced tumor [^{18}F]FLT uptake can be observed (NUV₆₀ (normalized to heart) baseline: 1.77 ± 0.11 , d1: 1.59 ± 0.10 , $P = 0.033$, d2: 1.06 ± 0.15 , $P = 0.0001$, $n = 4$) which is associated with reduced Ki67 at 48h ($P < 0.0001$) [168].

The HDAC inhibitor LAQ824 induces a dose-dependent growth reduction in human HCT116 colorectal xenografts. Tumor [^{18}F]FLT uptake is reduced in a dose- and time-dependent manner (NUV₆₀ vehicle vs. 5 mg/ml LAQ824: d2: 1.95 ± 0.16 vs. 1.89 ± 0.27 , d4: 2.16 ± 0.15 vs. 1.86 ± 0.13 ($P = 0.05$), d10: 2.77 ± 0.13 vs. 2.05 ± 0.17 ($P = 0.03$), $n = 6$ per group). The labeling index of Ki67 is significantly reduced to $38.0\% \pm 2.2\%$ ($P = 0.004$) and correlates with [^{18}F]FLT uptake ($r = 0.67$; $P = 0.003$). Also a decrease of TK1 protein and mRNA expression can be noted [169].

The HDAC inhibitor SAHA (N1-hydroxy-N8-phenyloctanediamide) and its iodinated derivative ISAHA were employed in a HepG2 hepatoma mouse model. 25 mg/kg and 100 mg/kg ISAHA effectively inhibit tumor growth ($P < 0.01$ relative to SAHA or vehicle on d22). [^{18}F]FLT PET performed one week after treatment initiation parallels the growth-inhibitory effect (T/M d0 vs. d8: control: 7.92 ± 0.52 vs. 8.10 ± 1.48 , $n = 3$; 100 mg/kg of SAHA: 7.85 ± 0.94 vs. 5.70 ± 0.73 , $n = 3$; 25 mg/kg of ISAHA: 7.24 ± 0.80 vs. 4.80 ± 0.54 , $n = 3$; 100 mg/kg of ISAHA: 7.70 ± 0.59 vs. 3.38 ± 0.06 , $n = 3$, all $P < 0.05$). There is a significant correlation of Ki67 staining after 1 week of therapy with [^{18}F]FLT PET ($r^2 = 0.98$, $P < 0.05$; relative staining intensity control: 0.54 ± 0.03 ; 100 mg/kg SAHA: 0.41 ± 0.08 , 25 mg/kg ISAHA: 0.37 ± 0.06 ; 100 mg/kg ISAHA: 0.24 ± 0.04) [170].

3.4.13 HSP90 inhibitors

HSP90 is a chaperone protein, which stabilizes a range of proteins required for survival of cancer cells. Inhibition of HSP90 by AUY922 in anaplastic large cell lymphoma leads to a significant reduction of [^{18}F]FLT uptake in responsive xenografts (SUDHL-1 mean T/B on d5 relative to baseline: untreated controls: $210\% \pm 60\%$, $P = 0.01$, $n = 4$; AUY922: $40\% \pm 20.7\%$, $P = 0.001$, $n = 12$; $P = 0.01$ between the two groups). This is consistent with reduced Ki67 staining (AUY922: $15.3\% \pm 0.8\%$, control: $63.3\% \pm 7\%$, $P = 0.03$). [^{18}F]FDG uptake is also significantly reduced but to a lesser extent. [^{18}F]FLT uptake is unchanged in a resistant lymphoma, whose growth is unaffected upon HSP90 inhibition and also Ki67 staining is not significantly reduced (Karpas299 mean [^{18}F]FLT T/B on d2 relative to baseline: control: $154\% \pm 35.5\%$, $n = 7$, AUY922: $149\% \pm 47.2\%$, $n = 10$, $P = 0.42$). Therefore, in this setting

[¹⁸F]FLT uptake appears to be a specific biomarker which is superior to [¹⁸F]FDG for monitoring treatment effects [144].

3.4.14 Cadherin inhibitors

P-cadherin (CDH3) is a membrane glycoprotein that mediates tumor cell adhesion, proliferation and invasiveness. PF-03732010 is a monoclonal antibody specifically targeting P-cadherin and therefore inhibiting cell adhesion and aggregation *in vitro*. *In vivo* it inhibits growth of primary tumors and metastatic progression of a range of P-cadherin overexpressing tumor cells, as shown here for MDA-MB-231-CDH3, MDA-MB-435HAL-CDH3 (both human breast cancer), 4T1-CDH3 (mouse breast cancer), HCT116 (human colorectal cancer), H1650 (human lung cancer), PC3M-CDH3 and DU145 (both human prostate cancers). Some of these tumors were genetically manipulated to overexpress CDH3. MDA-MB-435HAL-CDH3 were implanted into the subrenal capsule of mice. Primary tumors as well as lung metastases were imaged by [¹⁸F]FLT PET/CT on d42. 10 mg/ml and 20 mg/kg PF-03732010 significantly reduce uptake of [¹⁸F]FLT in the primary tumors by 26.8 % and 23.4 % ($P < 0.01$), respectively, and by 31.7 % and 37.8 % ($P < 0.01$) in the lung metastases ($n = 8$ per group), which is accompanied by reduced Ki67 staining. In this study, imaging was performed after 5 weeks of once-weekly drug administration. The authors interpret the reduction in [¹⁸F]FLT as an indication of a long-lasting treatment effect. At this time point also CT shows the reduction of lung tumor burden [171].

3.4.15 Inhibition of Ca²⁺ channels

Expression of the calcium channel K_{Ca}3.1 is associated with aggressiveness of non-small cell lung cancer and it is important for proliferation and migration of cells *in vitro*. When inhibited *in vivo* by senicapoc growth of A549 lung carcinoma is retarded (significant from d4 onwards), which is accompanied by reduced accumulation of [¹⁸F]FLT (relative change of %ID_{max}/ml (d 7/d 0): vehicle: 1.10 ± 0.07 , $n = 9$, senicapoc: 0.85 ± 0.04 , $n = 12$; $P = 0.0041$). Hence, reduction in [¹⁸F]FLT uptake reflects the growth-inhibitory effect of senicapoc [172].

3.4.16 Inhibition of arginine metabolism enzymes

The semi-essential amino acid arginine has numerous roles in cellular metabolism and is essential under periods of cell growth. It is the precursor of nitric oxide, which may influence tumor initiation, promotion and progression [173]. Arginine deaminase is known to degrade arginine. It inhibits both tumor growth and Ki67 labeling in SK-MEL-28 xenografts (Ki67 index: wk0: 62.7 ± 6.2 , wk1: 19.1 ± 0.3 , wk2: 16.5 ± 1.1 , wk3: 23.7 ± 2.9 , wk4: 22.3 ± 4.5 , all $P < 0.01$ relative to baseline). [¹⁸F]FLT uptake is not altered in treated (%ID/g of treated tumors: wk0: 3.3 ± 0.6 , wk1: 3.8 ± 0.4 , wk2: 3.6 ± 0.4 , wk3: 4.0 ± 0.5 , wk4: 5.4 ± 0.6 , $n = 5$) or untreated ($n = 3$) animals. The authors speculate that this discrepancy between proliferation in terms of tumor growth and [¹⁸F]FLT uptake could be explained by overexpression of TK1 caused by arginine deaminase induced degradation of the phosphatase PTEN which is followed by p53 downregulation. Indeed, TK1 levels are stable during the treatment period which is in accordance with unaltered [¹⁸F]FLT levels. Hence, due to the pharmacological properties of arginine deaminase [¹⁸F]FLT uptake may not be a suitable biomarker to evaluate anti-proliferative response to this treatment [174].

3.4.17 Inhibition of hypoxia induced gene regulation

BAY 87-2243 acts on the hypoxia-inducible factor 1- α pathway, principally by inhibiting the activity of mitochondrial complex I. Human lung cancer (H460) or human prostate cancer (PC3) xenografts respond to daily treatment with BAY 87-2243 as assessed by caliper measurements. Already on d1 after treatment a substantial decrease in [^{18}F]FLT uptake can be noted in these two sensitive models (%ID_{mean}/g vehicle vs. treatment: H460: 4.3 \pm 0.3 vs. 3.0 \pm 0.3, $P < 0.01$; PC3: 3.9 \pm 0.2 vs. 2.9 \pm 0.2, $P < 0.01$, $n = 6$ tumors per group) and this decrease is even more pronounced on d5 (H460: 4.1 \pm 0.3 vs. 3.0 \pm 0.3, $P < 0.01$, PC3: 4.0 \pm 0.2 vs. 2.4 \pm 0.2, $P < 0.01$, $n = 6$ tumors per group). [^{18}F]FDG uptake is unaffected in this study [175].

The proteasome inhibitor MG132 inhibits tumor cell proliferation and increases apoptosis. Furthermore, it suppresses the hypoxic response in tumors via hypoxia-inducible factor 1- α inactivation. When applied daily MG132 reduces [^{18}F]FLT uptake in colorectal HT29 xenografts on d2 ($n = 4$) [176].

3.4.18 Specific delivery of toxic molecules

VEGF₁₂₁/rGel is a vascular disruptive agent composed of the VEGF-A isoform VEGF₁₂₁ linked to the recombinant plant toxin gelonin, which is known to inhibit protein synthesis by inactivating ribosomes. In a breast cancer model [^{18}F]FLT is significantly reduced on d3 after administration of a single dose of this agent (%ID/g relative to baseline: d1: -13.0 % \pm 4.5 %, n.s., d3: -25.0 % \pm 4.4 %, $P < 0.01$, $n = 8$). On d7 tumor regrowth is detectable which is accompanied by normalization of [^{18}F]FLT levels. Ki67 staining index is consistent with [^{18}F]FLT uptake (baseline: 70 % \pm 5 %, d1: 56 % \pm 7 %, $P > 0.05$, d3: 37 % \pm 5 %, $P < 0.01$, d7: restores to baseline level, $P > 0.05$). [^{18}F]FDG fails to show any treatment effect [177]. Also in orthotopic U87-MG gliomas [^{18}F]FLT PET visualizes the efficacy of VEGF₁₂₁/rGel. Tracer accumulation, as well as Ki67 staining, are significantly reduced after 4 doses of this drug given in 2d intervals (%ID/g: control: 2.9 \pm 0.7, VEGF₁₂₁/rGel: 1.7 \pm 0.4, $P < 0.05$, $n = 3$; Ki67 index: control: 17 % \pm 4 %, treated: 5 % \pm 2 %) [178].

The α -folate receptor is overexpressed in several cancers. Hence, in an approach by Pillai et al. it was used to specifically target a thymidylate synthase inhibitor to the tumor. *In vitro* application of BGC 945 induces increase of [^3H]thymidine (2- to 3-fold increase after incubation for 2 h with 250 to 500 $\mu\text{g}/\text{ml}$) and membrane associated hENT1 levels (number of binding sites per cell: control: 55,720 \pm 6,101, 100 $\mu\text{g}/\text{ml}$ BGC 945: 130,800 \pm 10,800). In epidermal KB xenografts [^{18}F]FLT uptake more than doubled at early time points (NUV₆₀: control: 1.3 \pm 0.23, 1 h: 2.8 \pm 0.73*, $n = 8$, 4 h: 3.2 \pm 0.77*, $n = 3$, 24 h: 3.5 \pm 0.90*, $n = 3$, 48 h: 1.6 \pm 0.74, $n = 4$, * $P \leq 0.01$). Effective TS inhibition was verified by increased tumor deoxyuridine levels. Similar results can also be observed for the respective untargeted TS inhibitor BGC 9331. However, the untargeted variant also induces accumulation of [^{18}F]FLT in the intestine, a proliferative and TS-responsive tissue. Therefore, its activity is less tumor specific and [^{18}F]FLT helps to demonstrate the specificity of the drug and identifies possible toxic off-target effects [179].

3.4.19 Targeted radionuclide therapy

Targeted radionuclide therapy aims at local delivery of long-lived radionuclides to tumors. Veeravagu et al. employed Etaracizumab (Abegrin, MEDI-522), a monoclonal antibody to human integrin $\alpha_v\beta_3$, to specifically target [^{90}Y] to subcutaneous U87-MG glioblastoma xenografts. This therapy induces partial

tumor regression. [¹⁸F]FDG as well as [¹⁸F]FLT are decreased upon treatment (%ID/g of [¹⁸F]FLT: control: 3.04 ± 1.28, *n* = 5, [⁹⁰Y]IgG: 2.94 ± 1.5, *n* = 4, Etaracizumab: 2.39 ± 0.28, *n* = 5, [⁹⁰Y]Etaracizumab: 1.73 ± 0.1, *P* < 0.001, *n* = 5, imaging time point is not stated) which is in accordance with reduced Ki67 (%Ki67: control: 16.5 ± 0.7, [⁹⁰Y]IgG: 8.9 ± 1.2, Etaracizumab: 13.4 ± 2.1, [⁹⁰Y]Etaracizumab: 4.79 ± 0.42, *P* < 0.005) [180]. [⁹⁰Y]Ibritumomab tiuxetan (Zevalin), a monoclonal antibody targeting CD20 (see also 3.6.7), induces only a slight anti-proliferative effect in DoHH2 B-cell follicular lymphoma xenografts as determined by Ki67 immunohistochemistry after 48 h (%Ki67: control: 83.6 ± 3.2, treated: 78.8 ± 9.8, *P* = 0.014). [¹⁸F]FLT is not significantly affected at this time point (%ID/g: control: 5.4, treated: 5.8 ± 2.5, *n* = 10 per group), which the authors explain by tumor heterogeneity or delayed delivery of the therapeutic agent [81].

The urokinase plasminogen activator receptor (uPAR) is part of the plasminogen activation system and plays a role in tissue reorganization, necessary for cancer invasion and metastasis. Targeting uPAR is therefore an attractive approach for therapy of metastasizing cancers. Persson et al. applied a theranostic approach in a colorectal cancer model (uPAR-positive HT-29) by using the high affinity uPAR binding peptide DOTA-AE105 radiolabeled with [⁶⁴Cu] or [¹⁷⁷Lu] for PET imaging or radionuclide therapy, respectively. This specific peptide accumulates in the tumors and the [¹⁷⁷Lu] version significantly reduces tumor size. [¹⁸F]FLT uptake reduction precedes treatment response in this model as changes in tumor size correlate with changes in tracer uptake (size (d14/baseline) vs. [¹⁸F]FLT (d6/baseline): *R*² = 0.71, *P* = 0.001; and vs. [¹⁸F]FLT (d3/baseline): *R*² = 0.49 *P* = 0.02). However, no significant differences between the different treatment groups (¹⁷⁷Lu-DOTA-AE105 vs. vehicle control) can be noted by [¹⁸F]FLT PET on d1, d3 or d6 [181].

3.5 Imaging of response to radiotherapy

Radiation therapy employs ionizing radiation that damages DNA, which subsequently results in cell death. *In vitro* analysis of murine squamous cell carcinoma (SCCVII) irradiated with 10 Gy or 20 Gy reduces the number of cells in S-phase and increases the fraction in G₂/M-phase after 24 h. Irradiation of respective xenografts results in significantly delayed tumor growth. Uptake of [¹⁸F]FLT is significantly reduced after 24 h and 48 h (T/B ratio: control: baseline: 2.4 ± 0.3, 24 h: 2.5 ± 0.3, 48 h: 2.1 ± 0.7, *n* = 3; 10 Gy: baseline: 2.8 ± 0.5, 24 h: 1.3 ± 0.1, 48 h: 1.4 ± 0.2, *n* = 3; 20 Gy: baseline: 2.6 ± 0.2, 24 h: 1.3 ± 0.1, 48 h: 1.2 ± 0.1, *n* = 3; radiated relative to baseline: *P* = 0.027; radiated relative to control: *P* = 0.02), whereas [¹⁸F]FDG uptake is comparable to control tumors [182]. Sugiyama et al. report that [¹⁸F]FLT is superior to [¹⁸F]FDG in monitoring response to radiotherapy. Similar to the aforementioned study, the group irradiated SCCVII tumors with a single dose of 20 Gy, resulting in growth reduction on d7. This is accompanied by a significant reduction of [¹⁸F]FLT uptake (%ID/g: control: 9.7 ± 1.2, *n* = 4, 6 h: 5.9 ± 0.4*, *n* = 5, 12 h: 6.2 ± 0.6*, *n* = 5, 24 h: 6.1 ± 1.3*, *n* = 4, d3: 6.4 ± 1.1*, *n* = 5, d7: 9.3 ± 3.1, *n* = 4, **P* < 0.05), and a reduced PCNA labeling index (control: 53.2 ± 8.7, 6 h: 38.5 ± 5.3*, 24 h: 36.8 ± 5.3*, **P* < 0.05). [¹⁸F]FDG is significantly decreased only after 3 d [183].

Local irradiation with a dose of 22 Gy in six fractions over two weeks reduces volumes of HNX-OE head and neck cancer xenografts. [¹⁸F]FLT uptake significantly decreases on d4, which is followed by a further decrease in the second week. A maximum reduction of the T/B ratio is apparent on d12 (-49 ± 16%), whereas maximum decrease in [¹⁸F]FDG is observable on d8 (-42 ± 18%). The [¹⁸F]FDG signal is

significantly reduced from d4 onward and stays rather stable. A significant correlation of changes in tumor volume (d29/baseline) with changes in [¹⁸F]FLT signal d5/baseline (Spearman correlation = 0.65, *n* = 11) or d8/baseline (correlation = 0.70) can be noted, whereas no such correlation with [¹⁸F]FDG is apparent. The authors conclude that both tracers appear to be suitable to monitor therapy effects in this model [184].

Irradiation of MCK mammary carcinoma cells *in vitro* leads to a dose-dependent decrease of [¹⁸F]FLT uptake, which is not apparent at doses lower than 5 Gy (*in vitro* uptake, counts per minute: 0 Gy: 68,945 ± 3,385, 2.5 Gy: 65,737 ± 1,516, 5 Gy: 61,556 ± 3,794, 10 Gy: 53,493 ± 1,669*, 20 Gy: 42,674 ± 2,686*, **P* < 0.05). This reduction in [¹⁸F]FLT can probably be attributed to an increased amount of cells in G₂/M cycle after irradiation, as demonstrated by flow cytometry. Interestingly, when 10 Gy is given in four fractionated doses, the reduction in [¹⁸F]FLT uptake is no longer significant (*in vitro* uptake: 0 Gy: 27,428 ± 2,257, 2.5 Gy: 26,295 ± 606, 10 Gy: 21,558 ± 2,208 (*P* < 0.05), 4 x 2.5 Gy: 26,244 ± 1,549; absolute numbers differ from the previous experiment due to differences in the experimental setup) which can possibly be explained by a reduced cell number in G₂/M-phase compared to 10 Gy as a single dose. In an analogous *in vivo* model mice were bilaterally inoculated with these tumor cells and the right side irradiated with increasing doses. In tumors irradiated with more than 5 Gy [¹⁸F]FLT is decreased after 24 h (SUV of contralateral vs. irradiated tumor: 0 Gy: 1.69 ± 0.43 vs. 1.61 ± 0.31, *n* = 2, 2.5 Gy: 2.69 ± 1.39 vs. 1.93 ± 0.55, *n* = 3, 5 Gy: 2.11 ± 0.20 vs. 1.61 ± 0.24*, *n* = 5, 10 Gy: 1.99 ± 0.39 vs. 1.20 ± 0.11**, *n* = 4, 20 Gy: 1.19 ± 0.38 vs. 0.90 ± 0.26**, *n* = 4, 4 x 2.5 Gy: 2.72 ± 0.89 vs. 1.85 ± 0.50*, *n* = 4; **P* < 0.05 relative to control tumor; ***P* < 0.05 relative to 0 Gy dose). Single irradiation with 10 Gy has greater impact on tracer uptake than 4 x 2.5 Gy, consistent with the respective *in vitro* experiments [185].

In a study with SCCVII murine squamous cell carcinoma xenografts [¹⁸F]FLT uptake is significantly reduced 1 d after radiotherapy (SUV change relative to 0 Gy: 2 Gy -25.7 %, 6 Gy: -41.4 %, 20 Gy: -42.3 %, 60 Gy: -41.8 %, all *P* < 0.05 relative to control tumor, *n* = 3-4). However, no relationship between [¹⁸F]FLT decrease and radiation dose is evident, which may be explained by the fact that already with 6 Gy [¹⁸F]FLT accumulation decreases to levels which are undistinguishable from background. Tumor [¹⁸F]FLT uptake returns to control levels by d3 in tumors receiving 2 Gy and 6 Gy. The authors speculate that this might be attributed to sublethal DNA damage repair and subsequent repopulation. In tumors irradiated with 20 Gy or 60 Gy a significant reduction (*P* < 0.05) can still be noticed on d3, which persists until d7 for the 60 Gy dose. In this model, [¹⁸F]FDG is initially increased following low dose irradiation (2 Gy and 6 Gy), presumably caused by inflammation- or radiation-induced increase of glucose metabolism, as the authors hypothesize. A significant decrease of [¹⁸F]FDG is only detectable 7 d after high dose irradiation (20 Gy and 60 Gy) [186].

Radiation of two different colorectal xenografts leads to a dose-dependent reduction of [¹⁸F]FLT after 24 h, which is significant with the highest dose applied (T/B: SW480 tumors: 0 Gy: 3.65 ± 0.51, 5 Gy: 3.75 ± 0.71, 10 Gy: 3.04 ± 0.35, 20 Gy: 2.87 ± 0.47 (*P* < 0.01); SW620: 0 Gy: 2.22 ± 0.42, 5 Gy: 2.47 ± 0.59, 10 Gy: 2.10 ± 0.55, 20 Gy: 1.76 ± 0.45 (*P* < 0.05), *n* = 6 per group). A significant negative correlation can be noted between radiation dose and [¹⁸F]FLT uptake in both tumors (SW480: *r* = -0.727, *P* = 0.004, SW620: *r* = -0.664, *P* = 0.009). [¹⁸F]FDG uptake is also reduced, but to a lesser extent. Hence, again [¹⁸F]FLT seems to be superior to [¹⁸F]FDG for detection of response to radiotherapy [187].

In a pilot study two subcutaneous U251 glioma xenografts were irradiated with 16 Gy and [¹⁸F]FLT accumulation is decreased after one or two weeks (after 2 wk: -23 % and -64 % change). This is in concordance with decreased Ki67 staining [188].

During fractionated radiotherapy, tumor cells acquire increased capacity to regenerate, a phenomenon called “repopulation”. In human FaDu squamous cell carcinoma (SCC) daily irradiation for 12 or 18 days leads to reduced Ki67 and BrdU labeling at the end of treatment (BrdU labeling index: non-irradiated: 27.18 %, 12 f/12 d: 20.25 %, $P = 0.035$; 18 f/18 d: 11.18 %, $P < 0.001$), accompanied by reduced [¹⁸F]FLT uptake in the tumors (SUV_{max}: non-irradiated: 7.47, $n = 11$, 12 f/12 d: 3.61, $P < 0.001$; 18 f/18 d: 2.74, $P < 0.001$, $n = 5-8$ per irradiated group). When the same number of radiotherapy fractions is given in 2 d intervals, histological staining of tumor proliferation is indistinguishable from untreated tumors (BrdU : 12 f/24 d: 19.96 %, $P = 0.098$; 18 f/36 d: 26.63 %, $P = 1.000$), implying successful repopulation. Also [¹⁸F]FLT uptake is comparable to untreated tumors (SUV_{max}: 12 f/24 d: 7.03, $P = 1.000$, 18 f/36 d: 6.84, $P = 0.726$, $n = 5-8$ per group), indicating that [¹⁸F]FLT can visualize repopulation of tumors after fractionated radiotherapy. In this experimental approach [¹⁸F]FLT uptake (SUV_{max}) significantly correlates with Ki67 ($r^2 = 0.689$, $P < 0.001$) and BrdU ($r^2 = 0.779$, $P < 0.001$) labeling indices [189].

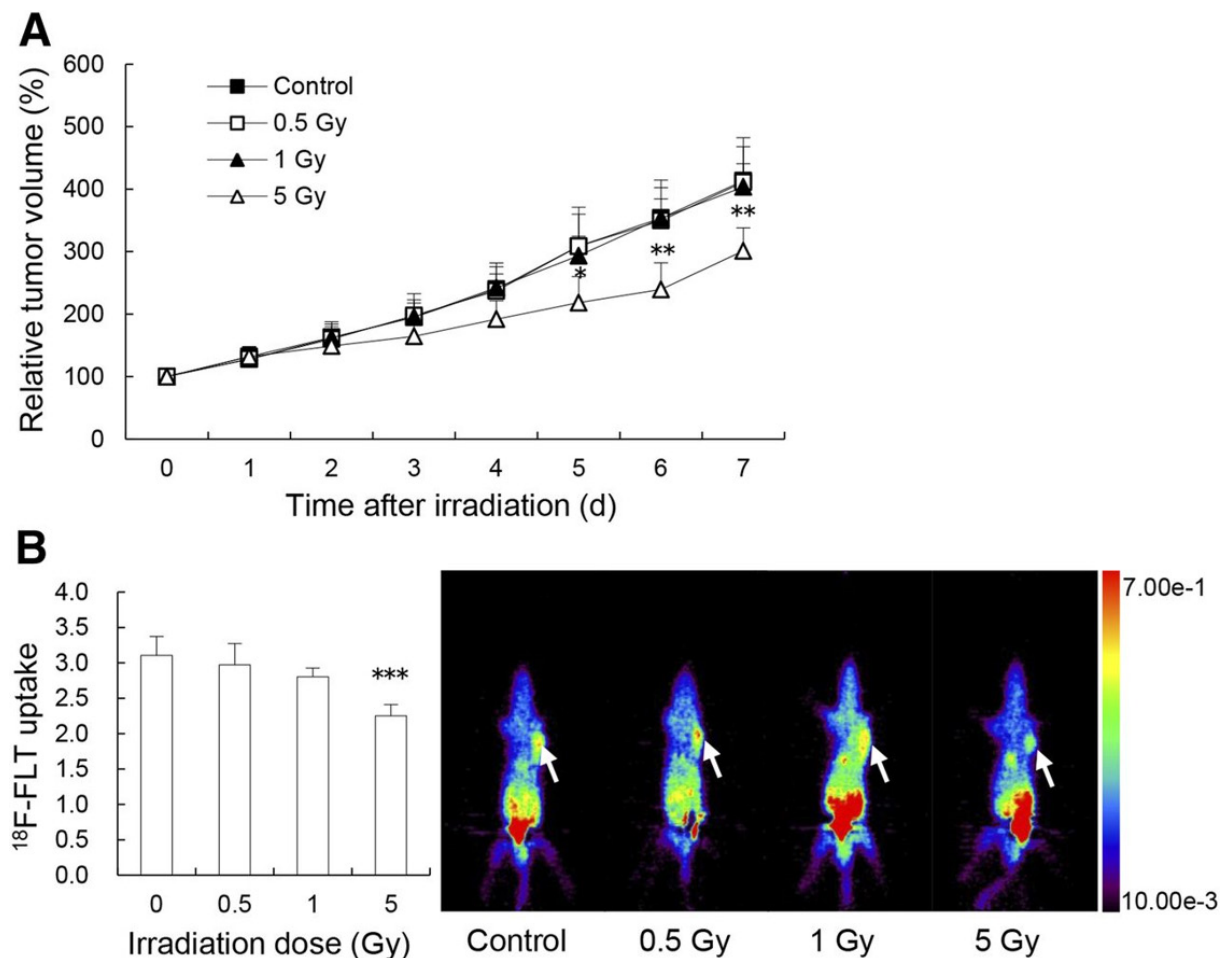
When subcutaneous A549 lung adenocarcinoma are irradiated with 20 Gy, [¹⁸F]FLT uptake is significantly reduced subsequently (%ID/g determined by well type detector: untreated control: 1.41 ± 0.38 , d1: $0.71 \pm 0.08^*$, d2: $0.33 \pm 0.07^*$, $n = 3$ per group; T/B: baseline: 3.3 ± 0.5 , d1: 1.7 ± 0.3 , d2: 1.2 ± 0.2 , $P < 0.05$, $n = 3$ per group). Again, [¹⁸F]FDG is unchanged [190].

Also in subcutaneous Eca-109 esophageal carcinomas [¹⁸F]FLT uptake decreases in response to radiotherapy (single dose of 10 Gy, T/B: baseline: 2.24 ± 0.06 , d1: 1.99 ± 0.09 , d7: 1.85 ± 0.04 , d15: 1.15 ± 0.10 , all $P < 0.05$ relative to baseline, $n = 6$). This correlates with reduced proliferation as determined by Ki67 and PCNA immunohistochemistry (labeling index PCNA: baseline: $60.0 \% \pm 3.6 \%$, d1: $47.5 \% \pm 2.1 \%$, d7: $40.5 \% \pm 3.7 \%$, d15: $35.3 \% \pm 3.9 \%$, $P < 0.05$; $r = 0.83$, $P < 0.001$; labeling index Ki67: baseline: $83.3 \% \pm 2.5 \%$, d1: $55.3 \% \pm 2.5 \%$, d7: $41.5 \% \pm 3.1 \%$, d15: $27.5 \% \pm 2.1 \%$, $P < 0.05$; $r = 0.88$, $P < 0.001$) [191].

A resistant and a sensitive nasopharyngeal squamous cell carcinoma cell line (CNE1 and CNE2) were employed to evaluate [¹⁸F]FLT changes 1 d after radiotherapy (15 Gy) in subcutaneous xenograft mouse models. [¹⁸F]FLT uptake in the radiosensitive CNE2 tumor is significantly decreased (T/M CNE2 before: 5.57 ± 1.30 , d1: 3.59 ± 1.06 , $P < 0.01$), whereas uptake in the resistant CNE1 model is unaltered ($n = 6$ per group). A significant correlation between changes in tracer uptake and changes in tumor volumes is apparent (Pearson correlation coefficient = 0.849, $P = 0.002$). Hence, in this study radiotherapy-induced changes in [¹⁸F]FLT uptake are specific for responsive tumors [192].

In addition to conventional radiotherapy with x-rays, charged particle therapy can also be employed for the treatment of tumors. In a study by Lin et al. proton and carbon therapy were applied in parallel to x-ray therapy to treat subcutaneous mouse colon 26 tumors in mice. Caliper measurements show that tumor growth is significantly retarded 4 d after proton irradiation, 3 d after carbon ion irradiation, and 5 d after x-irradiation, whereas [¹⁸F]FLT PET shows a signal decrease already on d1 (x-irradiation: 5 Gy: $P < 0.001$; proton irradiation: 0.5 Gy: $P < 0.01$, 1 Gy: $P < 0.001$, 5 Gy: $P < 0.001$; carbon ion irradiation: 0.5 Gy: $P < 0.05$, 1 Gy: $P < 0.01$, 5 Gy: $P < 0.001$; no absolute numbers provided, **Supplementary Fig. S5**). Since early changes in [¹⁸F]FLT parallel changes in tumor volume after irradiation with different

doses of various sources, [^{18}F]FLT PET is able to predict treatment response in this study. Additionally, [^{18}F]FLT is also reduced in respective *in vitro* experiments [193].



Supplementary Fig. S5: After radiotherapy changes in [^{18}F]FLT can be noted earlier than changes in tumor volume. After irradiation of colon 26 xenografts on d0, tumor volumes are significantly impaired 5 d after 5 Gy irradiation (A). This treatment causes reduced [^{18}F]FLT uptake already on d1. In line with unaltered tumor growth, [^{18}F]FLT is not changed with lower x-ray doses. *: $P < 0.05$, **: $P < 0.01$, ***: $P < 0.001$ relative to control group. This research was originally published in J Nucl Med [193].

[^{18}F]FLT also decreases in sensitive tumors after radiotherapy in other species. In two subcutaneous rat tumor models [^{18}F]FLT uptake is reduced following radiotherapy (change of SUV relative to before treatment: rhabdomyosarcoma: untreated control: $+12.45\% \pm 3.87\%$, $n = 14$; 15 Gy: $-20.0\% \pm 3.3\%$, $n = 8$; 20 Gy: $-33.6\% \pm 3.8\%$, $n = 9$, $P < 0.001$; 9L-glioma: untreated group: $13.3\% \pm 4.78\%$, $n = 15$; 40 Gy: $-10.2\% \pm 4.22\%$, $n = 10$, $P < 0.01$). The change in [^{18}F]FLT SUV significantly correlates with tumor growth delay (Pearson's r rhabdomyosarcomas: 0.76, $P < 0.0001$; 9L-gliomas: 0.35, $P < 0.05$) [194].

A case report describes repetitive imaging of a fibrosarcoma-bearing dog that undergoes radiotherapy (10 fractions, 4.5 Gy). [^{18}F]FLT is significantly decreased (SUV_{max}: before: 4.97, after 22.5 Gy: 3.68, after 45 Gy (completion of therapy): 3.72, 10 weeks after completing radiotherapy: 1.21; SUV_{mean}: before: 1.58, after 22.5 Gy: 1.75, after 45 Gy: 1.52, 10 weeks after completing radiotherapy: 0.87), along with decreased uptake of [^{18}F]FDG [195]. In a different study, a cohort of 22 canine patients with spontaneous sinonasal tumors underwent radiotherapy with 4.5 Gy or 5 Gy for 10 d and [^{18}F]FLT PET was carried

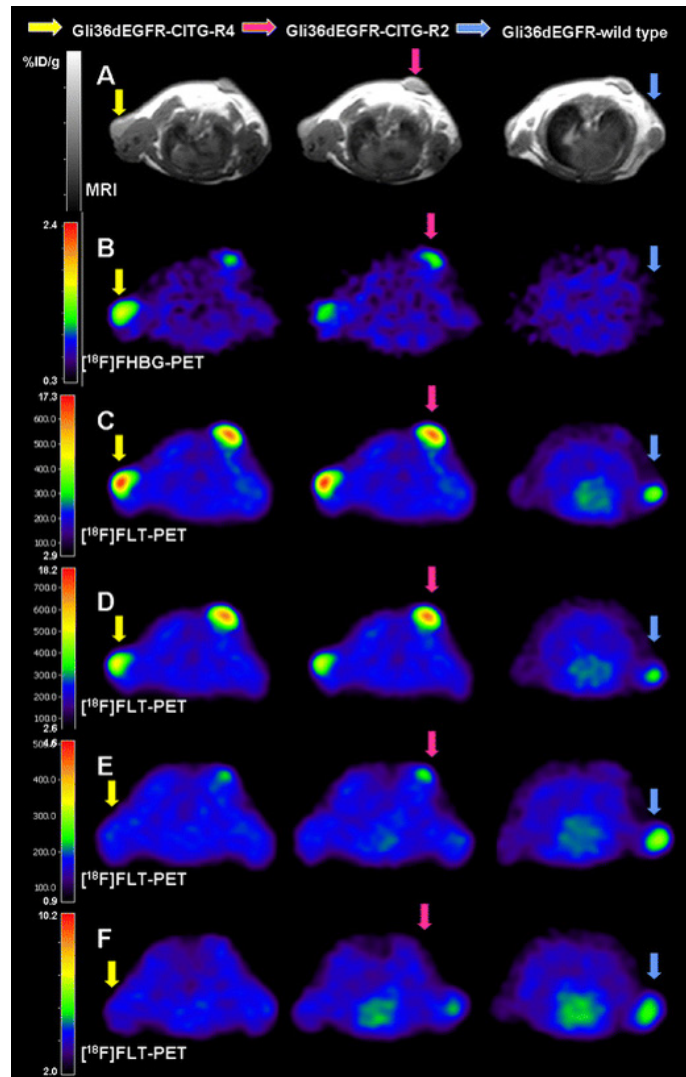
out after 2 doses. Univariable Cox proportional hazard regression shows that high [^{18}F]FLT SUV_{mean} ($P = 0.018$) and high [^{18}F]FLT SUV_{max} ($P = 0.006$) are significant predictors of worse outcome. On the other hand, an increase of [^{18}F]FLT SUV_{mean} relative to a pretreatment scan is positively associated with worse clinical outcome ($P = 0.013$). The authors speculate that the latter would be consistent with a theory that tumors with pronounced responses at the beginning of treatment would be more likely to regrow rapidly following radiation therapy, resulting in shorter progression-free intervals. In these dogs, no relations are detectable for [^{18}F]FDG [196].

Taken together, all these fifteen publications demonstrate that changes in [^{18}F]FLT uptake are reflecting changes in proliferation in response to radiation therapy, not only in rodents but also in canines. Furthermore, five of these studies show that [^{18}F]FLT appears to be superior to [^{18}F]FDG in the detection of radiotherapy response.

3.6 Imaging of response to other therapy approaches

3.6.1 Gene therapy

Gene therapy aims at specifically delivering therapeutic genes into targeted cells. These genes are supposed to aid in healing the respective disease. In case of cancer therapy, tumor cell death is the major aim. For example, Rueger et al. genetically manipulated Gli36dEGFR glioma cells so that they express therapeutically active genes (herpes simplex virus type 1 thymidine kinase (HSV-1-TK) and / or *Escherichia coli* cytosine deaminase (*E. coli* CD)). *In vivo* expression of HSV-1-TK can be demonstrated by [^{18}F]FHBG (9-[4-[^{18}F]fluoro-3-(hydroxymethyl)butyl]guanine) PET. Subsequent therapy with the appropriate prodrugs (i.e. ganciclovir for HSV-1-TK, 5-fluorocytosine for *E. coli* CD) results in successful glioma cell killing *in vivo* (significant reduction in tumor growth on d3 when both therapeutic genes are expressed, $P < 0.001$). On the third day of therapy [^{18}F]FLT is reduced significantly as compared to baseline (**Supplementary Fig. S6**) ($P = 0.015$ for R2 (low expression of both genes), $P = 0.006$ for R4 (high expression of both genes), $n = 3-6$ per group). Similar results can be obtained when only HSV-1-TK is expressed. [^{18}F]FLT uptake correlates with tumor growth rates ($r = 0.95$, $P < 0.001$) and therapeutic gene expression ([^{18}F]FHBG PET, $r = -0.81$, $P = 0.025$). Thus, [^{18}F]FLT appears to be a promising candidate for the evaluation of the outcome of anti-proliferative gene therapy approaches (**Supplementary Fig. S6**) [197].



Supplementary Fig. S6: [¹⁸F]FLT is capable of visualizing the treatment effect of a gene therapy approach employing HSV-1-TK and *E. coli* CD (CITG). Subcutaneous Gli36dEGFR gliomas encoding high (R4) and low (R2) amounts of CITG were treated by daily ganciclovir and 5-fluorocytosine administration. Wildtype gliomas served as control. (A) Tumors in the shoulder region can be delineated on MR images before therapy initiation. (B) [¹⁸F]FHBG reveals expression of the transgene HSV-1-TK in the transduced cells. [¹⁸F]FLT at baseline (C), on d1 (D), d3 (E), and d7 (F) of prodrug therapy shows a remarkable reduction of tumor proliferation in CITG expressing tumors, which is significant on d3 onward compared to baseline accumulation. With permission of Springer © Academy of Molecular Imaging and Society for Molecular Imaging 2010 [197].

Genetic manipulation of tumor cells *ex vivo* is an approach that cannot be translated to the clinical situation. However, transgenes can also be delivered directly into tumor tissue, e.g. with the help of viral vectors. Jacobs et al. successfully applied replication-conditional HSV-1 viruses in subcutaneous U87dEGFR tumors and show that expression of the transgene HSV-1-TK can readily be imaged by 2-[¹²⁴I]-fluoro-5-iodo-1-beta-D-arabinofuranosyl-uracil ([¹²⁴I]FIAU) PET [198]. In another study performed by this group, replication-deficient HSV-1 amplicon vectors coding for the same therapeutic genes as above (HSV-1-TK and *E. coli* CD) were directly injected into subcutaneous Gli36dEGFR gliomas. In that study, [¹⁸F]FLT PET is helpful in identifying the viable tumor tissue that could benefit from the therapy. Growth of most of the 22 tumors analyzed is retarded after respective prodrug therapy (4 complete responders (complete remission), 11 partial responders (28 % ± 16 % growth compared to control)).

PET imaging was performed in 11 of these mice on d4. Of these, 8 tumors respond to treatment in terms of [¹⁸F]FLT accumulation (%ID/g: control: 1.91 ± 1.12 , $n = 22$, transgene expression: 0.42 ± 1.31 , $P < 0.01$). [¹⁸F]FLT reduction correlates with expression of therapeutic genes ([¹⁸F]FHBG PET, $R = 0.73$, $P < 0.01$). In the responding tumors [¹⁸F]FLT decrease correlates with reduction in tumor volume ($R = 0.83$) [199].

In another gene therapy approach, squamous cell carcinoma of the head and neck (1483 SCCHN) were treated with EGFR antisense DNA. The plasmid DNA was injected directly into the tumor (5 d a week for 20 d). Compared to sense control tumors in the same mouse, tumor volumes in the antisense treated tumors are reduced in 4 out of 6 mice. This is accompanied by reduced Ki67 staining ($P = 0.0001$). The authors also report a reduction of [¹⁸F]FLT uptake after completion of therapy which they express as total proliferative volume (= total tumor volume x mean tumor SUV, antisense vs. sense: $P = 0.09$). However, it is not clear if the SUV of the tumor is altered at all as the reported PET results could have been primarily determined by the observed changes in tumor volume [200].

3.6.2 Oncolytic virotherapy

In some experimental therapy approaches replicating viruses are used to destroy tumor cells. Genetic manipulation of these viruses can aid in specifically targeting tumor tissues. Kuruppa et al. injected replication-conditional HSV-1 mutants into mouse MC26 colon cancer xenografts. Viral replication occurs in waves as shown by imaging of the firefly luciferase encoded by the virus. Application of the virus results in a reduction in tumor growth and induces necrosis in the core as shown by immunohistochemistry. 48 h after virus application [¹⁸F]FLT PET is capable of showing this spatial heterogeneities in tumors and signal intensity appears to be reduced. However, no quantification of [¹⁸F]FLT PET imaging data was reported and it is not clear if overall tumor uptake of tracer is related to treatment response [201].

Leyton et al. employed an adenovirus mutant for therapy of IGROV1 ovarian cancer xenografts. 2 d after intratumoral application of the virus [¹⁸F]FLT is reduced only marginally. However, a significant reduction can be observed at d7 (NUV₆₀: no treatment: 1.12 ± 0.08 , 2 d control virus (Ad LM-X): 1.24 ± 0.13 , 2 d modified virus (d/922-947): 0.98 ± 0.07 , 7 d control virus: 1.02 ± 0.13 , 7 d modified virus: 0.49 ± 0.12 ($P = 0.04$ relative to control virus), $n = 4$ per group, similar results were obtained for AUC and FRT). [¹⁸F]FLT uptake correlates with Ki67 ($r^2 = 0.893$) and TK1 ($r^2 = 0.936$) expression [202].

3.6.3 Photodynamic therapy

Photodynamic therapy (PDT) is performed by injecting a photosensitizer that accumulates preferentially in the tumor. Subsequent illumination with light with a specific wavelength induces the production of reactive oxygen that kills cells in the environment of the photosensitizer. 24 h after application of PDT in HeLa xenografts the PCNA labeling index (control: 83.2 ± 8.6 , PDT: 13.5 ± 12.7 , $P < 0.05$) as well as [¹⁸F]FLT accumulation (%ID/g: control: 11.1 ± 1.3 , $n = 4$, PDT: 4.0 ± 2.2 , $n = 4$, $P < 0.05$) are significantly reduced, whereas [¹⁸F]FDG uptake is unchanged. Hence, in this setting, reduction in [¹⁸F]FLT might be a promising biomarker for monitoring the anti-proliferative response to PDT [183].

3.6.4 Androgen depletion

Many prostate cancers depend on androgen. Hence, depletion of androgen can provide a therapeutic benefit. This can be performed by surgical castration or therapy with antiandrogens such as diethylstilbestrol. Both of these therapy approaches result in volume reduction in human CWR22 prostate cancer xenografts, accompanied by reduced [^{18}F]FLT uptake (T/M: control: baseline: 2.50 ± 0.61 , 1 wk: 2.30 ± 0.75 , 2 wk: 2.62 ($n = 2$), 3 wk: no mouse survived; diethylstilbestrol: baseline: 3.55 ± 0.59 , 1 wk: 1.31 ± 0.29 ($P = 0.01$), 2 wk: 1.49 ± 0.33 , 3 wk: 1.61 ± 0.49 ; castration: baseline: 2.52 ± 0.21 , 1 wk: 0.87 ± 0.29 ($P = 0.01$), 2 wk: 1.00 ± 0.20 , 3 wk: 1.00 ± 0.13) [203]. In two other prostate cancer models the therapeutic effect of castration is better visualized by [^{18}F]FDG than by [^{18}F]FLT (%ID/ml [^{18}F]FLT: CWR22: baseline: 1.38 ± 0.65 , $n = 17$, 3 wk after castration: 1.16 ± 0.65 , $n = 9$; PAC120: baseline: 1.13 ± 0.75 , $n = 15$, 2 wk after castration: 1.99 ± 0.75 , $n = 8$, $P = 0.015$). Failure of [^{18}F]FLT to predict treatment outcome is most likely related to low tracer uptake in these tumors at baseline [75].

3.6.5 Metformin

The antidiabetic compound metformin activates adenosine monophosphate-activated protein kinase, which inhibits the mTORC1 pathway, hence impeding energy-consuming processes such as DNA proliferation and protein synthesis. On the other hand it also activates ATP producing processes like glucose uptake. Treatment of two colorectal cancer models (human HT29 and murine MC26) results in increased *in vitro* uptake of [^{18}F]FDG and reduced [^{18}F]FLT after 24 h (% of initially added [^{18}F]FLT activity: HT29: control: 4.46 ± 0.07 , 0.1 mM MET: 3.02 ± 0.11 , $P < 0.001$, 1 mM MET: 4.19 ± 0.14 , $P < 0.001$, 10 mM MET: 2.63 ± 0.06 , $P < 0.0001$; MC26: control: 1.01 ± 0.03 , 0.1 mM MET: 0.92 ± 0.02 , $P < 0.01$, 1 mM MET: 0.82 ± 0.04 , $P < 0.001$, 10 mM MET: 0.40 ± 0.02 , $P < 0.0001$), consistent with a reduced percentage of cells in S-phase (HT29: control: 100.00 ± 1.09 , 10 mM MET: 63.58 ± 1.86 , $P < 0.001$; MC26: control: 100.00 ± 1.41 , 10 mM MET: 66.10 ± 0.96 , $P < 0.001$). A similar decrease in [^{18}F]FLT can also be noted after 24 h *in vivo* in subcutaneous HT29 tumors (SUV_{mean} : baseline: 1.18 ± 0.05 , 24 h: 0.89 ± 0.01 , $P < 0.05$, $n = 3$), whereas [^{18}F]FDG is increased. Hence, [^{18}F]FLT is a good alternative to [^{18}F]FDG when monitoring treatment response to agents altering glucose metabolism [204].

3.6.6 Interleukin-22

Interleukin-22 (IL-22) is a cytokine that mediates cellular inflammatory responses. It stimulates signaling pathways that are key players in the regulation of cell growth and proliferation. Weber et al. describe a murine mammary carcinoma cell line (EMT6) that expresses functional receptors for IL22. *In vitro* treatment of these cells with recombinant IL-22 induces a G₂/M-phase cell cycle arrest and *in vivo* treatment inhibits growth of the respective xenografts. This is accompanied by reduced [^{18}F]FLT accumulation in the tumors after 7 d treatment as demonstrated by *ex vivo* gamma counter measurements (%ID/g: vehicle control: 5.46 ± 0.34 , recombinant IL-22: 3.02 ± 0.42 , $P < 0.01$, $n = 6$) [205].

3.6.7 Immunotherapy

Buck et al. imaged the effect of immunotherapy on [^{18}F]FLT uptake in DoHH2 B-cell follicular lymphoma xenografts. They employed the CD20 targeting monoclonal antibody ibritumomab coupled to the chelator tiuxetan. The latter allows labeling with the radionuclide [^{90}Y] for radioimmunotherapy (see 3.4.19). The antibody binds to the CD20 antigen on the surface of B-cells and induces antibody-dependent cell-mediated cytotoxicity and apoptosis. 48 h after therapy a mild but significant reduction in Ki67 labeling can be detected in the analyzed xenografts (%Ki67: control: 83.6 ± 3.2 , treated: 77.6 ± 4.8 , $P = 0.0078$). A significant reduction of [^{18}F]FLT uptake cannot be observed (%ID/g: control: 5.4, treated: 3.9 ± 2.0 , $n = 10$ each). The authors speculate that this could owe to tumor heterogeneity. Furthermore, they hypothesize that in this setting later imaging time points could be more promising since monoclonal antibodies exert a delayed cytotoxic effect [81].

A clinical pilot trial shows that early after immunotherapy one might visualize a flare reaction with [^{18}F]FLT. Aarntzen et al. demonstrate increased [^{18}F]FLT uptake in lymph nodes injected with a dendritic cell vaccine for melanoma. This increased uptake is due to accumulation of the tracer in activated highly proliferative lymphocytes [206] (see also 3.2.2).

3.7 Imaging of response to combination therapies

In clinical practice a combination of different treatments is often applied as most single agents fail to induce the required response or rapidly lead to the development of resistance. Even though the use of single agents in a preclinical setting might help in evaluating the effect of a specific therapy on tracer uptake, like induction of TK1, imaging of combined therapies might be more informative for the clinical application of the agents.

3.7.1 Combinations of chemotherapeutic drugs

The combination of carboplatin and paclitaxel is a frequently used treatment paradigm in the clinical situation. The application of the two chemotherapeutic agents in A2780 ovarian cancer xenograft models results in impaired growth of the tumors. Jensen et al. demonstrate that [^{18}F]FDG and [^{18}F]FLT both detect therapy response. However, timing of imaging appears to be crucial. [^{18}F]FDG is decreased at later time points but reduction is more prolonged ([^{18}F]FDG % change of SUV_{max} relative to baseline: d4: control: 138 ± 9 , treated: 105 ± 4 , $P = 0.002$; d8: control: 167 ± 13 , treated: 125 ± 13 , $P = 0.05$, $n = 4$ per group). [^{18}F]FLT is non-significantly reduced early (d1) and transiently ([^{18}F]FLT % change of SUV_{max} relative to baseline: control: 109 ± 6 , treated: 89 ± 9 , $P = 0.08$; SUV_{mean} ratio: control: 113 ± 5 , treated: 96 ± 6 , $P = 0.05$, $n = 4$ per group). A missing reduction of [^{18}F]FLT uptake on d4 and d8 could be due to the gap between administration of the therapeutic agents (d0 and d5) and imaging, hence allowing the tumor cells to recover their proliferative capacity. The hypothesis that proliferation inhibition could last for less than 3 d is confirmed by unchanged Ki67 and TK1 immunohistochemical staining on d8 [207]. Katz et al. applied a different combination of a taxane with platinum. The combination of docetaxel and cisplatin exerts an anti-tumor effect but it induces only a marginal (and non-significant) reduction of [^{18}F]FDG (change of T_{max}/M : $-21 \% \pm 36 \%$, $P = 0.30$) in the Calu-6 NSCLC model investigated. [^{18}F]FLT is unaltered after 3d ($-2 \% \pm 7 \%$, $P = 0.67$, $n = 4$), consistent with unchanged Ki67. The authors report

that the analyzed Calu-6 tumor lacks functional p53. When DNA is damaged, p53 can mediate the down-regulation of TK1 followed by the inhibition of cell cycle progression. Hence, in p53 mutant cells, cell cycle progression is decoupled from TK1 activity, which could explain the lack of [¹⁸F]FLT reduction in response to the DNA damaging agents applied here [208]. The importance of p53 status for [¹⁸F]FLT uptake has also been described in another study [32].

Trifluridine/tipiracil (Lonsurf, TAS-102) is a combination of a TS inhibitor and a TP inhibitor impairing degradation of trifluridine. *In vitro* an increased uptake of [¹⁸F]FLT can be observed 0 h, 2 h and 24 h after 2 h incubation with trifluridine/tipiracil in colorectal HCT116, HT29, SW620 and HCT8 cells. 2 h after drug administration [¹⁸F]FLT accumulation is significantly increased in subcutaneous HT29 xenografts (SUV baseline vs. 2 h: vehicle: 0.86 ± 0.18 vs. 1.01 ± 0.50 , 30 mg/kg trifluridine/tipiracil: 0.91 ± 0.08 vs. 1.88 ± 0.67 ; 150 mg/kg trifluridine/tipiracil: 1.06 ± 0.20 vs. 1.65 ± 0.80 ; $P < 0.001$, $n = 6$ per group). A similar effect can be seen in SW620 xenografts 2 h and 8 d after daily administration of trifluridine/tipiracil, although results are less pronounced and not significant at the latter time point (absolute numbers not provided). *Ex vivo* studies show that Ki67 is unaltered at d8 and d15 of therapy with 150 mg/kg trifluridine/tipiracil. TK1 expression is increased as determined by western blot, whereas TK1 activity is only mildly elevated ($P = 0.12$, $n = 3$ per group) [209].

3.7.2 Combinations of targeted therapies

Haagensen et al. applied the MEK inhibitor PD 0325901 or the PI3K inhibitor GDC-0941 or a combination of these two agents in HT29 and HCT116 colorectal cancer xenograft-bearing mice. Both agents are able to reduce the growth of tumors, and a combination of both drugs is even more effective. Two days after treatment initiation [¹⁸F]FLT uptake in HCT116 tumors treated with a combination of the two drugs is significantly reduced (decrease of 18 % compared to baseline, $P < 0.005$, $n = 5-7$ mice per group). The single agents do not cause a change of [¹⁸F]FLT uptake [210]. This is in contrast to previous studies showing reduced [¹⁸F]FLT accumulation in responsive MEK- or PI3K-inhibited tumors [141,155,156,162]. However, these latter studies employed much higher inhibitor concentrations, which would not be tolerated in a combination treatment as used in this study.

Rituximab (Rituxan) is an antibody targeting CD20, which is frequently overexpressed in B-cell non-Hodgkin lymphomas (B-NHL). In these lymphomas increased expression of the anti-apoptotic protein survivin is typically observed. Interference with either CD20 or survivin inhibits growth of lymphomas. In three different B-NHL xenograft models (DB, WSU-DLCL-2, and Mino) the combination of these agents is more effective than either agent alone, as demonstrated by tumor growth inhibition and reduction of Ki67 staining. [¹⁸F]FDG as well as [¹⁸F]FLT are both able to detect this treatment effect 3 d after therapy initiation ([¹⁸F]FLT SUV_{max} in WSU-DLCL-2 change from baseline: control: 1.01 ± 0.04 , YM155: 0.69 ± 0.10 , $P < 0.05$ vs. control, rituximab: 0.97 ± 0.08 , combination: 0.62 ± 0.04 , $P < 0.01$ vs. control, $P < 0.05$ vs. rituximab monotherapy, $n = 4$ per group) [211].

BMS-754807 is an inhibitor of insulin-like growth factor-1 (IGF-1R) and insulin receptor (IR) with additional off-target activities e.g. against c-MET and aurora kinases. It synergizes with the EGFR inhibitor gefitinib *in vitro* with respect to anti-tumor activity. BMS-754807 increases the tumor growth-inhibitory efficacy of gefitinib in an H292 NSCLC xenograft model, whereas the drug alone exerts no effect. [¹⁸F]FLT is able to detect the combined effect of the two drugs after only 3 days of treatment

(SUV_{mean} d0 vs. d3: vehicle: 0.28 ± 0.13 vs. 0.49 ± 0.08 , $P < 0.01$, $n = 6$; combination: 0.51 ± 0.17 vs. 0.26 ± 0.15 , $P < 0.001$, $n = 6$; no difference can be observed with the respective single agent therapies). Even though it is also reduced upon the combination therapy, Ki67 staining is not in complete concordance with [¹⁸F]FLT accumulation, since it is also significantly reduced upon single agent gefitinib treatment. The authors speculate that this may be attributed to the fact that Ki67 is expressed during the entire mitotic process, whereas expression of TK1 is more timely regulated [212].

In Calu-6 xenografts a combined targeted therapy of TRAIL and sorafenib was applied by Katz et al. The therapy induces only a marginal reduction of [¹⁸F]FDG (change of T_{max}/M: $-8 \% \pm 36 \%$, $P = 0.59$), whereas [¹⁸F]FLT is significantly reduced on d3 post treatment ($-30 \% \pm 8 \%$, $P = 0.03$, $n = 4$). Hence, [¹⁸F]FLT appears to be superior to [¹⁸F]FDG in predicting therapy response to this therapeutic approach [208].

In Colo205 colorectal xenograft-bearing mice a combination of the BRAF inhibitor PLX4720 and the PI3K inhibitor BEZ235 results in decreased [¹⁸F]FLT uptake in the tumors on d4 of therapy (i.e. 1 d after the last treatment, $P = 0.0087$), whereas either agent alone does not alter accumulation of this tracer. Here, [¹⁸F]FLT reflects TK1 protein levels, whereas general proliferation, as assessed by Ki67 immunohistochemistry, is decreased with all therapeutic approaches applied. This study also comprises extensive *ex vivo* and *in vitro* analyses of further cell signaling events, demonstrating that [¹⁸F]FLT reflects the cellular processes altered by the drugs. Unfortunately, this study does not provide evidence that these changes ultimately lead to changes in tumor progression [128].

3.7.3 Combinations of chemotherapeutic and targeted agents

Cho et al. combined three different agents in a specific form of micelle: paclitaxel (cytotoxic agent), cyclopamine (hedgehog inhibitor) and gossypol (Bcl-2 inhibitor). When applied in ES-2 or SKOV3 ovarian tumor-bearing mice growth of tumors is severely inhibited compared to control mice and also compared to mice treated with micelles loaded with paclitaxel only. Treatment efficacy can nicely be demonstrated by bioluminescence imaging of luciferase-expressing tumors and by [¹⁸F]FLT PET of intraperitoneal ES-2 xenografts. Uptake of the radiotracer is significantly reduced on d17, but not on d7 (SUV_{mean} relative to baseline: vehicle: 263 %, paclitaxel: 164 %, 3-drug micelles: 86 %, $P < 0.01$ relative to control, $n = 4$ per group) [213].

Two different orthotopic glioma xenografts in rats (U87 and U251) were treated with temozolomide (TMZ) and / or bevacizumab. Bevacizumab alone has a minimal treatment effect, whereas treatment with TMZ or a combination of these two agents results in significant reduction of tumor volume, accompanied by reduced Ki67 staining. PET on d5 reveals reduced uptake of [¹⁸F]FDG and [¹⁸F]FLT in both tumor types ([¹⁸F]FLT SUV_{mean} on d5: U87: control: 0.93 ± 0.09 , $n = 7$, bevacizumab: 0.83 ± 0.13 , $n = 6$, TMZ: 0.47 ± 0.12 , $n = 6$, $P < 0.001$ vs. control, $P < 0.05$ vs. bevacizumab; combination: 0.36 ± 0.10 , $n = 6$, $P < 0.001$ vs. control, $P < 0.01$ vs. bevacizumab; U251: control: 0.66 ± 0.45 , $n = 5$, bevacizumab: 0.38 ± 0.25 , $n = 8$, TMZ: 0.24 ± 0.13 , $n = 8$, combination: 0.18 ± 0.11 , $n = 7$, $P < 0.05$ vs. control and bevacizumab). Furthermore, tracer uptake correlates with overall survival ([¹⁸F]FLT: U87: $R^2 = 0.42$, $P = 0.0007$, U251: $R^2 = 0.55$, $P < 0.0001$; [¹⁸F]FDG: U87: $R^2 = 0.38$, $P = 0.0016$, U251: $R^2 = 0.09$, not significant). Correlations as well as changes in tracer uptake are more pronounced with

[¹⁸F]FLT than [¹⁸F]FDG. Hence, the latter appears to be less predictive for therapy response in these models [214].

In a different study performed by the same group, the combination of the same two agents was employed to monitor the response of a recurrent intracranial glioblastoma model in rats (U251 cells). After treatment with TMZ for 5 d, regrowth of the tumor can readily be detected about 4 weeks later as determined by MRI. At this time point, a combined therapy of TMZ and bevacizumab or either agent alone was applied for 5 d. [¹⁸F]FDG PET was performed on d 4 and [¹⁸F]FLT PET on d 5 after the end of therapy. 2 weeks after the end of treatment, MRI tumor volumes reveal that the combination treatment is more effective than either treatment alone. Even though numerical values are not reported, the authors describe a reduction of [¹⁸F]FLT in treated tumors (control: $n = 5$, bevacizumab: $n = 4$, TMZ: $n = 6$, combination: $n = 7$, $P < 0.001$ vs. control, $P < 0.05$ vs. TMZ), which is consistent with the number of Ki67 positive cells (cells per mm²: control: 318 ± 48 ; bevacizumab: 193 ± 50 , $P < 0.05$ vs. control; TMZ: 291 ± 37 , combination: 91 ± 35 , $P < 0.01$ vs. control, $P < 0.001$ vs. TMZ). There is a negative correlation between [¹⁸F]FLT uptake and overall survival ($R^2 = 0.48$, $P = 0.0029$). No change in [¹⁸F]FDG uptake could be detected [215].

PXD101 (a histone deacetylase inhibitor) and irinotecan were applied in an HCT116 colon cancer xenograft model. Either agent alone inhibits tumor growth, while the combination provokes an even larger effect on tumor growth. On d8, [¹⁸F]FLT uptake is reduced in irinotecan-treated or irinotecan plus PXD101-treated tumors when compared to control tumors (change in SUV_{mean} relative to d0: vehicle: +36.5 %, $P < 0.05$; irinotecan: -55.2 %, $P < 0.05$ relative to d0, $P < 0.01$ relative to vehicle; combination: -63.7 %, $P = 0.0625$ relative to d0, $P < 0.01$ relative to vehicle; $n = 6$ per group). PXD101 alone appears to prevent an increase in tracer uptake as seen with the control tumors. [¹⁸F]FLT imaging results are paralleled by reduced TK1 expression in all treatment groups [216].

The group of Zhang et al. investigated PF-004477736, a checkpoint kinase 1 inhibitor, as a docetaxel-sensitizing agent in a Colo205 colorectal cancer model. Docetaxel activates the spindle checkpoint, which was shown to be abolished by a combination with PF-004477736. This combination is more effective than docetaxel alone in terms of inhibition of tumor growth (determined by caliper measurements and bioluminescence imaging). Anti-proliferative effects of docetaxel are observable by [¹⁸F]FLT PET on d2 and d16. However, this tracer is not able to show the potentiating effect of PF-004477736 (no exact values provided, both $P < 0.01$ relative to vehicle-treated group). The authors explain the missing difference in [¹⁸F]FLT tumor uptake in docetaxel vs. docetaxel plus PF-004477736 treated mice by the fact that the number of cells in S-phase does not differ between the two treatment paradigms [217].

A combination with docetaxel was also applied in a study by Honndorf et al. The MEK1/2 inhibitor selumetinib (AZD6244), docetaxel, and their combination were applied for 7 d in mice bearing subcutaneous HCT116 tumors. Ki67 analysis at the end of treatment shows a reduction of proliferation with all treatment approaches (control: $91 \% \pm 5 \%$, combination: $69 \% \pm 10 \%$, docetaxel: $59 \% \pm 4 \%$, selumetinib: $72 \% \pm 12 \%$), which on the other hand does not reflect the increased treatment efficiency of the combination treatment as determined by volumetric caliper measurements. [¹⁸F]FLT PET imaging was performed at baseline and on d 2, d 5 and d 7 ($n = 8$ per group). An increase in tracer uptake over time can be observed in all treatment groups, except for the control. This is inconsistent with the

observed reduction of Ki67 staining. Both drugs employed have been described to induce cell cycle arrest that could increase TK1 activity (see 3.2.4 for more details). A possible TK1 upregulation could explain an increase in [¹⁸F]FLT uptake that is independent of decreased Ki67 expression. TK1 analysis of the tumors would be needed to prove this hypothesis. In this study also [¹⁸F]FDG failed to show the treatment effects [218].

In a model analyzing lymph node infiltration of intravenously injected SU-DHL-8 diffuse large B-cell lymphoma a combination of sepantronium bromide (YM155, a survivin suppressant), bendamustine (an alkylating agent) and rituximab (an anti CD20 antibody) results in increased survival of mice compared to control mice or to mice treated with either agent alone. This is accompanied by reduced uptake of [¹⁸F]FLT in the lymph nodes (reduction of SUV_{max} in the lymph nodes relative to untreated controls: mandibular: $P < 0.05$, axillary: $P = 0.07$, inguinal: $P < 0.001$, $n = 5$, no numerical values provided) [219]. Fleuren et al. increased the anti-tumor activity of the mTOR inhibitor temsirolimus by combination with cisplatin or bevacizumab in an OS-1 osteosarcoma model. The combination therapies are more effective in inhibiting tumor growth than either agent alone as determined by caliper measurements. [¹⁸F]FLT uptake is also reduced (relative change temsirolimus + cisplatin: d7/d-2: SUV_{mean}: -35 %, SUV_{max}: -33 %; d28/d-2: SUV_{mean}: -33 %, SUV_{max}: -33 %; temsirolimus + bevacizumab: d7/d-2: SUV_{mean}: -36 %, SUV_{max}: -36 %; d28/d-2: SUV_{mean}: -48 % SUV_{max}: -43 %, $n = 2$ per group). Therefore, reduction in [¹⁸F]FLT signal precedes volumetric changes, potentially distinguishing responders from non-responders. On the other hand, Ki67 staining reveals that the number of proliferating cells is significantly reduced in bevacizumab-treated (-26 %, $P = 0.01$) and temsirolimus plus cisplatin-treated (-24 %, $P < 0.03$) tumors. Hence, no direct relation of Ki67 with [¹⁸F]FLT uptake can be observed. The authors hypothesize that this could be caused by the fact that Ki67 labels all cells that are not in G₀-phase whereas [¹⁸F]FLT is supposed to more specifically accumulate in cells in S-phase. Furthermore, dependence of the used cell line on the thymidine *de novo* pathway could hamper a relation of Ki67 with [¹⁸F]FLT. However, due to the low sample size, this study should be treated with caution [220].

Subcutaneous KB-V-1 cervix carcinoma and A2780 ovarian carcinoma were treated with a combination of doxorubicin, cyclosporine A and UIC2 (monoclonal antibody against P-glycoprotein, a multidrug pump). Growth is severely impaired in the treated tumors (caliper measurements significantly differ from d8 and d10 onwards in KB-V-1 and A2780, respectively) and [¹⁸F]FLT accumulation is diminished on d11-d16 after treatment ($P \leq 0.001$ in both tumors). Also [¹⁸F]FDG uptake is reduced. Hence, change in both tracers reflects tumor response to this combination treatment [221].

3.7.4 Combinations with radiotherapy

In the clinical situation chemotherapies and targeted therapies are often combined with radiotherapy. And also preclinical studies investigate this combination with respect to alterations in [¹⁸F]FLT uptake. Treatment response of the kinase inhibitor sorafenib with or without 20 Gy radiotherapy was evaluated in FSall fibrosarcoma tumor-bearing mice (d0 and d1: sorafenib, d2: radiotherapy). [¹⁸F]FLT PET shows that sorafenib exerts an anti-proliferative effect (T/B ratio: d2: control: $+9.5 \% \pm 10.7 \%$, $n = 7$, sorafenib: $-35.9 \% \pm 11.9 \%$, $n = 4$, $P < 0.05$ vs. d0). This effect cannot be increased by additional radiotherapy (d 3: control: $+0.9 \% \pm 9.9 \%$, $n = 7$, sorafenib plus irradiation: $-45.1 \% \pm 10.2 \%$, $n = 4$,

$P < 0.01$ vs. d0), which is in line with similarly reduced Ki67 (untreated: $74.6 \% \pm 7.1 \%$, sorafenib: $45.8 \% \pm 7.4 \%$, $P < 0.05$ relative to untreated, sorafenib plus irradiation: $39.3 \% \pm 6 \%$, $P < 0.05$ relative to untreated) [222].

Irradiation alone or irradiation combined with celecoxib (a cyclooxygenase-2 inhibitor) effectively inhibits tumor growth in two colorectal cancer models. The authors state that [^{18}F]FDG and [^{18}F]FLT accumulation are reduced in the tumors after 3 wk of radiotherapy and the effect is even more pronounced after combination of radiotherapy with celecoxib. However, the authors' conclusion is mostly based on analysis of tracer positive tumor volumes (data not mentioned here), which is not a commonly used method of PET quantification. [^{18}F]FLT tracer uptake itself appears to be little changed in HCT116 and reduced by celecoxib (but not irradiation) in HCA7 ([^{18}F]FLT T_{max}/L (and range): HCT116: control: 2.71 (1.59–5.29), celecoxib: 1 wk: 2.63 (2.4–3.45), 3 wk: n.d., irradiation (25 Gy): 1 wk: 2.46 (2.08–2.82), 3 wk: 2.69 (2.51–4.42), combination: 1 wk: 2.50 (1.86–3.65), 3 wk: 2.58 (1.79–3.86); HCA7: control: 4.29 (1.27–7.78), celecoxib: 1 wk: 3.32 (2.64–4.03), 3 wk: n.d., irradiation (40 Gy): 1 wk: n.d., 3 wk: 4.17 (2.67–7.41), combination: 1 wk: n.d., 3 wk: 3.47 (2.67–4.47); n.d. = not determined). Hence, results of more commonly applied modes of tracer uptake quantification give different results than analysis of tracer positive tumor volumes. The latter is probably primarily confounded by changes in tumor volumes. Caliper measurements alone already show that these are decreased after radiotherapy and combined therapy [223]. Further (statistical) analysis would be needed to draw a definite conclusion from these data. Since the outcome of this study is not clear, the respective data were not included in the quantitative data described in the summary of the changes of [^{18}F]FLT uptake in treated tumors..

Apisarnthanarax et al. applied a combination of radiotherapy (15 Gy) and docetaxel in SEG-1 esophageal adenocarcinoma. Liquid scintillation counter measurements of excised tumor tissue reveals a decline of [^3H]FLT uptake after treatment (d1: -72 %, $P = 0.006$; d2: -75 %, $P < 0.005$; d4: -76 %, $P < 0.005$, $n = 5$ mice per time point). A positive correlation between tracer uptake and Ki67 labeling index is observable ($r = 0.89$, $P < 0.001$). [^{18}F]FLT PET imaging on d2 reproduces the outcome of the *ex vivo* analyses (T/M ratio reduced by -58 %, $n = 2$ only). Preliminary autoradiography results imply a spatial relation of [^{18}F]FLT with Ki67 [224].

3.8 Summary of study designs

3.8.1 Experimental setup

A total of $n = 174$ publications were included in this review. These vary considerably in study design. We included all studies describing the use of [^{18}F]FLT in oncological research, irrespective of therapy approach or model system (*in vitro*, in mice, in rats, in dogs, or in rabbits).

The kinds of treatment differ substantially and the studies were sorted according to treatment. In general, only a limited number of studies further investigated a specific therapy approach. Also therapy protocols differ extensively. For instance, some drugs are given as a single dose, others several days in a row, or in weekly intervals. Upon that, the scheduling of the post treatment [^{18}F]FLT uptake assessment varies from 1 h after therapy to 80 d after start of therapy. Here, we stated the time of analysis after treatment initiation. Of note, this does not shed light on when [^{18}F]FLT analysis was performed with respect to the last drug or radiotherapy dose applied, since therapies were often applied more than once.

In the studies employing animals, the number of tumors analyzed ranges from $n = 1$ to $n = 29$ per group. The sample size of the majority of studies is below 10. We refrained from calculating the absolute number of mice analyzed due to several reasons. Some studies do not report the exact number of animals studied or indicate only a range (e.g. “ $n \geq 4$ ” or “ $n = 6 - 8$ ”). Furthermore, due to the differences in study design (e.g. multiple measurements of a single mouse, measurements of various groups), the number of scans or number of mice analyzed has a different meaning for the different experimental setups. Therefore, calculating the overall sum might be misleading.

Some studies employed more than one tumor model. We identified colorectal cancer as the most often studied tumor model, followed by glioma and lung cancer (**Supplementary Table S1**). Most of the tumors were originating from human tumor tissue and were grown as subcutaneous xenografts when employed *in vivo*.

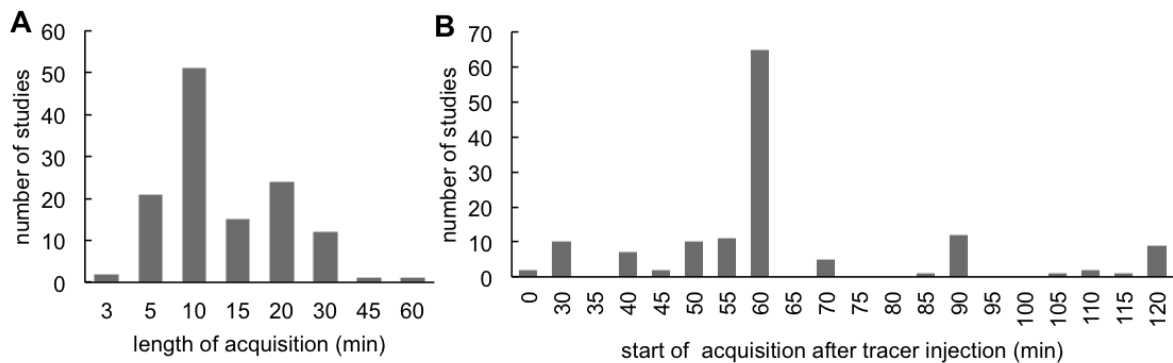
tumor type	number of studies
colorectal cancer	55
glioma	42
lung cancer	38
lymphoma	23
breast cancer	19
squamous cell carcinoma	15
sarcoma	12
ovarian cancer	11
prostate cancer	9
gastric cancer	8
epidermoid cancer	6
melanoma	6
pancreatic cancer	6
liver cancer	4
mesothelioma	3
cervical cancer	2
esophagus cancer	2
nose cancer	2
adrenocortical cancer	1
kidney cancer	1
leukemia	1

Supplementary Table S1. Tumor models investigated within the studies included in this review.

3.8.2 PET acquisition and quantification

The PET imaging studies differ substantially in the mode of [^{18}F]FLT acquisition and quantification. Acquisition times for static imaging in mice and rats vary between 3 min and 60 min, with 10 min being the most commonly used compromise between sufficiently high count numbers and fast imaging

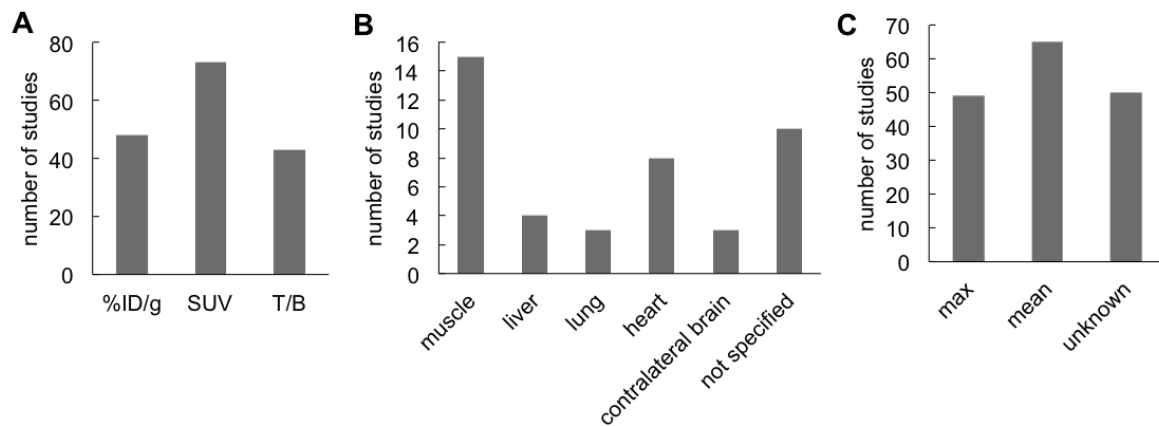
(**Supplementary Fig. S7A**). The majority of studies performed imaging around 60 min (**Supplementary Fig. S7B**). Dynamic scans provide the information that the plateau uptake in general starts at around 60 min, but it can also vary substantially from study to study, see e.g. [14,56,92,107,169]. Therefore, studies acquiring static imaging much earlier than 60 min should be treated with caution if no optimization was performed. Consequently, we recommend that when employing a new model, a dynamic scan should be performed in the beginning to determine the optimal window for static imaging. This might lead to different imaging time windows for different models [36,71].



Supplementary Fig. S7: [¹⁸F]FLT PET acquisition parameters in rodents. These data represent the details of static scans or the parameters of a dynamic scan that were used for static evaluations. (A) The duration of the image acquisition was extracted from the screened publications and presented as bar graph. (B) The time points of acquisition start relative to tracer injection time of static PET scans are shown here.

$n = 30$ studies started acquisition directly at the time of tracer injection. Of these, only $n = 6$ performed a kinetic evaluation (3-compartment model) [30,31,54,100,104,185]. Especially for agents affecting the vascularization (see also 3.4.2), kinetic analyses would be beneficial to shed light on tracer delivery. This has not been performed in any of the studies described within this review. It should be pointed out that kinetic analysis based on plasma samples from mice is extremely difficult [225,226].

Aside from compartmental modeling, $n = 9$ studies determine AUC and $n = 8$ calculate FRT. Most of the dynamic analyses also provide static evaluations. Here, we focus on the static parameters, which were mostly expressed as standardized uptake values (SUV) (see **Supplementary Fig. S8A**). In contrast to %ID/g, SUV takes into account weight of the animal studied. This is important in the clinical situation, although less so in rodent studies. One study did not correct for the injected dose of tracer and simply reported kBq/ml [107]. A range of studies refer uptake within the tumor to uptake in a background region (T/B), with muscle being the most commonly used background tissue (**Supplementary Fig. S8B**). Normalizing tracer uptake to a background region accounts for subtle differences in the imaging procedure like tracer dose and partially corrects for tracer delivery.



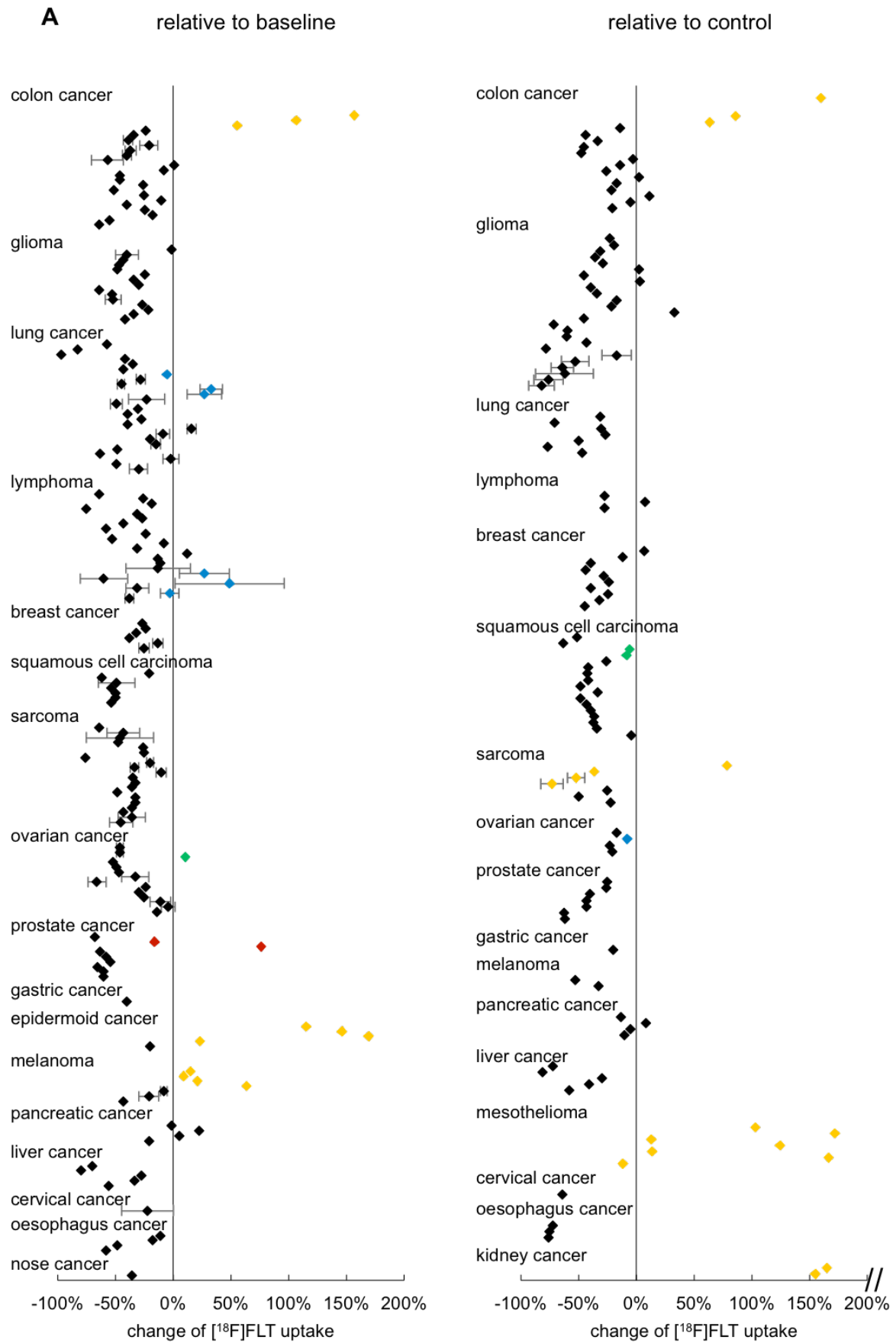
Supplementary Fig. S8: Modes of [¹⁸F]FLT PET quantification. (A) The graph presents the number of studies quantifying [¹⁸F]FLT PET imaging data as %ID/g, SUV, or tumor-to-background ratio (T/B, also named normalized uptake value (NUV) in some studies). Assuming a tissue density of 1 g/ml, studies using %ID/ml were combined with those employing %ID/g. (B) Most of the studies referring [¹⁸F]FLT uptake to background tissue use muscle as reference tissue. The contralateral brain is frequently used for intracranial brain tumors. (C) Analyses differ with respect to whether the maximum or the mean tracer uptake was analyzed. A high number of publications did not specify this in greater detail. It is likely that the mean tracer uptake was used. Of note, several studies employed more than one mode of data quantification, which are all included in these graphical demonstrations.

The mean tracer uptake is most frequently used for quantification of tumor tracer uptake (**Supplementary Fig. S8C**). Notably, some studies do not specify whether they used the mean or the maximum tracer accumulation. Averaging the tracer accumulation within the whole tumor is dependent on the tumor delineation method used and results can be biased if necrosis is present. Consequently, the overall signal of a necrotic tumor might decrease over time, without growth being impaired by successful therapy. On the other hand, maximum tracer uptake is easy to measure and it is less susceptible to inter-observer variabilities. But it might be influenced by image noise, pixel size [227] and motion artifacts [228]. Furthermore, results are more susceptible to outliers. Some studies try to circumvent these biases by setting a threshold and only averaging signals above 50 % [153], 60 % [34], 70 % [185] or 75 % [162] of the most intense pixel within the tumor region. Another approach is to not only include the most intense pixel, but to average its signal intensity with the pixels directly adjacent [31,100,184]. As an alternative approach, two studies calculated the total radioactivity within the tumor (total proliferative volume, i.e. tumor volume x SUV_{mean} [200], or μCi/tumor [76]).

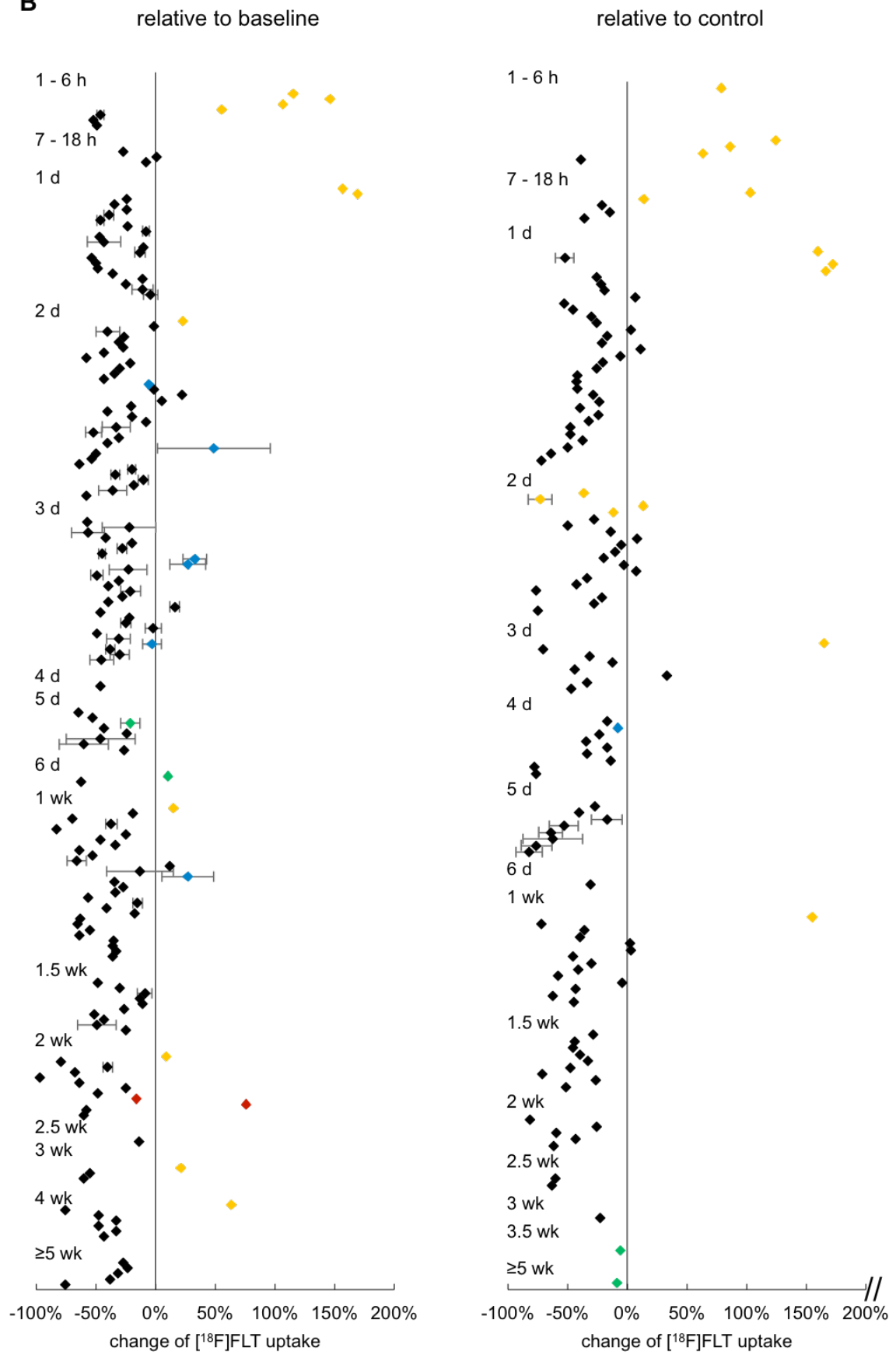
4 Supplementary Information: QuIC-ConCePT consortium participants.

AstraZeneca, European Organisation for Research and Treatment of Cancer (EORTC), University of Cambridge, University of Manchester, Westfälische Wilhelms-Universität Münster, Radboud University Nijmegen Medical Center, Institut National de la Santé et de la Recherche Medical, Stichting Maastricht Radiation Oncology 'Maastricht Clinic', VUmc Amsterdam, King's College London, Universitair Ziekenhuis Antwerpen, Institute of Cancer Research – Royal Cancer Hospital, Erasmus Universitair Medisch Centrum Rotterdam, Imperial College of Science Technology and Medicine, Keosys S.A.S., Eidgenössische Technische Hochschule Zürich, Amgen NV, Eli Lilly and Company Ltd., GlaxoSmithKline Research & Development Limited, Merck KGa, Pfizer Limited, F. Hoffmann – La Roche Ltd., Sanofi–Aventis Research and Development.

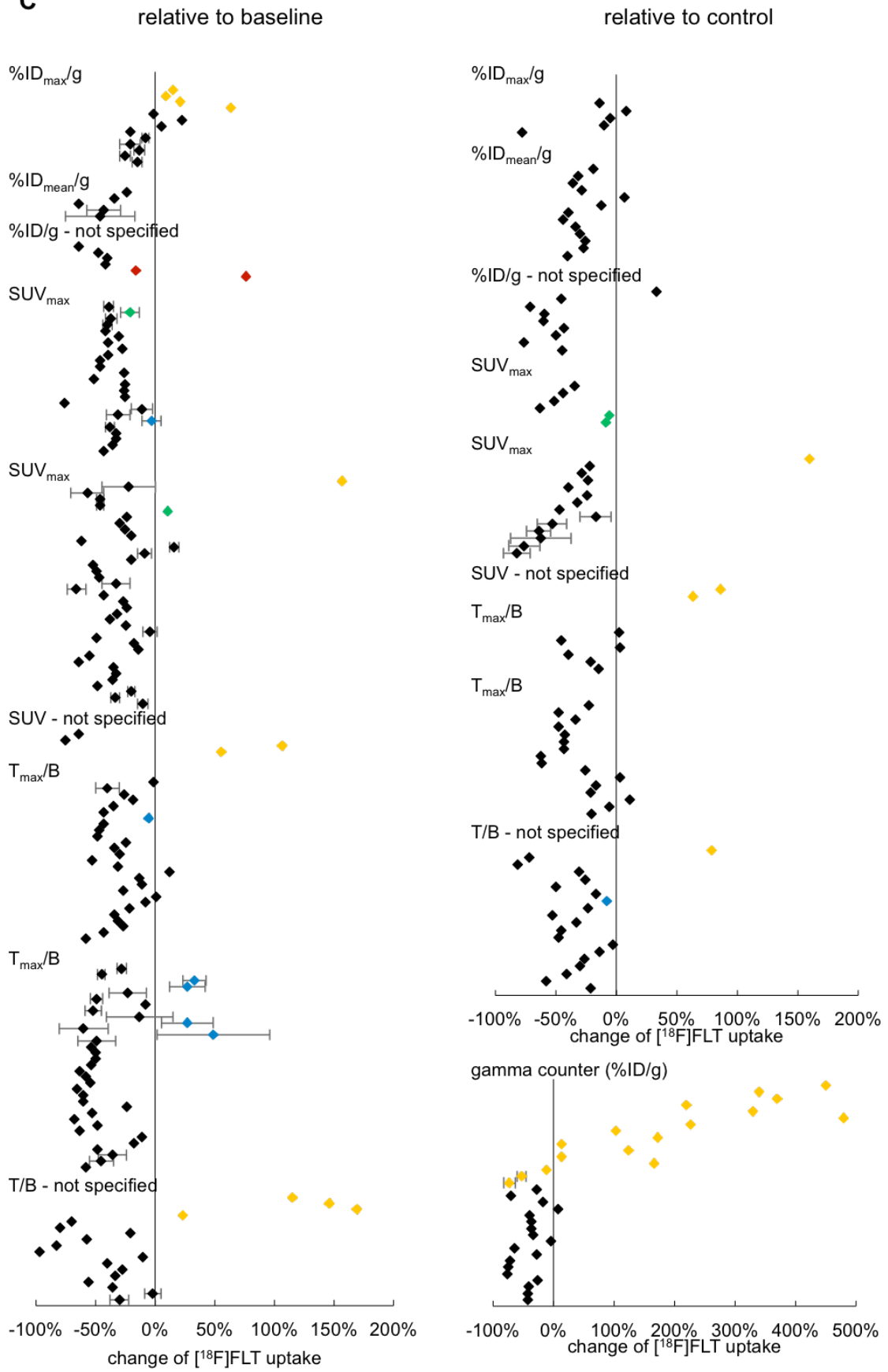
5 Supplementary Figures



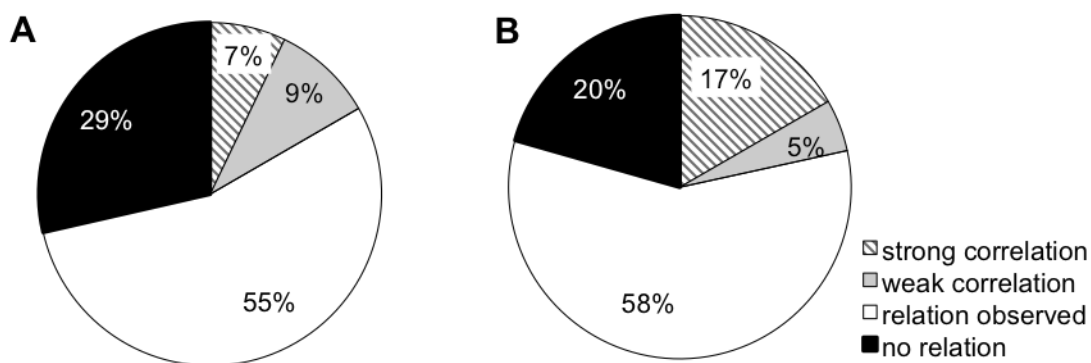
B



C



Supplementary Fig. S9: Relative change of [¹⁸F]FLT uptake in relation to (A) tumor type, (B) time after treatment initiation, and (C) quantification mode. The data presented in Fig. 4 was sorted according to the above mentioned parameters to further investigate if one of these factors is related to the change of [¹⁸F]FLT uptake in tumors upon therapy. Changes were calculated either relative to baseline (left panel) or to control (right panel). Each rectangle represents one data point. Some studies provide more than one data point. Yellow indicates data points from studies investigating TS inhibiting agents. Blue represents data points from resistant tumor models. Green represents time points where the authors of the respective publication describe a recovery of the tumor tissue. Red rectangles originate from studies using tumor models with very low baseline [¹⁸F]FLT uptake. When provided, standard deviations were displayed as error bars. Of note, the x-axis of the right graph in A and B is truncated so that all graphs are displayed with the same scaling. Hence, a few data point from studies analyzing TS inhibitors are not shown.



Supplementary Fig. S10: Overview of relations of [¹⁸F]FLT with parameters of cellular proliferation. These charts reflect the data presented in Fig. 5, sorted for TK1 and other proliferation markers. (A) Relation of [¹⁸F]FLT to TK1 expression and activity as assessed by a vast variety of methods, including western blots, and immunohistochemistry. (B) Relation of [¹⁸F]FLT with histological markers of proliferation, such as Ki67, PCNA and BrdU. Correlations with a correlation coefficient > 0.7 were considered strong.

6 Supplementary Tables

6.1 Supplementary Table S1: PRISMA 2009 checklist.

Section/topic	#	Checklist item	Reported on page #
TITLE			
Title	1	Identify the report as a systematic review, meta-analysis, or both.	40
ABSTRACT			
Structured summary	2	Provide a structured summary including, as applicable: background; objectives; data sources; study eligibility criteria, participants, and interventions; study appraisal and synthesis methods; results; limitations; conclusions and implications of key findings; systematic review registration number.	40
INTRODUCTION			
Rationale	3	Describe the rationale for the review in the context of what is already known.	41
Objectives	4	Provide an explicit statement of questions being addressed with reference to participants, interventions, comparisons, outcomes, and study design (PICOS).	41
METHODS			
Protocol and registration	5	Indicate if a review protocol exists, if and where it can be accessed (e.g., Web address), and, if available, provide registration information including registration number.	not applicable
Eligibility criteria	6	Specify study characteristics (e.g., PICOS, length of follow-up) and report characteristics (e.g., years considered, language, publication status) used as criteria for eligibility, giving rationale.	41
Information sources	7	Describe all information sources (e.g., databases with dates of coverage, contact with study authors to identify additional studies) in the search and date last searched.	41
Search	8	Present full electronic search strategy for at least one database, including any limits used, such that it could be repeated.	S4
Study selection	9	State the process for selecting studies (i.e., screening, eligibility, included in systematic review, and, if applicable, included in the meta-analysis).	41 / S4

Section/topic	#	Checklist item	Reported on page #
Data collection process	10	Describe method of data extraction from reports (e.g., piloted forms, independently, in duplicate) and any processes for obtaining and confirming data from investigators.	S5
Data items	11	List and define all variables for which data were sought (e.g., PICOS, funding sources) and any assumptions and simplifications made.	S4 / S5
Risk of bias in individual studies	12	Describe methods used for assessing risk of bias of individual studies (including specification of whether this was done at the study or outcome level), and how this information is to be used in any data synthesis.	S4
Summary measures	13	State the principal summary measures (e.g., risk ratio, difference in means).	not applicable
Synthesis of results	14	Describe the methods of handling data and combining results of studies, if done, including measures of consistency (e.g., I^2) for each meta-analysis.	S5
Risk of bias across studies	15	Specify any assessment of risk of bias that may affect the cumulative evidence (e.g., publication bias, selective reporting within studies).	not applicable
Additional analyses	16	Describe methods of additional analyses (e.g., sensitivity or subgroup analyses, meta-regression), if done, indicating which were pre-specified.	S5
RESULTS			
Study selection	17	Give numbers of studies screened, assessed for eligibility, and included in the review, with reasons for exclusions at each stage, ideally with a flow diagram.	42, Fig. 2
Study characteristics	18	For each study, present characteristics for which data were extracted (e.g., study size, PICOS, follow-up period) and provide the citations.	S6 – S53
Risk of bias within studies	19	Present data on risk of bias of each study and, if available, any outcome level assessment (see item 12).	not applicable
Results of individual studies	20	For all outcomes considered (benefits or harms), present, for each study: (a) simple summary data for each intervention group (b) effect estimates and confidence intervals, ideally with a forest plot.	S6 – S53
Synthesis of results	21	Present results of each meta-analysis done, including confidence intervals and measures of consistency.	not applicable
Risk of bias across studies	22	Present results of any assessment of risk of bias across studies (see Item 15).	not applicable
Additional analysis	23	Give results of additional analyses, if done (e.g., sensitivity or subgroup analyses, meta-regression [see Item 16]).	43 – 46, S53-S56

Section/topic	#	Checklist item	Reported on page #
DISCUSSION			
Summary of evidence	24	Summarize the main findings including the strength of evidence for each main outcome; consider their relevance to key groups (e.g., healthcare providers, users, and policy makers).	46
Limitations	25	Discuss limitations at study and outcome level (e.g., risk of bias), and at review-level (e.g., incomplete retrieval of identified research, reporting bias).	47
Conclusions	26	Provide a general interpretation of the results in the context of other evidence, and implications for future research.	48
FUNDING			
Funding	27	Describe sources of funding for the systematic review and other support (e.g., supply of data); role of funders for the systematic review.	49

From: Moher D, Liberati A, Tetzlaff J, Altman DG, The PRISMA Group (2009). Preferred Reporting Items for Systematic Reviews and Meta-Analyses: The PRISMA Statement. PLoS Med 6(6): e1000097. doi:10.1371/journal.pmed1000097

6.2 Supplementary Table S2: Quantitative data (relative changes) from the studies included in this review.

Chemotherapies													
reference	quantification mode	cell line	therapy	imaging time	relative to baseline			n =	relative to control			n = *	comment
					change	stdev	significance		change	stdev	significance		
[113,114]	SUV	dogs non-Hodgkin's lymphoma	GS-9219	d5	-64%		$P = 0.016$	4					
				4wk	-76%		$P < 0.031$	5					
[80]	T_{max}/M_{mean}	subcutaneous glioma (Gli36)	TMZ	d2	-1%			8			$P < 0.01$	9 / 8	
	T_{max}/B	intracranial glioma (Gli36)			-40%	10%	$P = 0.015$	5			$P < 0.05$	4 / 5	
[81]	%ID/g	follicular lymphoma (DoHH2)	cyclophosphamide	d2					-28%		$P = 0.0005$	10 / 10	gamma counter
[82]	T_{max}/L	leukemic mantle cell lymphoma (Granta-519)	cyclophosphamide	d2	-26%		n.a.	5					
				d7	-19%		n.a.	5					
[87]	T/M	hepatoma (HepG2)	doxosome® (doxorubicin)	d7	-70%		$P < 0.01$	≥ 5	-72%				
				d14	-79%		$P < 0.01$	≥ 5	-81%				
[85]	T/B	diffuse large B-cell lymphoma (SUDHL-4)	25 µg doxorubicin	d2	-31%		$P = 0.02$	6					
			50 µg doxorubicin		-27%		$P = 0.037$	6					
			100 µg doxorubicin		-43%		$P = 0.008$	3					
			200 µg doxorubicin		-58%		$P = 0.001$	3					
[88]	T/M	head and neck squamous cancer (UM-SCC-22B)	doxil	48h	-21%		$P < 0.005$	6					
[89]	%ID _{mean} /g	colon (C26) (10 ⁵ inoculated)	lipo-DOX	d1	-24%		$P < 0.05$	5					
		colon (C26) (10 ⁶ inoculated)			-34%		$P < 0.05$	5					
[84]	T_{mean}/B	diffuse large B-cell lymphoma (SUDHL-4)	doxorubicin	d1	-24%		$P = 0.048$	6					
				d5	-53%		$P = 0.068$	4					
[86]	T/M	lung cancer H460	doxorubicin	d6					-31%		$P < 0.05$	4 / 4	
[83]	SUV _{max}	colon (HCT116)	irinotecan	d1	-39%	4%	$P < 0.012$	6					
				d5	-21%	8%	n.s.	4					recovery
				d8	-37%	5%	$P < 0.012$	6					
				d15	-40%	4%	$P < 0.012$	6					
[92]	NUV ₆₀	radiation-induced fibrosarcoma 1 (RIF-1)	cisplatin	d1					-25%		$P = 0.03$	4 / 4	
				d2					-50%		$P = 0.03$	4 / 4	

[94]	NUV ₆₀	ovarian (PEO1)	cisplatin	d4					-17%		<i>P</i> < 0.05	6 / 6	
		ovarian (PEO4)	cisplatin						-8%		n.s.	6 / 6	resistant
			cisplatin plus API-2							-23%		<i>P</i> < 0.0005	6 / 6
[95]	T _{mean} /M	prostate (22Rv1)	docetaxel	d14	-68%		<i>P</i> < 0.05	6	-26%			6 / 6	
[99]	SUV _{mean}	sarcoma (RIF-1)	patupilone	d1					-22%		<i>P</i> = 0.002	5 / 5	
[96]	NUV	NSCLC (Calu-6)	docetaxel	d3	-58%		<i>P</i> = 0.149	4					
				d7	-83%		<i>P</i> < 0.05	4					
				d14	-97%		<i>P</i> < 0.01	4					
[100]	SUV _{mean}	cervix (KB-V1)	JAC106	d3									
		colorectal (SW620)											
[101]	ID/ml	rhabdomyosarcoma	vincristine	d14	-64%		<i>P</i> = 0.002	n.a.					
				d28	-48%		<i>P</i> = 0.045	n.a.					
[121]	SUV _{mean}	ovarian(A2780)	TP202377	6h	-46%	3%	<i>P</i> < 0.001	8 – 16					
				d1	-46%	3%	<i>P</i> < 0.001	8 – 16					
				d6	11%		n.s.	8 – 16					recovery
[123]	SUV _{mean}	ovary (A2780)	APO866	d1	-23%		<i>P</i> < 0.001	10					
				d2	-30%		<i>P</i> < 0.001	10					
				d7	-25%		<i>P</i> < 0.001	10					

Targeted therapies													
reference	quantification mode	cell line	therapy	imaging time	relative to baseline			<i>n</i> =	relative to control			<i>n</i> = *	comment
					change	stdev	significance		change	stdev	significance		
[126]	(%ID/g) x kg	lung (H1975)	cetuximab	d3					-70%		<i>P</i> < 0.001	5 / 4	gamma counter
	SUV _{max}				-41%		<i>P</i> < 0.01	4					
[130]	%ID _{max} /ml / mediastinum	lung (HCC827)	erlotinib	d2	-35%		<i>P</i> = 0.04	7					
		lung (PC9)			-43%		<i>P</i> = 0.04	8					
		lung (H1975)			-5%		n.s.	12				resistant model	
[34]	SUV _{mean}	epidermoid (A431)	erlotinib	d3	-20%						<i>P</i> = 0.005	5 / 5	
		HNSCC (SCC-1)	cetuximab	d6	-62%						<i>P</i> = 0.05	3 / 4	
[131]	T _{max} /B	NSCLC (HCC827)	erlotinib 50 mg/kg	d3	-28%	4%	n.s.	≥ 4					
			erlotinib 150 mg/kg		-45%	3%	<i>P</i> < 0.01	≥ 4					
		NSCLC (H1975)	erlotinib 50 mg/kg		33%	10%	n.s.	≥ 4					resistant model
			erlotinib 150 mg/kg		27%	15%	n.s.	≥ 4					
		NSCLC (H1650)	erlotinib 50 mg/kg		-23%	16%	n.s.	≥ 4					
			erlotinib 150 mg/kg		-49%	5%	<i>P</i> ≤ 0.01	≥ 4					

[157]	%ID _{max} /ml	pancreatic cancer	anti-EGFR	d2	-1%		n.s.	8	-14%				
			anti-HER2		22%		$P \leq 0.01$	8	8%				
			anti-HER3		5%		n.s.	8	-5%				
			anti-pan-HER		-21%		$P \leq 0.01$	8	-10%				
[129]	SUV _{max}	NSCLC	50 mg/kg erlotinib	d3	-30%		$P < 0.05$	≥ 4					
			100 mg/kg erlotinib	d3	-39%		$P < 0.05$	≥ 4					
[68]	T _{mean} /B	glioma (human spheroids)	bevacizumab	wk 3					-23%		$P < 0.05$	4 / 4	
[134]	%ID _{max} /g	melanoma (MDA-MB-435)	VEGFR-2 inhibitor	d1	-8%	3%	$P < 0.05$	8					
				d3	-21%	9%	$P < 0.01$	8					
				d3	-21%	9%	$P < 0.01$						
[161]	%ID _{mean} /g	glioma (U87-MG)	axitinib	d1					-19%		n.s.	7 / 7	
				d3					-31%		$P < 0.05$	7 / 7	
				d7					-36%		$P < 0.01$	7 / 7	
				d10					-29%		$P < 0.05$	7 / 7	
		breast (MDA-MB-231)	d1					6%		n.s.		4 / 4	
			d3					-12%		n.s.		4 / 4	
			d7					-40%		$P < 0.01$		4 / 4	
			d10					-44%		$P < 0.01$		4 / 4	
[137]	T/B	glioma (U87)	low dose Ficlaturzumab	d5	-43%		$P < 0.0001$	7					
				d8	-47%		$P < 0.0001$	7	2%		8 / 7		
				d11	-48%		$P < 0.0001$	7	-45%		8 / 7		
			high dose Ficlaturzumab	d5	-24%		$P = 0.2581$	8					
				d8	-34%		$P = 0.2581$	8	3%		8 / 8		
				d11	-30%		$P = 0.2581$	8	-40%		8 / 8		
[140]	%ID/cc	gastric cancer (Hs746T)	c-Met inhibitor BAY 853474	d2	-40%		$P < 0.05$	5					
[138]	%ID _{mean} /g	glioma (U87)	rilotumumab	d7	-64%		$P < 0.001$	6					
[139]	T/B	glioma (U87-MG)	crizotinib	d8	-53%		$P < 0.001$	7-8					
[129]	SUV _{max}	NSCLC (H1933)	50 mg/kg crizotinib	d3	-28%		$P < 0.05$	≥ 4					
			100 mg/kg crizotinib	d3	-40%		$P < 0.01$	≥ 4					
[143]	SUV _{mean}	lung (H727)	everolimus	d3	16%	4%	$P < 0.05$	8					
				d10	-9%	6%		8			$P = 0.010$	8 / 8	
[149]	SUV _{max}	glioma (U87)	AZD8055	d4					-35%		$P = 0.0003$	11 / 9	
	%ID/g			d4					-17%		$P > 0.05$	10 / 9	gamma-counter
[146]	SUV _{mean}	lung (H596)	everolimus	d2	-20%		$P < 0.01$	10					
[144]	T _{mean} /B	lymphoma (Karpas299)	everolimus	d2	-8%			8			$P = 0.001$	7 / 8	

[148]	SUV _{mean}	ovarian (A2780)	Top216	2h	-52%		$P < 0.001$	5 - 10					
				6h	-49%		$P = 0.002$	5 - 10					
				d1	-47%		$P < 0.001$	5 - 10					
[145]	SUV _{mean}	ovarian (SKOV3)	everolimus	d2	-0.33	0.12	$P = 0.003$	7		$P = 0.0008$	7 / 7		
				d7	-0.66	0.08	$P < 0.001$	7		$P = 0.01$	7 / 7		
[147]	T _{mean} /B	glioma (U87)	rapamycin	d2	-52%	7%	$P < 0.01$	6					
[82]	T _{max} /L	leukemic mantle cell lymphoma (Granta-519)	temsirolimus	d2	-31%		n.a.						
				d7	12%		n.a.						
				d9	-13%		n.a.						
				d11	-11%		n.a.						
[141]	NUV _{max}	glioma (U87)	PI3K inhibitor GDC-09	18h	-27%		$P < 0.01$	6	-21%			5 / 6	
	NUV _{max}	colon (HCT116)		18h	1%		n.s.	5	-14%			4 / 5	primary tumor - no growth inhibition
	NUV _{max}			18h	-8%		$P = 0.05$	3					liver metastasis model
	SUV _{max}	colon (HT29)		dominant negative PI3K subunit	3d	-46%		$P < 0.05$	n.a.	-44%			n.a.
[150]	SUV _{max}	colon (HCT116)	TAK-901	d4	-46%		$P < 0.001$	n.a.					
				d9	-26%		$P < 0.001$	n.a.					
				d11	-51%		$P < 0.001$	n.a.					
				d15	-25%		$P < 0.001$	n.a.					
[69]	%ID _{mean} /g	colorectal (Lim2405)	PLX4720	d4					-34%	$P = 0.0079$	5 / 5		
[155]	NUV ₆₀	melanoma (SKMEL-28)	PD0325901	d1					-53%	$P = 0.045$	4 / 4		
				d10					-33%	$P = 0.03$	4 / 4		
		colon (HCT116)		d1					-45%	$P = 0.03$	4 / 4		
				d10					-47%	$P = 0.04$	4 / 4		
[156]	SUV _{mean}	melanoma (SKMEL-28)	PD0325901	wk1	-43%		n.a.	n.a.					
[158]	%ID _{mean} /g	sarcoma (A673)	Sorafenib	d1	-43%	14%	$P = 0.04$	15					
				d5	-46%	29%	$P = 0.003$	7					
[162]	SUV _{max25}	gastric (N87, MKN45, MKN28)	BEZ235	d2					-20%	$P < 0.05$	8 / 8		
[163]	T _{mean} /B	large cell lymphoma (SU-DHL-1)	BGT226	d7	-13%	28%					$P = 0.0007$	7 / 10	
		large cell lymphoma (Karpas299)			27%	22%					$P = 0.2$	3 / 5	resistant model
[164]	T _{max} /M	glioma (U87)	sunitinib	d3	-22%		$P < 0.001$	n.a.					
				d7	-34%		$P < 0.001$	n.a.					

[165]	%ID _{mean} /g	glioma (U87)	sunitinib	d3					33%		n.a.	6 / 6		
				d7						-45%		<i>P</i> < 0.05	6 / 6	
				d10						-71%		<i>P</i> < 0.05	6 / 6	
				d14						-59%		<i>P</i> < 0.05	6 / 6	
				d16						-60%		<i>P</i> < 0.05	6 / 6	
[168]	NUV ₆₀	colo (HCT116)	C1A	d1	-10%		<i>P</i> = 0.033	4						
				d2	-40%		<i>P</i> = 0.0001	4						
[169]	NUV ₆₀	colo (HCT116)	LAQ824	d2					-3%		n.s.	6 / 6		
				d4						-14%		<i>P</i> = 0.05	6 / 6	
				d10						-26%		<i>P</i> = 0.03	6 / 6	
[170]	T/M	HepG2 hepatoma	100 mg/kg SAHA	d8	-27%		<i>P</i> < 0.05	3	-30%			3 / 3		
			25 mg/kg ISAHA		-34%		<i>P</i> < 0.05	3	-41%			3 / 3		
			100 mg/kg ISAHA		-56%		<i>P</i> < 0.05	3	-58%			3 / 3		
[144]	T _{mean} /M	anaplastic large cell lymphoma (ALCL) (SU-DHL-1)	HSP90 inhibitor NVP-AUY922 or mTOR inhibitor everolimus	d5	-60%	21%	<i>P</i> = 0.001	12			<i>P</i> = 0.001	4 / 12		
		anaplastic large cell lymphoma (ALCL) (Karpas299)		d2	49%	47%	<i>P</i> = 0.42	10					resistant model	
[171]	SUV _{mean}	mammary (MDA MB 431)	10 mg/kg PF-03732010,	wk5	-27%		<i>P</i> < 0.01	8					primary tumor	
			20 mg/kg PF-03732010		-23%		<i>P</i> < 0.01	8						
			10 mg/kg PF-03732010		-32%		<i>P</i> < 0.01	8				lung lesion		
			20 mg/kg PF-03732010		-38%		<i>P</i> < 0.01	8						
[177]	%ID _{max} /g	breast cancer (MDA-MB-435)	VEGF121/rGel fusion protein	d1	-13%	5%	n.s.	8						
				d3	-25%	4%	<i>P</i> < 0.01	8						
[178]	%ID/g	glioma (U87-MG-fLuc)	VEGF121/rGel	d8	-41%		<i>P</i> < 0.05	3						
[172]	%ID _{max} /ml	lung (A549)	senicapoc	d7	-15%	4%	<i>P</i> = 0.0041	12						
[175]	%ID _{mean} /g	lung (H460)	BAY 87-2243	d1					-30%		<i>P</i> < 0.01	6 / 6		
		prostate (PC3)							-26%		<i>P</i> < 0.01	6 / 6		
		lung (H460)		d5					-27%		<i>P</i> < 0.01	6 / 6		
		prostate (PC3)							-40%		<i>P</i> < 0.01	6 / 6		
[180]	%ID/g	glioma (U87)	90Y-Abegrin	n.a.					-43%		<i>P</i> < 0.001	5 / 5		
[81]	%ID/g	follicular lymphoma (DoHH2)	radioimmuno-therapy	d2					7%		n.s.	10 / 10	gamma counter	

Radiotherapy																			
reference	quantification mode	cell line	therapy	imaging time	relative to baseline			n =	relative to control			n = *	comment						
					change	stdev	significance		change	stdev	significance								
[189]	SUV _{max}	SCC (FaDu)	12f/12d	d12					-52%		<i>P</i> < 0.001	11 / 5-8							
			18f/18d	d18					-63%		<i>P</i> < 0.001	11 / 5-8							
			12f/24d	d24					-6%		<i>P</i> = 1.000	11 / 5-8	repopulation						
			18f/36d	d36					-8%		<i>P</i> = 0.726	11 / 5-8	repopulation						
[187]	T/NT (lung)	colon (SW480)	5 Gy	24h					3%		n.s.	6 / 6							
			10 Gy						-17%		n.s.	6 / 6							
			20 Gy						-21%		<i>P</i> < 0.01	6 / 6							
		colon (SW620)	5 Gy	24h						11%		n.s.	6 / 6						
			10 Gy							-5%		n.s.	6 / 6						
			20 Gy							-21%		<i>P</i> < 0.05	6 / 6						
[186]	SUV	murine squamous cell carcinoma (SCCVII)	2 Gy	d1					-26%		<i>P</i> < 0.05	3-4	gamma counter						
			6 Gy						-41%		<i>P</i> < 0.05	3-4							
			20 Gy						-42%		<i>P</i> < 0.05	3-4							
			60 Gy						-42%		<i>P</i> < 0.05	3-4							
[185]	SUV _{mean}	mammary (MCAK)	2.5 Gy	d1					-28%		n.s.	3 / 3							
			5 Gy						-24%		<i>P</i> < 0.05	5 / 5							
			10 Gy						-40%		<i>P</i> < 0.05	4 / 4							
			20 Gy						-24%		n.s.	4 / 4							
			4 x 2.5 Gy						-32%		<i>P</i> < 0.05	4 / 4	repopulation						
[184]	T/B	head and neck (HNX-OE)	22 Gy	d12	-49%	16%	n.a.	11											
[182]	T/B	murine squamous cell carcinoma (SCCVII)	10 Gy	d1					-54%		<i>P</i> = 0.027	3	-48%		<i>P</i> = 0.02	3 / 3			
				d2					-50%		<i>P</i> = 0.027	3	-33%		<i>P</i> = 0.02	3 / 3			
			20 Gy	d1					-50%		<i>P</i> = 0.027	3	-48%		<i>P</i> = 0.02	3 / 3			
				d2					-54%		<i>P</i> = 0.027	3	-43%		<i>P</i> = 0.02	3 / 3			
[183]	%ID/g	murine squamous cell carcinoma (SCCVII)	20 Gy	6 h									-39%		<i>P</i> < 0.05	4 / 5	gamma counter		
				12 h											-36%			<i>P</i> < 0.05	4 / 5
				d1											-37%			<i>P</i> < 0.05	4 / 4
				d3											-34%			<i>P</i> < 0.05	4 / 5
				d7											-4%			n.s.	4 / 4
[190]	%ID/g	lung A549	20 Gy	d1									-50%		<i>P</i> < 0.05	3 / 3			
				d2											-77%		<i>P</i> < 0.05	3 / 3	
	T/B			d1											-48%		<i>P</i> < 0.05	3	
				d2											-64%		<i>P</i> < 0.05	3	

[195]	SUV _{max}	fibrosarcoma	4.5 Gy in 10 fractions	d5	-26%			1					
				d10	-25%			1					
				d80	-76%			1					
[194]	SUV	rhabdomyosarcoma	15Gy	d2	-20%	3%	$P < 0.001$	8					
			20Gy	d2	-34%	4%	$P < 0.001$	9					
			40Gy	d2	-10%	4%	$P < 0.01$	10					
[192]	T/M	CNE1 and CNE2 nasopharyngeal	15 Gy	d1	-36%		$P < 0.01$	6					
[191]	T/B	oesophagus Eca-109	10 Gy	d1	-11%		$P < 0.05$	6					
				d7	-17%		$P < 0.05$	6					
				d15	-49%		$P < 0.05$	6					

Other therapies													
reference	quantification mode	cell line	therapy	imaging time	relative to baseline			n =	relative to control			n = *	comment
					change	stdev	significance		change	stdev	significance		
[199]	%ID _{max} /g	glioma (Gli36)	gene therapy	d4					-78%		$P < 0.01$	22 / 8	
[202]	NUV ₆₀	ovarian (IGROV1)	virotherapy	d2					-21%		$P = 0.04$	4 / 4	
[183]	%ID/g	cervix (HeLa)	PDT	d1					-64%		$P < 0.05$	4 / 4	gamma counter
[75]	ID/ml	prostate (CWR22)	castration	wk2	-16%		n.s.	17 / 9					low baseline uptake
		prostate (PAC120)	castration	wk2	76%		$P = 0.015$	15 / 8					low baseline uptake
[203]	T _{mean} /M	prostate (CWR22)	diethylstilbestrol	wk1	-63%		$P = 0.01$	n.a.	-43%		n.a.	n.a.	
				wk2	-58%		n.a.	n.a.	-43%		n.a.	n.a.	
				wk3	-55%		n.a.	n.a.					
			castration	wk1	-65%		$P = 0.01$	n.a.	-62%		n.a.	n.a.	
				wk2	-60%		n.a.	n.a.	-62%		n.a.	n.a.	
wk3	-60%		n.a.	n.a.									
[204]	SUV _{mean}	colon (HT29)	metformin	24 h	-25%		$P < 0.05$	3					
[205]	%ID/g	breast (EMT-6)	IL-22	d7					-45%		$P < 0.01$	n.a. (6 / 6 or 3 / 3)	
[81]	%ID/g	lymphoma (DoHH2)	immunotherapy	d2					-28%		n.s.	10 / 10	gamma counter

Combination therapies													
reference	quantification mode	cell line	therapy	imaging time	relative to baseline			n =	relative to control			n = *	comment
					change	stdev	significance		change	stdev	significance		
[208]	T/M	NSCLC (Calu-6)	docetaxel plus cisplatin	d3	-2%	7%	$P = 0.67$	3					unchanged Ki67
[207]	SUV _{max}	ovarian (A2780)	paclitaxel plus carboplatin	d1	-11%	9%		4			$P = 0.08$	4 / 4	
	SUV _{mean}				-4%	6%		4			$P = 0.05$	4 / 4	

[212]	SUV _{mean}	NSCLC (H292)	IGF-1R inhibitor plus gefitinib	d3					-47%		$P < 0.001$	6 / 6		
[210]	SUV _{mean}	colon (HCT116)	MEK inhibitor plus PI3K inhibitor	d2	-18%		$P < 0.005$	5 - 7						
[211]	SUV _{max}	B-NHL (WSU-DLCL-2)	survivin suppressant	d3	-31%	10%		4			$P < 0.05$	4 / 4		
			rituximab		-3%	8%		4		n.s.	4 / 4	resistant model		
			survivin suppressant plus rituximab		-38%	4%		4		$P < 0.01$	4 / 4			
[208]	T/M	NSCLC (Calu-6)	TRAIL plus sorafenib	d3	-30%	8%	$P = 0.03$	4						
[213]	SUV _{mean}	ovarian (ES-2)	micelles containing paclitaxel	d17	-14%			4			$P < 0.01$	4 / 4		
[214]	SUV _{mean}	glioma (U87)	bevacizumab	d5					-17%	13%	n.s.	7 / 6		
			TMZ						-53%	12%	$P < 0.001$	7 / 6		
			bevacizumab plus TMZ						-64%	10%	$P < 0.001$	7 / 6		
		glioma (U251)	bevacizumab						-62%	25%	n.s.	5 / 8		
			TMZ						-76%	13%	n.s.	5 / 8		
			bevacizumab plus TMZ						-82%	11%	$P < 0.05$	5 / 7		
[216]	SUV _{mean}	colon (HCT116)	irinotecan	d8	-55%		$P < 0.05$	6			$P < 0.01$	6 / 6		
			irinotecan plus HDAC inhibitor		-64%		$P = 0.0625$	6		$P < 0.01$	6 / 6			
[220]	SUV _{mean}	osteosarcoma	temsirolimus + cisplatin	d7	-35%			2						
				d28	-33%			2						
			temsirolimus + bevacizumab	d7	-36%			2						
				d28	-48%			2						
	SUV _{max}		temsirolimus + cisplatin	d7	-33%			2						
				d28	-33%			2						
		temsirolimus + bevacizumab	d7	-36%			2							
			d28	-43%			2							
[222]	T/B	fibrosarcoma (FSall)	sorafenib	d2	-36%	12%	$P < 0.05$	4						
			sorafenib plus radiation	d3	-45%	10%	$P < 0.01$	4						
[224]	%ID/g	esophagus (SEG-1)	docetaxel plus radiation	d1					-72%		$P = 0.006$	5 / 5	scintillation counter	
				d2					-75%		$P < 0.005$	5 / 5		
				d4					-76%		$P < 0.005$	5 / 5		
	T/M			d2	-58%		n.a.	2				PET		

TS inhibitors													
reference	quantification mode	cell line	therapy	imaging time	relative to baseline				relative to control				comment
					change	stdev	significance	n =	change	stdev	significance	n = *	
[104]	SUV _{mean}	colorectal cancer (HT29)	5FU	d1	157%		P < 0.05	8	160%			8 / 8	
[56]	NUV ₆₀	fibrosarcoma (RIF-1)	5FU	2 h					79%		P = 0.0016	5 / 8	
[45]	FRT	fibrosarcoma (RIF-1)	5FU	d2					-36%		P = 0.026	3 / 3	
				d1					-52%	8%	P < 0.01	8 - 12	gamma counter
				d2					-73%	10%	P < 0.001	8 - 12	
[107]	%ID/g	Burkitt lymphoma (Ramos)	FdUrd	1 h					450%		P < 0.001	4 / 4	gamma counter
		3 h						340%		P < 0.001	3 / 3		
		breast (MDA-MB-231)		2 h					370%		P < 0.05	5 / 5	
		breast (SKBR3)		2 h					220%		P < 0.05	5 / 5	
		colon (LS 174T)		2 h					330%		P < 0.05	3 / 3	
		colon (WiDr)		2 h					480%		P < 0.05	3 / 3	
[115]	%ID/g	mesothelioma (MSTO211H, Ds#4)	pemetrexed	1 h					226%		P < 0.01	3 - 5	liquid scintillation counting
				12 h					103%		P < 0.01	3 - 5	
				d1					172%		P < 0.01	3 - 5	
				d2					13%		n.s.	3 - 5	
		mesothelioma (MSTO211H, Tu#6)		1 h					124%		P < 0.01	3 - 5	
				12 h					14%		n.s.	3 - 5	
				d1					167%		P < 0.01	3 - 5	
				d2					-11%		n.s.	3 - 5	
[159]	(%ID/g) × kg	renal cell carcinoma (A498)	sorafenib	d3					165%		P < 0.01		autoradiography
				d7					155%		P < 0.01		
[179]	NUV ₆₀	epidermoid cancer (KB)	BGC 945	1 h	115%		P ≤ 0.01	8					
				4 h	146%		P ≤ 0.01	3					
				d1	169%		P ≤ 0.01	3					
				d2	23%		n.s.	4					
[174]	%ID _{max} /g	melanoma (SK-MEL-28)	arginine deaminase	wk1	15%		n.a.	5					
				wk2	9%		n.a.	5					
				wk3	21%		n.a.	5					
				wk4	64%		n.a.	5					
[209]	SUV	colorectal cancer	30mg/kg TAS-102	2h	107%		P < 0.001	6	86%				
			150mg/kg TAS-102	2h	56%		P < 0.001	6	63%				

* number of control tumors / number of treated tumors

stdev: standard deviation

n.s.: not significant

n.a.: not available

6.3 Supplementary Table S3: Correlation data from the studies included in this review.

reference	tumor type	treatment	correlation type	proliferation marker	quantification mode	correlation coefficient	significance
[40]	colorectal	none	Spearman	TK1	%ID _{mean} /g	$r = 0.36$	$P < 0.05$
[35]	lymphoma	none	linear regression	TK1	AUC	$r = 0.68$	$P = 0.046$
[33]	various (<i>in vitro</i>)	none	?	TK1	disintegrations per minute / cells	$r^2 = 0.80$	$P < 0.0001$
[36]	various	none	Spearman	TK1	SUV _{mean}	$r = 0.59$	$P = 0.017$
				Ki67		$r = 0.66$	$P = 0.002$
[106]	colorectal	5-FU	Spearman	TK1	SUV _{mean}	$\rho = 0.890$	$P < 0.001$
[45]	fibrosarcoma	5-FU	linear regression	PCNA	%ID/g (gamma-counter)	$r = 0.71$	$P = 0.031$
				tumor volume		$r = 0.59$	$P = 0.001$
[80]	glioma (subcutaneous)	temozolomide	Pearson	tumor volume	T/M	$r = 0.76$	$P < 0.0001$
	glioma (intracranial)				T/B	$r = 0.83$	$P = 0.0039$
[92]	fibrosarcoma	cisplatin	linear regression	PCNA	NUV ₆₀	$r = 0.89$	$P = 0.001$
[123]	ovarian cancer	NAMPT inhibition	linear regression	Ki67	SUV _{max}	$r^2 = 0.75$	$P < 0.001$
[130]	lung cancer	EGFR inhibitor	?	Ki67	%ID _{max} /g	$r = 0.87$	$P < 0.001$
[68]	glioma	VEGF inhibitor	Pearson	Ki67	T/B	$r = 0.95$	$P = 0.004$
[143]	lung cancer	mTOR inhibitor	linear regression	tumor volume	SUV _{mean}	$r^2 = 0.87$	$P < 0.001$
[36]	glioma	mTOR inhibitor	?	Ki67	SUV _{max}	$r = 0.63$	$P < 0.05$
[146]	lung cancer	mTOR inhibitor	Spearman	Ki67	SUV _{mean}	$r = 0.60$	$P = 0.04$
[148]	ovarian cancer	mTOR inhibitor	?	tumor volume	SUV _{mean}	$r^2 = 0.61$	$P = 0.04$
[141]	glioma and colon cancer	PI3K inhibitor	?	tumor volume	NUV ₆₀	$R^2 = 0.32$	$P < 0.05$
[155]	melanoma and colorectal	MEK1/2 inhibitor	Pearson	Ki67	NUV ₆₀	$r = 0.63$	$P = 0.001$
[164]	glioma	multiple kinase inhibitor	?	Ki67	T/M	$r = 0.79$?
[167]	ovarian cancer	HDAC inhibitor	linear regression	tumor volume	SUV _{mean}	$r^2 = 0.67$	$P = 0.02$
[169]	colon cancer	HDAC inhibitor	linear regression (Pearson)	Ki67	NUV ₆₀	$r = 0.67$	$P = 0.003$
[170]	liver cancer	HDAC inhibitor	linear regression	Ki67	T/M	$r^2 = 0.98$	$P < 0.05$
[181]	colorectal cancer	radionuclide therapy	linear regression	tumor volume	%ID _{mean} /g	$R^2 = 0.71$	$P = 0.001$
[189]	squamous cell carcinoma	radiotherapy	Spearman's rho	Ki67	SUV _{max}	$r^2 = 0.69$	$P < 0.001$
					SUV _{mean}	$r^2 = 0.68$	$P < 0.001$
					T/NT	$r^2 = 0.88$	$P < 0.001$
				BrdU	SUV _{max}	$r^2 = 0.78$	$P < 0.001$
					SUV _{mean}	$r^2 = 0.77$	$P < 0.001$
					T/NT	$r^2 = 0.88$	$P < 0.001$
[184]	head and neck cancer	radiotherapy	Spearman's rho	tumor volume	T/NT	$r = 0.70$	
[155]	melanoma and colon cancer	MEK1/2 inhibitor	Pearson	TK1	NUV ₆₀	$r = 0.52$	$P = 0.002$
[202]	ovarian cancer	adenovirus	?	TK1	NUV ₆₀	$r^2 = 0.94$?
[194]	rhabdomyosarcoma	radiotherapy	Pearson	tumor volume	SUV _{mean}	$r = 0.76$	$P < 0.01$
	glioma					$r = 0.35$	$P < 0.05$

[192]	nose	radiotherapy	Pearson	tumor volume	T/M	$r = 0.849$	$P = 0.002$
[191]	esophagus cancer	radiotherapy	linear regression	Ki67	T_{mean}/B	$r = 0.88$	$P < 0.001$
				PCNA		$r = 0.83$	$P < 0.001$
[197]	glioma	gene therapy	?	tumor volume	%ID/g	$r = 0.95$	$P < 0.001$
[199]	glioma	gene therapy	?	tumor volume	ID/g	$R = 0.83$	
[202]	ovarian	virotherapy	?	Ki67	NUV ₆₀	$r^2 = 0.89$	
[214]	glioma (U87)	TMZ plus bevacizumab	linear regression	tumor volume	SUV	$R^2 = 0.42$	$P = 0.0007$
	glioma (U251)					$R^2 = 0.55$	$P = 0.0001$
[215]	glioma (U251)	TMZ plus bevacizumab	linear regression	tumor volume	SUV	$R^2 = 0.48$	$P = 0.0029$
[224]	esophagus cancer	docetaxel plus radiation	linear regression	Ki67	T/M_{mean}	$r = 0.89$	$P < 0.001$

6.4 Supplementary Table S4: Number of studies reported on in this review sorted for major characteristics and therapy approach.

	no therapy	chemo-therapy	targeted therapy	radio-therapy	other therapies	combination therapies	sum
number of studies	45	42	59	15	11	20	192

therapy response							
[¹⁸ F]FLT predictive		29	52	15	9	17	122
[¹⁸ F]FLT failed		4	5		2	2	13
[¹⁸ F]FLT increased		9	2			1	12

[¹⁸ F]FDG comparison							
[¹⁸ F]FLT better than [¹⁸ F]FDG		7	15	5	2	4	33
[¹⁸ F]FLT = [¹⁸ F]FDG		3	6	2		6	17
[¹⁸ F]FDG better than [¹⁸ F]FLT		3	3		1		7

ex vivo relations							
Ki67* correlation	1	3	8	4	1	1	18
Ki67* relation	4	15	30	2	2	6	59
no Ki67* relation	7	2	5		1	6	21
TK1 correlation	4	1	1		1		7
TK1 relation	2	5	13			3	23
no TK1 relation	5	5	2				12
growth correlation		2	5	3	2	2	14

* also including PCNA and BrdU analysis

number of tumor models							
colorectal cancer	20	5	15	3	3	9	55
glioma	14	4	14	2	5	3	42
lung cancer	13	2	19	1		3	38
lymphoma	4	6	8		1	4	23
breast cancer	7	3	7	1	1		19
squamous cell carcinoma	4	3	1	6	1		15
sarcoma	3	3	1	2		3	12
ovarian cancer		3	3		1	4	11
prostate cancer	2	1	1		5		9
gastric cancer	2	1	5				8
epidermoid cancer	3		2				6
melanoma	1		5				6
pancreatic cancer	5		1				6
liver cancer	1	2	1				4
mesotheliom	2	1					3
cervical cancer		1			1		2
esophagus cancer				1		1	2
nose cancer				2			2
adrenocortical cancer		1					1
kidney cancer			1				1
leukemia	1						1
sum	82	36	84	18	18	27	266
resistant models		4	9	1			14

6.5 Supplementary Table S5: Number of studies sorted for acquisition and quantification protocols.

start of image acquisition relative to tracer static injection														
minute	0	30	40	45	50	55	60	70	85	90	105	110	115	120
no. of studies	2	10	7	2	10	11	65	5	1	12	1	2	1	9

acquisition duration								
minute	3	5	10	15	20	30	45	60
no. of studies	2	21	51	15	24	12	1	1

mode of [¹⁸ F]FLT uptake quantification												
mode	%ID _{max} /g	%ID _{mean} /g	%ID _? /g	SUV _{max}	SUV _{mean}	SUV _?	T _{max} /B	T _{mean} /B	T _? /B	AUC	FRT	kinetic
no. of studies	12	15	21	28	39	6	9	11	23	9	8	6

background region used for calculation of T/B						
background region	muscle	liver	lung	heart	contralateral brain	not specified
no. of studies	15	4	3	8	3	10

6.6 Supplementary Table S6: Number of treatment studies and datapoints providing quantitative data.

	TS inhibitors	chemo-therapy	targeted therapy	radio-therapy	other therapies	combination therapies	sum
no. of studies	9	20	40	12	8	12	101
no. of datapoints	34	47	121	47	18	32	299

number of datapoints relative to treatment initiation																
time	hours		days						weeks							
	1-6	7-18	1	2	3	4	5	6	1	1.5	2	2.5	3	3.5	4	≥ 5
no. of datapoint	19	8	54	53	35	10	16	3	43	19	17	3	4	1	7	6

7 References

1. Shields AF, Grierson JR, Dohmen BM, Machulla HJ, Stayanoff JC, Lawhorn-Crews JM, et al. Imaging proliferation in vivo with [F-18]FLT and positron emission tomography. *Nat Med.* 1998 Nov;4(11):1334–6.
2. Shields AF, Grierson JR, Muzik O, Stayanoff JC, Lawhorn-Crews JM, Obradovich JE, et al. Kinetics of 3'-deoxy-3'-[F-18]fluorothymidine uptake and retention in dogs. *Mol Imaging Biol.* 2002 Jan;4(1):83–90.
3. Mankoff DA, Shields AF, Krohn KA. PET imaging of cellular proliferation. *Radiol Clin North Am.* 2005 Jan;43(1):153–67.
4. Janjigian YY, Viola-Villegas N, Holland JP, Divilov V, Carlin SD, Gomes-DaGama EM, et al. Monitoring afatinib treatment in HER2-positive gastric cancer with 18F-FDG and 89Zr-trastuzumab PET. *J Nucl Med.* 2013 Jun;54(6):936–43.
5. Lu L, Jiang L, Guan H, Gao Y, Lu H. Imaging proliferation in human leukemia-tumor bearing mice with 18F-FLT: Comparison with 18F-FDG PET. *Hell J Nucl Med.* 2012;15(3):206–9.
6. Ekshyyan O, Sibley D, Caldito GC, Sunderland J, Vascoe C, Nathan C-AO. 18F-fluorodeoxythymidine micro-positron-emission tomography versus 18F-fluorodeoxyglucose micro-positron-emission tomography for in vivo minimal residual disease imaging. *Laryngoscope.* 2013;123(1):107–11.
7. Krieger-Hinck N, Gustke H, Valentiner U, Mikecz P, Buchert R, Mester J, et al. Visualisation of neuroblastoma growth in a Scid mouse model using [18F]FDG and [18F]FLT-PET. *Anticancer Res.* 2006;26(5 A):3467–72.
8. Valentiner U, Haane C, Peldschus K, Gustke H, Brenner W, Wilke F, et al. [18F]FDG and [18F]FLT PET-CT and MR imaging of human neuroblastomas in a SCID mouse xenograft model. *Anticancer Res.* 2008;28(5 A):2561–8.
9. Pantaleo MA, Landuzzi L, Nicoletti G, Nanni C, Boschi S, Piazzini G, et al. Advances in preclinical therapeutics development using small animal imaging and molecular analyses: The gastrointestinal stromal tumors model. *Clin Exp Med.* 2009;9(3):199–205.
10. Haldorsen IS, Popa M, Fonnes T, Brekke N, Kopperud R, Visser NC, et al. Multimodal Imaging of Orthotopic Mouse Model of Endometrial Carcinoma. *PLoS One.* 2015 Jan 7;10(8):e0135220.
11. Cheng Z, Wei R, Wu C, Qing H, Jiang X, Lu H, et al. Ex-vivo biodistribution and micro-PET/CT imaging of 18F-FDG, 18F-FLT, 18F-FMISO, and 18F-AIF-NOTA-PRGD2 in a prostate tumor-bearing nude mouse model. *Nucl Med Commun.* 2015 Sep;36(9):914–21.
12. Alberini J-L, Boisgard R, Guillermet S, Siquier K, Jego B, Thézé B, et al. Multimodal In Vivo Imaging of Tumorigenesis and Response to Chemotherapy in a Transgenic Mouse Model of Mammary Cancer. *Mol imaging Biol.* 2016 Aug;18(4):617–26.
13. Probst S, Wiehr S, Mantlik F, Schmidt H, Kolb A, Münch P, et al. Evaluation of Positron Emission Tomographic Tracers for Imaging of Papillomavirus-Induced Tumors in Rabbits. *Mol Imaging.* 2014;13(1):1–9.
14. Fuchs K, Kukuk D, Mahling M, Quintanilla-Martinez L, Reischl G, Reutershan J, et al. Impact of anesthetics on 3'-[18F]fluoro-3'-deoxythymidine ([18F]FLT) uptake in animal models of cancer and inflammation. *Mol Imaging.* 2013 Jan;12(5):277–87.
15. Jost SC, Wanebo JE, Song S-K, Chicoine MR, Rich KM, Woolsey TA, et al. In vivo imaging in a murine model of glioblastoma. *Neurosurgery.* 2007;60(2):360–70.
16. Huang Y-C, Huang H-L, Yeh C-N, Lin K-J, Yu C-S. Investigation of brain tumors using (18)F-

- fluorobutyl ethacrynic amide and its metabolite with positron emission tomography. *Onco Targets Ther.* 2015 Jan 24;8:1877–85.
17. Thorsen F, Fite B, Mahakian LM, Seo JW, Qin S, Harrison V, et al. Multimodal imaging enables early detection and characterization of changes in tumor permeability of brain metastases. *J Control Release.* 2013;172(3):812–22.
 18. Schelhaas S, Wachsmuth L, Viel T, Honess DJ, Heinzmann K, Smith D-M, et al. Variability of proliferation and diffusion in different lung cancer models as measured by 3'-deoxy-3'-18F-fluorothymidine PET and diffusion-weighted MR imaging. *J Nucl Med.* 2014 Apr;55(6):983–8.
 19. Viel T, Talasila KM, Monfared P, Wang J, Jikeli JF, Waerzeggers Y, et al. Analysis of the growth dynamics of angiogenesis-dependent and -independent experimental glioblastomas by multimodal small-animal PET and MRI. *J Nucl Med.* 2012;53(7):1135–45.
 20. Wang H, Zhang J, Tian J, Qu B, Li T, Chen Y, et al. Using dual-tracer PET to predict the biologic behavior of human colorectal cancer. *J Nucl Med.* 2009 Nov;50(11):1857–64.
 21. Lee TS, Ahn SH, Moon BS, Chun KS, Kang JH, Cheon GJ, et al. Comparison of 18F-FDG, 18F-FET and 18F-FLT for differentiation between tumor and inflammation in rats. *Nucl Med Biol.* 2009;36(6):681–6.
 22. Van Waarde A, Cobben DCP, Suurmeijer AJH, Maas B, Vaalburg W, De Vries EFJ, et al. Selectivity of 18F-FLT and 18F-FDG for differentiating tumor from inflammation in a rodent model. *J Nucl Med.* 2004;45(4):695–700.
 23. Van Waarde A, Jager PL, Ishiwata K, Dierckx RA, Elsinga PH. Comparison of sigma-ligands and metabolic PET Tracers for differentiating tumor from inflammation. *J Nucl Med.* 2006;47(1):150–4.
 24. Zhao S, Kuge Y, Kohanawa M, Takahashi T, Zhao Y, Yi M, et al. Usefulness of 11C-methionine for differentiating tumors from granulomas in experimental rat models: A comparison with 18F-FDG and 18F-FLT. *J Nucl Med.* 2008;49(1):135–41.
 25. Ye Y-X, Calcagno C, Binderup T, Courties G, Keliher EJ, Wojtkiewicz GR, et al. Imaging Macrophage and Hematopoietic Progenitor Proliferation in Atherosclerosis. *Circ Res.* 2015 Oct 23;117(10):835–45.
 26. Troost EGC, Vogel W V, Merckx MAW, Slootweg PJ, Marres HAM, Peeters WJM, et al. 18F-FLT PET does not discriminate between reactive and metastatic lymph nodes in primary head and neck cancer patients. *J Nucl Med.* 2007 May;48(5):726–35.
 27. Cobben DCP, van der Laan BFAM, Maas B, Vaalburg W, Suurmeijer AJH, Hoekstra HJ, et al. 18F-FLT PET for visualization of laryngeal cancer: comparison with 18F-FDG PET. *J Nucl Med.* 2004 Feb;45(2):226–31.
 28. Rayamajhi SJ, Mittal BR, Maturu VN, Agarwal R, Bal A, Dey P, et al. (18)F-FDG and (18)F-FLT PET/CT imaging in the characterization of mediastinal lymph nodes. *Ann Nucl Med.* 2016 Apr;30(3):207–16.
 29. Tseng JR, Dandekar M, Subbarayan M, Cheng Z, Park JM, Louie S, et al. Reproducibility of 3'-deoxy-3'-18F-fluorothymidine microPET studies in tumor xenografts in mice. *J Nucl Med.* 2005;46(11):1851–7.
 30. Whisenant JG, Peterson TE, Fluckiger JU, Tantawy MN, Ayers GD, Yankeelov TE. Reproducibility of static and dynamic (18)F-FDG, (18)F-FLT, and (18)F-FMISO MicroPET studies in a murine model of HER2+ breast cancer. *Mol imaging Biol.* 2013 Feb;15(1):87–96.
 31. Choi SJ, Kim SY, Kim SJ, Lee JS, Lee SJ, Park SA, et al. Reproducibility of the kinetic analysis of 3'-deoxy-3'-[(18)F]fluorothymidine positron emission tomography in mouse tumor models. *Nucl Med Biol.* 2009 Oct;36(7):711–9.

32. Rasey JS, Grierson JR, Wiens LW, Kolb PD, Schwartz JL. Validation of FLT uptake as a measure of thymidine kinase-1 activity in A549 carcinoma cells. *J Nucl Med.* 2002 Sep;43(9):1210–7.
33. Schwartz JL, Tamura Y, Jordan R, Grierson JR, Krohn KA. Monitoring tumor cell proliferation by targeting DNA synthetic processes with thymidine and thymidine analogs. *J Nucl Med.* 2003 Dec;44(12):2027–32.
34. Atkinson DM, Clarke MJ, Mladek AC, Carlson BL, Trump DP, Jacobson MS, et al. Using fluorodeoxythymidine to monitor anti-egfr inhibitor therapy in squamous cell carcinoma xenografts. *Head Neck.* 2008 Jun;30(6):790–9.
35. Barthel H, Perumal M, Latigo J, He Q, Brady F, Luthra SK, et al. The uptake of 3'-deoxy-3'-[18F]fluorothymidine into L5178Y tumours in vivo is dependent on thymidine kinase 1 protein levels. *Eur J Nucl Med Mol Imaging.* 2005;32(3):257–63.
36. Keen H, Pichler B, Kukuk D, Duchamp O, Raguin O, Shannon A, et al. An evaluation of 2-deoxy-2-[18F]fluoro-D-glucose and 3'-deoxy-3'-[18F]-fluorothymidine uptake in human tumor xenograft models. *Mol Imaging Biol.* 2012 Jun;14(3):355–65.
37. von Forstner C, Egberts J-H, Ammerpohl O, Niedzielska D, Buchert R, Mikecz P, et al. Gene expression patterns and tumor uptake of 18F-FDG, 18F-FLT, and 18F-FEC in PET/MRI of an orthotopic mouse xenotransplantation model of pancreatic cancer. *J Nucl Med.* 2008 Aug;49(8):1362–70.
38. Seitz U, Wagner M, Neumaier B, Wawra E, Glattig G, Leder G, et al. Evaluation of pyrimidine metabolising enzymes and in vitro uptake of 3'-[(18)F]fluoro-3'-deoxythymidine ([18F]FLT) in pancreatic cancer cell lines. *Eur J Nucl Med Mol Imaging.* 2002 Sep;29(9):1174–81.
39. Foekens JA, Romain S, Look MP, Martin PM, Klijn JG. Thymidine kinase and thymidylate synthase in advanced breast cancer: response to tamoxifen and chemotherapy. *Cancer Res.* 2001 Feb 15;61(4):1421–5.
40. McKinley ET, Ayers GD, Smith RA, Saleh SA, Zhao P, Washington MK, et al. Limits of [18F]-FLT PET as a biomarker of proliferation in oncology. *PLoS One.* 2013;8(3):e58938.
41. Rose MG, Farrell MP, Schmitz JC. Thymidylate synthase: a critical target for cancer chemotherapy. *Clin Colorectal Cancer.* 2002 Feb;1(4):220–9.
42. Van Triest B, Pinedo HM, Giaccone G, Peters GJ. Downstream molecular determinants of response to 5-fluorouracil and antifolate thymidylate synthase inhibitors. *Ann Oncol.* 2000 Apr;11(4):385–91.
43. Voeller DM, Grem JL, Pommier Y, Paull K, Allegra CJ. Identification and proposed mechanism of action of thymidine kinase inhibition associated with cellular exposure to camptothecin analogs. *Cancer Chemother Pharmacol.* 2000 Jan;45(5):409–16.
44. Schiepers C, Chen W, Dahlbom M, Cloughesy T, Hoh CK, Huang S-C. 18F-fluorothymidine kinetics of malignant brain tumors. *Eur J Nucl Med Mol Imaging.* 2007 Jul;34(7):1003–11.
45. Barthel H, Cleij MC, Collingridge DR, Hutchinson OC, Osman S, He Q, et al. 3'-deoxy-3'-[18F]fluorothymidine as a new marker for monitoring tumor response to antiproliferative therapy in vivo with positron emission tomography. *Cancer Res.* 2003 Jul;63(13):3791–8.
46. Van Waarde A, Been LB, Ishiwata K, Dierckx RA, Elsinga PH. Early response of (sigma)-receptor ligands and metabolic PET tracers to 3 forms of chemotherapy: An in vitro study in glioma cells. *J Nucl Med.* 2006;47(9):1538–45.
47. Direcks WGE, Berndsen SC, Proost N, Peters GJ, Balzarini J, Spreuwenberg MD, et al. [18F]FDG and [18F]FLT uptake in human breast cancer cells in relation to the effects of chemotherapy: an in vitro study. *Br J Cancer.* 2008 Aug 5;99(3):481–7.
48. Munch-Petersen B, Cloos L, Tyrsted G, Eriksson S. Diverging substrate specificity of pure human

- thymidine kinases 1 and 2 against antiviral dideoxynucleosides. *J Biol Chem*. 1991 May 15;266(14):9032–8.
49. Eriksson S, Kierdaszuk B, Munch-Petersen B, Oberg B, Johansson NG. Comparison of the substrate specificities of human thymidine kinase 1 and 2 and deoxycytidine kinase toward antiviral and cytostatic nucleoside analogs. *Biochem Biophys Res Commun*. 1991 May 30;176(2):586–92.
 50. Eriksson S, Munch-Petersen B, Johansson K, Eklund H. Structure and function of cellular deoxyribonucleoside kinases. *Cell Mol Life Sci*. 2002 Aug;59(8):1327–46.
 51. Sala R, Nguyen Q-D, Patel CBK, Mann D, Steinke JHG, Vilar R, et al. Phosphorylation status of thymidine kinase 1 following antiproliferative drug treatment mediates 3'-deoxy-3'-[18F]-fluorothymidine cellular retention. *PLoS One*. 2014;9(7):e101366.
 52. Tsuji AB, Sogawa C, Sugyo A, Sudo H, Toyohara J, Koizumi M, et al. Comparison of conventional and novel PET tracers for imaging mesothelioma in nude mice with subcutaneous and intrapleural xenografts. *Nucl Med Biol*. 2009 May;36(4):379–88.
 53. Paproski RJ, Ng AML, Yao SYM, Graham K, Young JD, Cass CE. The role of human nucleoside transporters in uptake of 3'-deoxy-3'-fluorothymidine. *Mol Pharmacol*. 2008 Nov;74(5):1372–80.
 54. Paproski RJ, Wuest M, Jans H-S, Graham K, Gati WP, McQuarrie S, et al. Biodistribution and uptake of 3'-deoxy-3'-fluorothymidine in ENT1-knockout mice and in an ENT1-knockdown tumor model. *J Nucl Med*. 2010 Sep;51(9):1447–55.
 55. Plotnik DA, Asher C, Chu SK, Miyaoka RS, Garwin GG, Johnson BW, et al. Levels of human equilibrative nucleoside transporter-1 are higher in proliferating regions of A549 tumor cells grown as tumor xenografts in vivo. *Nucl Med Biol*. 2012 Nov;39(8):1161–6.
 56. Perumal M, Pillai RG, Barthel H, Leyton J, Latigo JR, Forster M, et al. Redistribution of nucleoside transporters to the cell membrane provides a novel approach for imaging thymidylate synthase inhibition by positron emission tomography. *Cancer Res*. 2006;66(17):8558–64.
 57. Zhang CC, Yan Z, Li W, Kuszpit K, Painter CL, Zhang Q, et al. [(18)F]FLT-PET imaging does not always “light up” proliferating tumor cells. *Clin Cancer Res*. 2012 Mar;18(5):1303–12.
 58. Poliakov E, Managadze D, Rogozin IB. Generalized portrait of cancer metabolic pathways inferred from a list of genes overexpressed in cancer. *Genet Res Int*. 2014 Jan;2014:646193.
 59. Nottebrock H, Then R. Thymidine concentrations in serum and urine of different animal species and man. *Biochem Pharmacol*. 1977 Nov 15;26(22):2175–9.
 60. Li KM, Clarke SJ, Rivory LP. Quantitation of plasma thymidine by high-performance liquid chromatography—atmospheric pressure chemical ionization mass spectrometry and its application to pharmacodynamic studies in cancer patients. *Anal Chim Acta*. 2003 Jun;486(1):51–61.
 61. Li KM, Rivory LP, Hoskins J, Sharma R, Clarke SJ. Altered deoxyuridine and thymidine in plasma following capecitabine treatment in colorectal cancer patients. *Br J Clin Pharmacol*. 2007;63(1):67–74.
 62. Lee SJ, Yeo JS, Lee HJ, Lee EJ, Kim SY, Jang SJ, et al. Thymidine phosphorylase influences [(18)F]fluorothymidine uptake in cancer cells and patients with non-small cell lung cancer. *Eur J Nucl Med Mol Imaging*. 2014 Jul;41(7):1327–35.
 63. Li X-F, Huang T, Jiang H, Wang X, Shen B, Wang X, et al. Combined Injection of (18)F-Fluorodeoxyglucose and 3'-Deoxy-3'-[(18)F]fluorothymidine PET Achieves More Complete Identification of Viable Lung Cancer Cells in Mice and Patients than Individual Radiopharmaceutical: A Proof-of-Concept Study. *Transl Oncol*. 2013 Dec;6(6):775–83.
 64. Huang T, Civelek AC, Li J, Jiang H, Ng CK, Postel GC, et al. Tumor microenvironment-dependent

- 18F-FDG, 18F-fluorothymidine, and 18F-misonidazole uptake: a pilot study in mouse models of human non-small cell lung cancer. *J Nucl Med*. 2012 Aug;53(8):1262–8.
65. Dence CS, Ponde DE, Welch MJ, Lewis JS. Autoradiographic and small-animal PET comparisons between (18)F-FMISO, (18)F-FDG, (18)F-FLT and the hypoxic selective (64)Cu-ATSM in a rodent model of cancer. *Nucl Med Biol*. 2008 Aug;35(6):713–20.
 66. Bruns CJ, Harbison MT, Davis DW, Portera CA, Tsan R, McConkey DJ, et al. Epidermal growth factor receptor blockade with C225 plus gemcitabine results in regression of human pancreatic carcinoma growing orthotopically in nude mice by antiangiogenic mechanisms. *Clin Cancer Res*. 2000 May;6(5):1936–48.
 67. Van Cruijssen H, Giaccone G, Hoekman K. Epidermal growth factor receptor and angiogenesis: Opportunities for combined anticancer strategies. *Int J Cancer*. 2005;117(6):883–8.
 68. Viel T, Boehm-Sturm P, Rapic S, Monfared P, Neumaier B, Hoehn M, et al. Non-invasive imaging of glioma vessel size and densities in correlation with tumour cell proliferation by small animal PET and MRI. *Eur J Nucl Med Mol Imaging*. 2013 Oct;40(10):1595–606.
 69. McKinley ET, Smith RA, Zhao P, Fu A, Saleh SA, Uddin MI, et al. 3'-Deoxy-3'-18F-fluorothymidine PET predicts response to (V600E)BRAF-targeted therapy in preclinical models of colorectal cancer. *J Nucl Med*. 2013 Mar;54(3):424–30.
 70. Miles KA, Williams RE. Warburg revisited: imaging tumour blood flow and metabolism. *Cancer Imaging*. 2008 Jan;8:81–6.
 71. Fuchs K, Kukuk D, Reischl G, Foller M, Eichner M, Reutershan J, et al. Oxygen breathing affects 3'-Deoxy-3'-18F-fluorothymidine uptake in mouse models of arthritis and cancer. *J Nucl Med*. 2012;53(5):823–30.
 72. Caretti V, Zondervan I, Meijer DH, Idema S, Vos W, Hamans B, et al. Monitoring of tumor growth and post-irradiation recurrence in a diffuse intrinsic pontine glioma mouse model. *Brain Pathol*. 2011 Jul;21(4):441–51.
 73. Muzi M, Spence AM, O'Sullivan F, Mankoff DA, Wells JM, Grierson JR, et al. Kinetic analysis of 3'-deoxy-3'-18F-fluorothymidine in patients with gliomas. *J Nucl Med*. 2006 Oct;47(10):1612–21.
 74. Axente M, He J, Bass CP, Hirsch JI, Sundaresan G, Williamson J, et al. Tumour microenvironment heterogeneity affects the perceived spatial concordance between the intratumoural patterns of cell proliferation and 18F-fluorothymidine uptake. *Radiother Oncol*. 2012;105(1):49–56.
 75. Kukuk D, Reischl G, Raguin O, Wiehr S, Judenhofer MS, Calaminus C, et al. Assessment of PET tracer uptake in hormone-independent and hormone-dependent xenograft prostate cancer mouse models. *J Nucl Med*. 2011 Oct;52(10):1654–63.
 76. Moroz MA, Kochetkov T, Cai S, Wu J, Shamis M, Nair J, et al. Imaging colon cancer response following treatment with AZD1152: a preclinical analysis of [18F]fluoro-2-deoxyglucose and 3'-deoxy-3'-[18F]fluorothymidine imaging. *Clin Cancer Res*. 2011 Mar;17(5):1099–110.
 77. Shah C, Miller TW, Wyatt SK, McKinley ET, Olivares MG, Sanchez V, et al. Imaging biomarkers predict response to Anti-HER2 (ErbB2) therapy in preclinical models of breast cancer. *Clin Cancer Res*. 2009 Jul;15(14):4712–21.
 78. Kanamaru R, Asamura M, Sato H, Saito S, Wakui A, Saito T. Studies on the mechanism of action of ACNU, 1-(4-amino-2-methylpyrimidine-5-yl) methyl-3-(2-chloroethyl)-3-nitrosourea hydrochloride: effects on cultured HeLa S3 cells. *Tohoku J Exp Med*. 1980 Dec;132(4):431–41.
 79. Kawai H, Toyohara J, Kado H, Nakagawa T, Takamatsu S, Furukawa T, et al. Acquisition of resistance to antitumor alkylating agent ACNU: A possible target of positron emission tomography monitoring. *Nucl Med Biol*. 2006;33(1):29–35.

80. Viel T, Schelhaas S, Wagner S, Wachsmuth L, Schwegmann K, Kuhlmann M, et al. Early assessment of the efficacy of temozolomide chemotherapy in experimental glioblastoma using [18F]FLT-PET imaging. *PLoS One*. 2013;8(7):e67911.
81. Buck AK, Kratochwil C, Glatting G, Juweid M, Bommer M, Tepsic D, et al. Early assessment of therapy response in malignant lymphoma with the thymidine analogue [18F]FLT. *Eur J Nucl Med Mol Imaging*. 2007 Nov;34(11):1775–82.
82. Brepoels L, Stroobants S, Verhoef G, De Groot T, Mortelmans L, De Wolf-Peeters C. (18)F-FDG and (18)F-FLT uptake early after cyclophosphamide and mTOR inhibition in an experimental lymphoma model. *J Nucl Med*. 2009 Jul;50(7):1102–9.
83. Mudd SR, Holich KD, Voorbach MJ, Cole TB, Reuter DR, Tapang P, et al. Pharmacodynamic evaluation of irinotecan therapy by FDG and FLT PET/CT imaging in a colorectal cancer xenograft model. *Mol Imaging Biol*. 2012 Oct;14(5):617–24.
84. Graf N, Herrmann K, den Hollander J, Fend F, Schuster T, Wester H-J, et al. Imaging proliferation to monitor early response of lymphoma to cytotoxic treatment. *Mol Imaging Biol*. 2008;10(6):349–55.
85. Graf N, Herrmann K, Numberger B, Zwisler D, Aichler M, Feuchtinger A, et al. [18F]FLT is superior to [18F]FDG for predicting early response to antiproliferative treatment in high-grade lymphoma in a dose-dependent manner. *Eur J Nucl Med Mol Imaging*. 2013 Jan;40(1):34–43.
86. Kwak W, Ha YS, Soni N, Lee W, Park S-I, Ahn H, et al. Apoptosis imaging studies in various animal models using radio-iodinated peptide. *Apoptosis*. 2015;20(1):110–21.
87. Wu C-Y, Chou L-S, Chan P-C, Ho C-H, Lin M-H, Shen C-C, et al. Monitoring tumor response with radiolabeled nucleoside analogs in a hepatoma-bearing mouse model early after doxosome((R)) treatment. *Mol imaging Biol*. 2013 Jun;15(3):326–35.
88. Zhang F, Zhu L, Liu G, Hida N, Lu G, Eden HS, et al. Multimodality imaging of tumor response to Doxil. *Theranostics*. 2011;1(1):302–9.
89. Lee T-W, Lee W-C, Chang C-H, Ho C-L, Chen L-C, Wu Y-H, et al. Early detection of tumor response by FLT/MicroPET imaging in a C26 murine colon carcinoma solid tumor animal model. *J Biomed Biotechnol*. 2011;2011(535902).
90. Sherley JL, Kelly TJ. Regulation of human thymidine kinase during the cell cycle. *J Biol Chem*. 1988;263(17):8350–8.
91. Dittmann H, Dohmen BM, Kehlbach R, Bartusek G, Pritzkow M, Sarbia M, et al. Early changes in [18F]FLT uptake after chemotherapy: an experimental study. *Eur J Nucl Med Mol Imaging*. 2002 Nov;29(11):1462–9.
92. Leyton J, Latigo J, M P, Dhaliwal H, He Q, Aboagye E. Early detection of tumor response to chemotherapy by 3'-deoxy- 3'-[18F]fluorothymidine positron emission tomography: The effect of cisplatin on a fibrosarcoma tumor model in vivo. *Cancer Res*. 2005;65(10):4202–10.
93. Stronach EA, Alfraidi A, Rama N, Datler C, Studd JB, Agarwal R, et al. HDAC4-regulated STAT1 activation mediates platinum resistance in ovarian cancer. *Cancer Res*. 2011 Jul 1;71(13):4412–22.
94. Perumal M, Stronach EA, Gabra H, Aboagye EO. Evaluation of 2-deoxy-2-[18F]fluoro-D-glucose- and 3'-deoxy-3'-[18F]fluorothymidine-positron emission tomography as biomarkers of therapy response in platinum-resistant ovarian cancer. *Mol imaging Biol*. 2012 Dec;14(6):753–61.
95. Oyama N, Hasegawa Y, Kiyono Y, Kobayashi M, Fujibayashi Y, Ponde DE, et al. Early response assessment in prostate carcinoma by 18F- fluorothymidine following anticancer therapy with docetaxel using preclinical tumour models. *Eur J Nucl Med Mol Imaging*. 2011 Jan;38(1):81–9.

96. Fushiki H, Miyoshi S, Noda A, Murakami Y, Sasaki H, Jitsuoka M, et al. Pre-clinical validation of orthotopically-implanted pulmonary tumor by imaging with ¹⁸F-fluorothymidine-positron emission tomography/computed tomography. *Anticancer Res.* 2013 Nov;33(11):4741–50.
97. Honndorf VS, Schmidt H, Wehrl HF, Wiehr S, Ehrlichmann W, Quintanilla-Martinez L, et al. Quantitative correlation at the molecular level of tumor response to docetaxel by multimodal diffusion-weighted magnetic resonance imaging and [¹⁸F]FDG/[¹⁸F]FLT positron emission tomography. *Mol Imaging.* 2014 Jan;13.
98. Cao Q, Li, Z-B, Chen K, Wu Z, He L, Neamati N, et al. Evaluation of biodistribution and anti-tumor effect of a dimeric RGD peptide-paclitaxel conjugate in mice with breast cancer. *Eur J Nucl Med Mol Imaging.* 2008;35(8):1489–98.
99. Ebenhan T, Honer M, Ametamey SM, Schubiger PA, Becquet M, Ferretti S, et al. Comparison of [¹⁸F]-Tracers in various experimental tumor models by PET imaging and identification of an early response biomarker for the novel microtubule stabilizer patupilone. *Mol Imaging Biol.* 2009;11(5):308–21.
100. Lee SJ, Kang HY, Kim SY, Chung JH, Oh SJ, Ryu J-S, et al. Early assessment of tumor response to JAC106, an anti-tubulin agent, by 3'-deoxy-3'-[(1)(8)F]fluorothymidine in preclinical tumor models. *Eur J Nucl Med Mol Imaging.* 2011 Aug;38(8):1436–48.
101. Armeanu-Ebinger S, Griessinger CM, Herrmann D, Fuchs J, Kneilling M, Pichler BJ, et al. PET/MR imaging and optical imaging of metastatic rhabdomyosarcoma in mice. *J Nucl Med.* 2014 Sep;55(9):1545–51.
102. Longley DB, Harkin DP, Johnston PG. 5-fluorouracil: mechanisms of action and clinical strategies. *Nat Rev Cancer.* 2003 May;3(5):330–8.
103. Mirjoleit JF, Didelot C, Barberi-Heyob M, Merlin JL. G1/S but not G0/G1 cell fraction is related to 5-fluorouracil cytotoxicity. *Cytometry.* 2002;48(1):6–13.
104. Lee SJ, Kim SY, Chung JH, Oh SJ, Ryu JS, Hong YS, et al. Induction of thymidine kinase 1 after 5-fluorouracil as a mechanism for 3'-deoxy-3'-[¹⁸F]fluorothymidine flare. *Biochem Pharmacol.* 2010 Nov;80(10):1528–36.
105. Plotnik DA, McLaughlin LJ, Krohn KA, Schwartz JL. The effects of 5-fluorouracil treatment on 3'-fluoro-3'-deoxythymidine (FLT) transport and metabolism in proliferating and non-proliferating cultures of human tumor cells. *Nucl Med Biol.* 2012 Oct;39(7):970–6.
106. Hong IK, Kim SY, Chung JH, Lee SJ, Oh SJ, Lee SJ, et al. 3'-Deoxy-3'-[¹⁸F]fluorothymidine positron emission tomography imaging of thymidine kinase 1 activity after 5-fluorouracil treatment in a mouse tumor model. *Anticancer Res.* 2014 Feb;34(2):759–66.
107. Viertl D, Bischof Delaloye A, Lanz B, Poitry-Yamate C, Gruetter R, Mlynarik V, et al. Increase of [(18)F]FLT tumor uptake in vivo mediated by FdUrd: toward improving cell proliferation positron emission tomography. *Mol imaging Biol.* 2011 Apr;13(2):321–31.
108. Prakasha Gowda AS, Polizzi JM, Eckert KA, Spratt TE. Incorporation of gemcitabine and cytarabine into DNA by DNA polymerase beta and ligase III/XRCC1. *Biochemistry.* 2010 Jun 15;49(23):4833–40.
109. Mini E, Nobili S, Caciagli B, Landini I, Mazzei T. Cellular pharmacology of gemcitabine. *Ann Oncol.* 2006 May;17 Suppl 5:v7–12.
110. Honeywell RJ, Ruiz van Haperen VWT, Veerman G, Smid K, Peters GJ. Inhibition of thymidylate synthase by 2',2'-difluoro-2'-deoxycytidine (Gemcitabine) and its metabolite 2',2'-difluoro-2'-deoxyuridine. *Int J Biochem Cell Biol.* 2015 Mar;60:73–81.
111. Paposki RJ, Young JD, Cass CE. Predicting gemcitabine transport and toxicity in human pancreatic cancer cell lines with the positron emission tomography tracer 3'-deoxy-3'-fluorothymidine. *Biochem Pharmacol.* 2010 Feb;79(4):587–95.

112. Kramata P, Downey KM, Paborsky LR. Incorporation and Excision of 9-(2-Phosphonylmethoxyethyl)guanine (PMEG) by DNA Polymerase and in Vitro. *J Biol Chem.* 1998 Aug 21;273(34):21966–71.
113. Vail DM, Thamm DH, Reiser H, Ray AS, Wolfgang GHI, Watkins WJ, et al. Assessment of GS-9219 in a pet dog model of non-Hodgkin's lymphoma. *Clin Cancer Res.* 2009 May;15(10):3503–10.
114. Lawrence J, Vanderhoek M, Barbee D, Jeraj R, Tumas DB, Vail DM. Use of 3'-deoxy-3'-[18F]fluorothymidine PET/CT for evaluating response to cytotoxic chemotherapy in dogs with non-Hodgkin's lymphoma. *Vet Radiol Ultrasound.* Jan;50(6):660–8.
115. Saito Y, Furukawa T, Arano Y, Fujibayashi Y, Saga T. Comparison of semiquantitative fluorescence imaging and PET tracer uptake in mesothelioma models as a monitoring system for growth and therapeutic effects. *Nucl Med Biol.* 2008 Nov;35(8):851–60.
116. Kenny L, Coombes RC, Vigushin DM, Al-Nahhas A, Shousha S, Aboagye EO. Imaging early changes in proliferation at 1 week post chemotherapy: a pilot study in breast cancer patients with 3'-deoxy-3'-[18F]fluorothymidine positron emission tomography. *Eur J Nucl Med Mol Imaging.* 2007 Sep;34(9):1339–47.
117. Challapalli A, Barwick T, Pearson RA, Merchant S, Mauri F, Howell EC, et al. 3'-Deoxy-3'-¹⁸F-fluorothymidine positron emission tomography as an early predictor of disease progression in patients with advanced and metastatic pancreatic cancer. *Eur J Nucl Med Mol Imaging.* 2015 May;42(6):831–40.
118. Kenny LM, Contractor KB, Stebbing J, Al-Nahhas A, Palmieri C, Shousha S, et al. Altered tissue 3'-deoxy-3'-[18F]fluorothymidine pharmacokinetics in human breast cancer following capecitabine treatment detected by positron emission tomography. *Clin Cancer Res.* 2009 Nov;15(21):6649–57.
119. Hong YS, Kim HO, Kim K, Lee J-L, Kim HJ, Lee SJ, et al. 3'-Deoxy-3'-¹⁸F-fluorothymidine PET for the early prediction of response to leucovorin, 5-fluorouracil, and oxaliplatin therapy in patients with metastatic colorectal cancer. *J Nucl Med.* 2013 Aug;54(8):1209–16.
120. Frings V, van der Veldt AAM, Boellaard R, Herder GJM, Giovannetti E, Honeywell R, et al. Pemetrexed induced thymidylate synthase inhibition in non-small cell lung cancer patients: a pilot study with 3'-deoxy-3'-[(1)(8)F]fluorothymidine positron emission tomography. *PLoS One.* 2013;8(5):e63705.
121. Munk Jensen M, Erichsen KD, Bjorkling F, Madsen J, Jensen PB, Sehested M, et al. [18F]FLT PET for Non-Invasive Assessment of Tumor Sensitivity to Chemotherapy: Studies with Experimental Chemotherapy TP202377 in Human Cancer Xenografts in Mice. *PLoS One.* 2012;7(11):e50618.
122. Wang X, Zhang F, Yang L, Mei Y, Long H, Zhang X, et al. Ursolic acid inhibits proliferation and induces apoptosis of cancer cells in vitro and in vivo. *J Biomed Biotechnol.* 2011;2011:419343.
123. Jensen MM, Erichsen KD, Johnbeck CB, Bjorkling F, Madsen J, Bzorek M, et al. [18F]FLT and [18F]FDG PET for Non-invasive Treatment Monitoring of the Nicotinamide Phosphoribosyltransferase Inhibitor APO866 in Human Xenografts. *PLoS One.* 2013;8(1):e53410.
124. Lindhe O, Skogseid B. Mitotane effects in a H295R xenograft model of adjuvant treatment of adrenocortical cancer. *Horm Metab Res.* 2010 Sep;42(10):725–30.
125. Hanahan D, Weinberg RA. Hallmarks of cancer: the next generation. *Cell.* 2011 Mar 4;144(5):646–74.
126. Takeuchi S, Zhao S, Kuge Y, Zhao Y, Nishijima K-I, Hatano T, et al. ¹⁸F-fluorothymidine PET/CT as an early predictor of tumor response to treatment with cetuximab in human lung cancer

- xenografts. *Oncol Rep*. 2011 Sep;26(3):725–30.
127. Manning HC, Merchant NB, Foutch AC, Virostko JM, Wyatt SK, Shah C, et al. Molecular imaging of therapeutic response to epidermal growth factor receptor blockade in colorectal cancer. *Clin Cancer Res*. 2008 Nov;14(22):7413–22.
 128. McKinley ET, Zhao P, Coffey RJ, Washington MK, Manning HC. 3'-deoxy-3'-[18F]-fluorothymidine PET imaging reflects PI3K-mTOR-mediated pro-survival response to targeted therapy in colorectal cancer. *PLoS One*. 2014;9(9).
 129. Iommelli F, De Rosa V, Gargiulo S, Panico M, Monti M, Greco A, et al. Monitoring Reversal of MET-Mediated Resistance to EGFR Tyrosine Kinase Inhibitors in Non-Small Cell Lung Cancer Using 3'-Deoxy-3'-[18F]-Fluorothymidine Positron Emission Tomography. *Clin Cancer Res*. 2014 Jul;20(18):4806–15.
 130. Ullrich RT, Zander T, Neumaier B, Koker M, Shimamura T, Waerzeggers Y, et al. Early detection of erlotinib treatment response in NSCLC by 3'-deoxy-3'-[F]-fluoro-L-thymidine ([F]FLT) positron emission tomography (PET). *PLoS One*. 2008;3(12):e3908.
 131. Zannetti A, Iommelli F, Speranza A, Salvatore M, Del Vecchio S. 3'-Deoxy-3'-18F-fluorothymidine PET/CT to guide therapy with epidermal growth factor receptor antagonists and Bcl-xL inhibitors in non-small cell lung cancer. *J Nucl Med*. 2012;53(3):443–50.
 132. McKinley ET, Watchmaker JM, Chakravarthy AB, Meyerhardt JA, Engelman JA, Walker RC, et al. [(18)F]-FLT PET to predict early response to neoadjuvant therapy in KRAS wild-type rectal cancer: a pilot study. *Ann Nucl Med*. 2015 Jul;29(6):535–42.
 133. Xu Y, Chang E, Liu H, Jiang H, Gambhir SS, Cheng Z. Proof-of-concept study of monitoring cancer drug therapy with cerenkov luminescence imaging. *J Nucl Med*. 2012 Feb;53(2):312–7.
 134. Yang M, Gao H, Yan Y, Sun X, Chen K, Quan Q, et al. PET imaging of early response to the tyrosine kinase inhibitor ZD4190. *Eur J Nucl Med Mol Imaging*. 2011 Jul;38(7):1237–47.
 135. Dimitroff CJ, Klohs W, Sharma A, Pera P, Driscoll D, Veith J, et al. Anti-Angiogenic Activity of Selected Receptor Tyrosine Kinase Inhibitors, PD166285 and PD173074: Implications for Combination Treatment with Photodynamic Therapy. *Invest New Drugs*. 1999;17(2):121–35.
 136. Pardo OE, Latigo J, Jeffery RE, Nye E, Poulson R, Spencer-Dene B, et al. The fibroblast growth factor receptor inhibitor PD173074 blocks small cell lung cancer growth in vitro and in vivo. *Cancer Res*. 2009 Nov;69(22):8645–51.
 137. Mittra ES, Fan-Minogue H, Lin FI, Karamchandani J, Sriram V, Han M, et al. Preclinical efficacy of the anti-hepatocyte growth factor antibody ficlatuzumab in a mouse brain orthotopic glioma model evaluated by bioluminescence, PET, and MRI. *Clin Cancer Res*. 2013 Oct;19(20):5711–21.
 138. Rex K, Lewis XZ, Gobalakrishnan S, Glaus C, Silva MD, Radinsky R, et al. Evaluation of the antitumor effects of rilotumumab by PET imaging in a U-87 MG mouse xenograft model. *Nucl Med Biol*. 2013 May;40(4):458–63.
 139. Cullinane C, Dorow DS, Jackson S, Solomon B, Bogatyreva E, Binns D, et al. Differential (18)F-FDG and 3'-deoxy-3'-(18)F-fluorothymidine PET responses to pharmacologic inhibition of the c-MET receptor in preclinical tumor models. *J Nucl Med*. 2011 Aug;52(8):1261–7.
 140. Wiehr S, von Ahsen O, Rose L, Mueller A, Mannheim JG, Honndorf V, et al. Preclinical evaluation of a novel c-Met inhibitor in a gastric cancer xenograft model using small animal PET. *Mol Imaging Biol*. 2013 Apr;15(2):203–11.
 141. Cawthorne C, Burrows N, Gieling RG, Morrow CJ, Forster D, Gregory J, et al. [18F]-FLT positron emission tomography can be used to image the response of sensitive tumors to PI3-kinase inhibition with the novel agent GDC-0941. *Mol Cancer Ther*. 2013 May;12(5):819–28.

142. Nguyen Q-D, Perumal M, Waldman TA, Aboagye EO. Glucose metabolism measured by [¹⁸F]fluorodeoxyglucose positron emission tomography is independent of PTEN/AKT status in human colon carcinoma cells. *Transl Oncol.* 2011 Aug;4(4):241–8.
143. Johnbeck CB, Jensen MM, Haagen Nielsen C, Fisker Hag AM, Knigge U, Kjaer A. 18F-FDG and 18F-FLT-PET imaging for monitoring everolimus effect on tumor-growth in neuroendocrine tumors: studies in human tumor xenografts in mice. *PLoS One.* 2014;9(3):e91387.
144. Li Z, Graf N, Herrmann K, Junger A, Aichler M, Feuchtinger A, et al. FLT-PET is superior to FDG-PET for very early response prediction in NPM-ALK-positive lymphoma treated with targeted therapy. *Cancer Res.* 2012 Oct;72(19):5014–24.
145. Aide N, Kinross K, Cullinane C, Roselt P, Waldeck K, Neels O, et al. 18F-FLT PET as a surrogate marker of drug efficacy during mTOR inhibition by everolimus in a preclinical cisplatin-resistant ovarian tumor model. *J Nucl Med.* 2010 Oct;51(10):1559–64.
146. Honer M, Ebenhan T, Allegrini PR, Ametamey SM, Becquet M, Cannet C, et al. Anti-angiogenic/vascular effects of the mTOR inhibitor everolimus are not detectable by FDG/FLT-PET. *Transl Oncol.* 2010;3(4):264–75.
147. Wei LH, Su H, Hildebrandt IJ, Phelps ME, Czernin J, Weber WA. Changes in tumor metabolism as readout for Mammalian target of rapamycin kinase inhibition by rapamycin in glioblastoma. *Clin Cancer Res.* 2008 Jun;14(11):3416–26.
148. Jensen MM, Erichsen KD, Bjorkling F, Madsen J, Jensen PB, Hojgaard L, et al. Early detection of response to experimental chemotherapeutic Top216 with [¹⁸F]FLT and [¹⁸F]FDG PET in human ovary cancer xenografts in mice. *PLoS One.* 2010;5(9):e12965.
149. Keen HG, Ricketts S-A, Maynard J, Logie A, Odedra R, Shannon AM, et al. Examining changes in [¹⁸F]FDG and [¹⁸F]FLT uptake in U87-MG glioma xenografts as early response biomarkers to treatment with the dual mTOR1/2 inhibitor AZD8055. *Mol Imaging Biol.* 2014 Jun;16(3):421–30.
150. Cullinane C, Waldeck KL, Binns D, Bogatyreva E, Bradley DP, de Jong R, et al. Preclinical FLT-PET and FDG-PET imaging of tumor response to the multi-targeted Aurora B kinase inhibitor, TAK-901. *Nucl Med Biol.* 2014 Feb;41(2):148–54.
151. Manfredi MG, Ecsedy JA, Chakravarty A, Silverman L, Zhang M, Hoar KM, et al. Characterization of alisertib (MLN8237), an investigational small-molecule inhibitor of Aurora A kinase using novel in vivo pharmacodynamic assays. *Clin Cancer Res.* 2011 Dec;17(24):7614–24.
152. Chan F, Sun C, Perumal M, Nguyen Q-D, Bavetsias V, McDonald E, et al. Mechanism of action of the Aurora kinase inhibitor CCT129202 and in vivo quantification of biological activity. *Mol Cancer Ther.* 2007 Dec;6(12):3147–57.
153. Geven EJW, Evers S, Nayak TK, Bergstrom M, Su F, Gerrits D, et al. Therapy response monitoring of the early effects of a new BRAF inhibitor on melanoma xenograft in mice: evaluation of F-FDG-PET and F-FLT-PET. *Contrast Media Mol Imaging.* 2014 Sep;
154. Solit DB, Garraway LA, Pratilas CA, Sawai A, Getz G, Basso A, et al. BRAF mutation predicts sensitivity to MEK inhibition. *Nature.* 2006 Jan 19;439(7074):358–62.
155. Leyton J, Smith G, Lees M, Perumal M, Nguyen Q, Aigbirhio FI, et al. Noninvasive imaging of cell proliferation following mitogenic extracellular kinase inhibition by PD0325901. *Mol Cancer Ther.* 2008 Sep;7(9):3112–21.
156. Solit DB, Santos E, Pratilas CA, Lobo J, Moroz M, Cai S, et al. 3'-Deoxy-3'-[¹⁸F]fluorothymidine positron emission tomography is a sensitive method for imaging the response of BRAF-dependent tumors to MEK inhibition. *Cancer Res.* 2007;67(23):11463–9.
157. Nielsen CH, Jensen MM, Kristensen LK, Dahlman A, Fröhlich C, Jacobsen HJ, et al. In vivo imaging of therapy response to a novel Pan-HER antibody mixture using FDG and FLT positron

- emission tomography. Vol. 6, *Oncotarget*. 2015. p. 37486–99.
158. Li Z, Herrmann K, Pirsig S, Philipp-Abbrederis K, Henninger M, Aichler M, et al. Molecular imaging for early prediction of response to Sorafenib treatment in sarcoma. *Am J Nucl Med Mol Imaging*. 2013;4(1):70–9.
 159. Murakami M, Zhao S, Zhao Y, Yu W, Fatema CN, Nishijima K-I, et al. Increased intratumoral fluorothymidine uptake levels following multikinase inhibitor sorafenib treatment in a human renal cell carcinoma xenograft model. *Oncol Lett*. 2013 Sep;6(3):667–72.
 160. Takeuchi A, Shiota M, Tatsugami K, Yokomizo A, Eto M, Inokuchi J, et al. Sorafenib augments cytotoxic effect of S-1 in vitro and in vivo through TS suppression. *Cancer Chemother Pharmacol*. 2011 Dec;68(6):1557–64.
 161. Goggi JL, Bejot R, Moonshi SS, Bhakoo KK. Stratification of 18F-labeled PET imaging agents for the assessment of antiangiogenic therapy responses in tumors. *J Nucl Med*. 2013;54(9):1630–6.
 162. Fuereder T, Wanek T, Pfliegerl P, Jaeger-Lansky A, Hoeflmayer D, Strommer S, et al. Gastric cancer growth control by BEZ235 in vivo does not correlate with PI3K/mTOR target inhibition but with [18F]FLT uptake. *Clin Cancer Res*. 2011 Aug;17(16):5322–32.
 163. Graf N, Li Z, Herrmann K, Weh D, Aichler M, Slawska J, et al. Positron emission tomographic monitoring of dual phosphatidylinositol-3-kinase and mTOR inhibition in anaplastic large cell lymphoma. *Onco Targets Ther*. 2014;7:789–98.
 164. Bao X, Wang M-W, Zhang Y-P, Zhang Y-J. Early monitoring antiangiogenesis treatment response of Sunitinib in U87MG Tumor Xenograft by (18)F-FLT MicroPET/CT imaging. *Biomed Res Int*. 2014;2014:218578.
 165. Moonshi SS, Bejot R, Atcha Z, Vijayaragavan V, Bhakoo KK, Goggi JL. A comparison of PET imaging agents for the assessment of therapy efficacy in a rodent model of glioma. *Am J Nucl Med Mol Imaging*. 2013;3(5):397–407.
 166. Tumber A, Collins LS, Petersen KD, Thougard A, Christiansen SJ, Dejligbjerg M, et al. The histone deacetylase inhibitor PXD101 synergises with 5-fluorouracil to inhibit colon cancer cell growth in vitro and in vivo. *Cancer Chemother Pharmacol*. 2007 Jul;60(2):275–83.
 167. Jensen MM, Erichsen KD, Johnbeck CB, Bjorkling F, Madsen J, Jensen PB, et al. [18F]FDG and [18F]FLT positron emission tomography imaging following treatment with belinostat in human ovary cancer xenografts in mice. *BMC Cancer*. 2013;13:168.
 168. Kaliszczak M, Trousil S, Aberg O, Perumal M, Nguyen Q-D, Aboagye EO. A novel small molecule hydroxamate preferentially inhibits HDAC6 activity and tumour growth. *Br J Cancer*. 2013 Feb;108(2):342–50.
 169. Leyton J, Alao JP, Da Costa M, Stavropoulou A V, Latigo JR, Perumal M, et al. In vivo biological activity of the histone deacetylase inhibitor LAQ824 is detectable with 3'-deoxy-3'-[18F]fluorothymidine positron emission tomography. *Cancer Res*. 2006 Aug;66(15):7621–9.
 170. Chan P-C, Wu C-Y, Chou L-S, Ho C-H, Chang C-W, Chiou S-H, et al. Monitoring Tumor Response After Histone Deacetylase Inhibitor Treatment Using 3'-Deoxy-3'-[18F]-fluorothymidine PET. *Mol Imaging Biol*. 2015 Jun;17(3):394–402.
 171. Zhang CC, Yan Z, Zhang Q, Kuszpit K, Zasadny K, Qiu M, et al. PF-03732010: A fully human monoclonal antibody against P-cadherin with antitumor and antimetastatic activity. *Clin Cancer Res*. 2010 Nov;16(21):5177–88.
 172. Bulk E, Ay A-S, Hammadi M, Ouadid-Ahidouch H, Schelhaas S, Hascher A, et al. Epigenetic dysregulation of KCa 3.1 channels induces poor prognosis in lung cancer. *Int J Cancer*. 2015 Sep 15;137(6):1306–17.

173. Lind DS. Arginine and Cancer. *J Nutr.* 2004 Oct 1;134(10):2837S – 2841S.
174. Stelter L, Fuchs S, Jungbluth AA, Ritter G, Longo VA, Zanzonico P, et al. Evaluation of arginine deiminase treatment in melanoma xenografts using 18F-FLT PET. *Mol Imaging Biol.* 2013;15(6):768–75.
175. Chang E, Liu H, Unterschemmann K, Ellinghaus P, Liu S, Gekeler V, et al. 18F-FAZA PET imaging response tracks the reoxygenation of tumors in mice upon treatment with the mitochondrial complex I inhibitor BAY 87-2243. *Clin Cancer Res.* 2015 Jan 15;21(2):335–46.
176. Yoshii Y, Furukawa T, Waki A, Okuyama H, Inoue M, Itoh M, et al. High-throughput screening with nanoimprinting 3D culture for efficient drug development by mimicking the tumor environment. *Biomaterials.* 2015 May;51:278–89.
177. Yang M, Gao H, Sun X, Yan Y, Quan Q, Zhang W, et al. Multiplexed PET probes for imaging breast cancer early response to VEGF(1)(2)(1)/rGel treatment. *Mol Pharm.* 2011 Apr;8(2):621–8.
178. Hsu AR, Cai W, Veeravagu A, Mohamedali KA, Chen K, Kim S, et al. Multimodality molecular imaging of glioblastoma growth inhibition with vasculature-targeting fusion toxin VEGF121/rGel. *J Nucl Med.* 2007;48(3):445–54.
179. Pillai RG, Forster M, Perumal M, Mitchell F, Leyton J, Aibgirhio FI, et al. Imaging pharmacodynamics of the alpha-folate receptor-targeted thymidylate synthase inhibitor BGC 945. *Cancer Res.* 2008 May;68(10):3827–34.
180. Veeravagu A, Liu Z, Niu G, Chen K, Jia B, Cai W, et al. Integrin alphavbeta3-targeted radioimmunotherapy of glioblastoma multiforme. *Clin Cancer Res.* 2008 Nov;14(22):7330–9.
181. Persson M, Rasmussen P, Madsen J, Ploug M, Kjaer A. New peptide receptor radionuclide therapy of invasive cancer cells: in vivo studies using 177Lu-DOTA-AE105 targeting uPAR in human colorectal cancer xenografts. *Nucl Med Biol.* 2012 Oct;39(7):962–9.
182. Yang Y-J, Ryu J-S, Kim S-Y, Seung JO, Ki CI, Lee H, et al. Use of 3'-deoxy-3'-[18F]fluorothymidine PET to monitor early responses to radiation therapy in murine SCCVII tumors. *Eur J Nucl Med Mol Imaging.* 2006;33(4):412–9.
183. Sugiyama M, Sakahara H, Sato K, Harada N, Fukumoto D, Kakiuchi T, et al. Evaluation of 3'-deoxy-3'-18F-fluorothymidine for monitoring tumor response to radiotherapy and photodynamic therapy in mice. *J Nucl Med.* 2004 Oct;45(10):1754–8.
184. Molthoff CFM, Klabbers BM, Berkhof J, Felten JT, van Gelder M, Windhorst AD, et al. Monitoring response to radiotherapy in human squamous cell cancer bearing nude mice: comparison of 2'-deoxy-2'-[18F]fluoro-D-glucose (FDG) and 3'-[18F]fluoro-3'-deoxythymidine (FLT). *Mol imaging Biol.* 2007;9(6):340–7.
185. Pan MH, Huang SC, Liao YP, Schae D, Wang CC, Stout DB, et al. FLT-PET imaging of radiation responses in murine tumors. *Mol Imaging Biol.* 2008;10(6):325–34.
186. Murayama C, Harada N, Kakiuchi T, Fukumoto D, Kamijo A, Kawaguchi AT, et al. Evaluation of D-18F-FMT, 18F-FDG, L- 11C-MET, and 18F-FLT for monitoring the response of tumors to radiotherapy in mice. *J Nucl Med.* 2009;50(2):290–5.
187. Wang H, Liu B, Tian J-H, Xu B-X, Guan Z-W, Qu B-L, et al. Monitoring early responses to irradiation with dual-tracer micro-PET in dual-tumor bearing mice. *World J Gastroenterol.* 2010;16(43):5416–23.
188. Chandrasekaran S, Hollander A, Xu X, Benci JL, Davis JJ, Dorsey JF, et al. 18F-fluorothymidine-pet imaging of glioblastoma multiforme: effects of radiation therapy on radiotracer uptake and molecular biomarker patterns. *ScientificWorldJournal.* 2013;2013:796029.
189. Yue J-B, Yang J, Liu J, Lee J, Cabrera AR, Sun X-D, et al. Histopathologic validation of 3'-deoxy-

- 3'-(18)F-fluorothymidine PET for detecting tumor repopulation during fractionated radiotherapy of human FaDu squamous cell carcinoma in nude mice(18)F-FLT PET repopulation. *Radiother Oncol.* 2014 Jun;111(3):475–81.
190. Qu B, Wang H, Yu W, Zhang J, Zhang H, Tian J. Evaluation of Therapeutic Effects of Radiotherapy during Treatment of Lung Adenocarcinoma in Mice with Positron Emission Tomography Imaging of 18F-FLT and 18F-FDG. *Trop J Pharm Res.* 2015 Aug 6;14(7):1293.
191. Jiang M, Huang Q, Chen P, Ruan X, Luo Z, Zhao L, et al. Monitoring the early biologic response of esophageal carcinoma after irradiation with 18F-FLT: an in-vitro and in-vivo study. *Nucl Med Commun.* 2014 Sep;
192. Zheng Y, Yang Z, Zhang Y, Shi Q, Bao X, Zhang J, et al. The preliminary study of 18F-FLT micro-PET/CT in predicting radiosensitivity of human nasopharyngeal carcinoma xenografts. *Ann Nucl Med.* 2015 Jan;29(1):29–36.
193. Lin C, Kume K, Mori T, Martinez ME, Okazawa H, Kiyono Y. Predictive Value of Early-Stage Uptake of 3'-Deoxy-3'-18F-Fluorothymidine in Cancer Cells Treated with Charged Particle Irradiation. *J Nucl Med.* 2015 Jun 1;56(6):945–50.
194. Tran L-B-A, Bol A, Labar D, Karroum O, Mignon L, Bol V, et al. DW-MRI and 18 F-FLT PET for early assessment of response to radiation therapy associated with hypoxia-driven interventions. Preclinical studies using manipulation of oxygenation and/or dose escalation. *Contrast Media Mol Imaging.* 2015 Oct 7;115–21.
195. Zornhagen K, Clausen M, Hansen A, Law I, McEvoy F, Engelholm S, et al. Use of Molecular Imaging Markers of Glycolysis, Hypoxia and Proliferation (18F-FDG, 64Cu-ATSM and 18F-FLT) in a Dog with Fibrosarcoma: The Importance of Individualized Treatment Planning and Monitoring. *Diagnostics.* 2015 Sep 11;5(3):372–82.
196. Bradshaw TJ, Bowen SR, Deveau MA, Kubicek L, White P, Bentzen SM, et al. Molecular imaging biomarkers of resistance to radiation therapy for spontaneous nasal tumors in canines. *Int J Radiat Oncol Biol Phys.* 2015 Mar 15;91(4):787–95.
197. Rueger MA, Ameli M, Li H, Winkeler A, Rueckriem B, Vollmar S, et al. [18F]FLT PET for non-invasive monitoring of early response to gene therapy in experimental gliomas. *Mol Imaging Biol.* 2011 Jun;13(3):547–57.
198. Jacobs A, Tjuvajev JG, Dubrovin M, Akhurst T, Balatoni J, Beattie B, et al. Positron emission tomography-based imaging of transgene expression mediated by replication-conditional, oncolytic herpes simplex virus type 1 mutant vectors in vivo. *Cancer Res.* 2001 Apr 1;61(7):2983–95.
199. Jacobs AH, Rueger MA, Winkeler A, Li H, Vollmar S, Waerzeggers Y, et al. Imaging-guided gene therapy of experimental gliomas. *Cancer Res. United States;* 2007 Feb;67(4):1706–15.
200. Mason NS, Lopresti BJ, Ruszkiewicz J, Dong X, Joyce S, Leef G, et al. Utility of 3'-[(18)F]fluoro-3'-deoxythymidine as a PET tracer to monitor response to gene therapy in a xenograft model of head and neck carcinoma. *Am J Nucl Med Mol Imaging.* 2013;3(1):16–31.
201. Kuruppu D, Brownell A-L, Shah K, Mahmood U, Tanabe KK. Molecular imaging with bioluminescence and PET reveals viral oncolysis kinetics and tumor viability. *Cancer Res.* 2014 Aug;74(15):4111–21.
202. Leyton J, Lockley M, Aerts JL, Baird SK, Aboagye EO, Lemoine NR, et al. Quantifying the activity of adenoviral E1A CR2 deletion mutants using Renilla luciferase bioluminescence and 3'-deoxy-3'-[18F]fluorothymidine positron emission tomography imaging. *Cancer Res.* 2006 Sep;66(18):9178–85.
203. Oyama N, Ponde DE, Dence C, Kim J, Tai Y-C, Welch MJ. Monitoring of therapy in androgen-dependent prostate tumor model by measuring tumor proliferation. *J Nucl Med.* 2004;45(3):519–25.

204. Habibollahi P, van den Berg NS, Kuruppu D, Loda M, Mahmood U. Metformin--an adjunct antineoplastic therapy--divergently modulates tumor metabolism and proliferation, interfering with early response prediction by 18F-FDG PET imaging. *J Nucl Med.* 2013 Feb;54(2):252–8.
205. Weber GF, Gaertner FC, Erl W, Janssen K-P, Blechert B, Holzmann B, et al. IL-22-mediated tumor growth reduction correlates with inhibition of ERK1/2 and AKT phosphorylation and induction of cell cycle arrest in the G 2-M phase. *J Immunol.* 2006;177(11):8266–72.
206. Aarntzen EHJG, Srinivas M, De Wilt JHW, Jacobs JFM, Lesterhuis WJ, Windhorst AD, et al. Early identification of antigen-specific immune responses in vivo by [18F]-labeled 3'-fluoro-3'-deoxy-thymidine ([18F]FLT) PET imaging. *Proc Natl Acad Sci.* 2011 Nov;108(45):18396–9.
207. Jensen MM, Erichsen KD, Bjorkling F, Madsen J, Jensen PB, Sehested M, et al. Imaging of treatment response to the combination of carboplatin and paclitaxel in human ovarian cancer xenograft tumors in mice using FDG and FLT PET. *PLoS One.* 2013;8(12):e85126.
208. Katz SI, Zhou L, Ferrara TA, Wang W, Mayes PA, Smith CD, et al. FLT-PET may not be a reliable indicator of therapeutic response in p53-null malignancy. *Int J Oncol.* 2011 Jul;39(1):91–100.
209. Lee HJ, Oh SJ, Lee EJ, Chung JH, Kim Y, Ryu J-S, et al. Positron emission tomography imaging of human colon cancer xenografts in mice with [18F]fluorothymidine after TAS-102 treatment. *Cancer Chemother Pharmacol.* 2015 May;75(5):1005–13.
210. Haagensen EJ, Thomas HD, Wilson I, Harnor SJ, Payne SL, Rennison T, et al. The enhanced in vivo activity of the combination of a MEK and a PI3K inhibitor correlates with [18F]-FLT PET in human colorectal cancer xenograft tumour-bearing mice. *PLoS One.* 2013;8(12):e81763.
211. Kita A, Mitsuoka K, Kaneko N, Nakata M, Yamanaka K, Jitsuoka M, et al. Sepantronium bromide (YM155) enhances response of human B-cell non-hodgkin lymphoma to rituximab. *J Pharmacol Exp Ther.* 2012 Oct;343(1):178–83.
212. Lee SJ, Kim EJ, Lee HJ, Kim SY, Oh SJ, Ryu JS, et al. A pilot study for the early assessment of the effects of BMS-754807 plus gefitinib in an H292 tumor model by [(18)F]fluorothymidine-positron emission tomography. *Invest New Drugs.* 2013 Jun;31(3):506–15.
213. Cho H, Lai TC, Kwon GS. Poly(ethylene glycol)-block-poly((epsilon)-caprolactone) micelles for combination drug delivery: Evaluation of paclitaxel, cyclopamine and gossypol in intraperitoneal xenograft models of ovarian cancer. *J Control Release.* 2013 Feb;166(1):1–9.
214. Corroyer-Dulmont A, Peres EA, Petit E, Guillamo J-S, Varoqueaux N, Roussel S, et al. Detection of glioblastoma response to temozolomide combined with bevacizumab based on muMRI and muPET imaging reveals [18F]-fluoro-L-thymidine as an early and robust predictive marker for treatment efficacy. *Neuro Oncol.* 2013 Jan;15(1):41–56.
215. Corroyer-Dulmont A, Pérès EA, Gérault AN, Savina A, Bouquet F, Divoux D, et al. Multimodal imaging based on MRI and PET reveals [18F]FLT PET as a specific and early indicator of treatment efficacy in a preclinical model of recurrent glioblastoma. *Eur J Nucl Med Mol Imaging.* 2016;43(4):682–94.
216. Na Y-S, Jung K-A, Kim S-M, Hong YS, Ryu M-H, Jang SJ, et al. The histone deacetylase inhibitor PXD101 increases the efficacy of irinotecan in in vitro and in vivo colon cancer models. *Cancer Chemother Pharmacol.* 2011 Aug;68(2):389–98.
217. Zhang C, Yan Z, Painter CL, Zhang Q, Chen E, Arango ME, et al. PF-00477736 mediates checkpoint kinase 1 signaling pathway and potentiates docetaxel-induced efficacy in xenografts. *Clin Cancer Res.* 2009 Jul;15(14):4630–40.
218. Honndorf VS, Schmidt H, Wiehr S, Wehr HF, Quintanilla-Martinez L, Stahlschmidt A, et al. The Synergistic Effect of Selumetinib/Docetaxel Combination Therapy Monitored by [(18) F]FDG/[(18) F]FLT PET and Diffusion-Weighted Magnetic Resonance Imaging in a Colorectal Tumor Xenograft Model. *Mol imaging Biol.* 2016 Apr;18(2):249–57.

219. Kaneko N, Mitsuoka K, Amino N, Yamanaka K, Kita A, Mori M, et al. Combination of YM155, a survivin suppressant, with bendamustine and rituximab: A new combination therapy to treat relapsed/refractory diffuse large B-cell lymphoma. *Clin Cancer Res.* 2014 Apr;20(7):1814–22.
220. Fleuren EDG, Versleijen-Jonkers YMH, Roeffen MHS, Franssen GM, Flucke UE, Houghton PJ, et al. Temsirolimus combined with cisplatin or bevacizumab is active in osteosarcoma models. *Int J Cancer.* 2014 Apr;135(12):2770–82.
221. Trencsényi G, Márián T, Lajtos I, Krasznai Z, Balkay L, Emri M, et al. ¹⁸F-FDG, [¹⁸F]FLT, [¹⁸F]FAZA, and ¹¹C-methionine are suitable tracers for the diagnosis and in vivo follow-up of the efficacy of chemotherapy by miniPET in both multidrug resistant and sensitive human gynecologic tumor xenografts. *Biomed Res Int.* 2014 Jan;2014:787365.
222. Karroum O, Mignon L, Kengen J, Karmani L, Leveque P, Danhier P, et al. Multimodal imaging of tumor response to sorafenib combined with radiation therapy: Comparison between diffusion-weighted MRI, choline spectroscopy and ¹⁸F-FLT PET imaging. *Contrast Media Mol Imaging.* 2013;8(3):274–80.
223. Debucquoy A, Devos E, Vermaelen P, Landuyt W, De Weer S, Van Den Heuvel F, et al. ¹⁸F-FLT and ¹⁸F-FDG PET to measure response to radiotherapy combined with celecoxib in two colorectal xenograft models. *Int J Radiat Biol.* 2009 Sep;85(9):763–71.
224. Apisarnthanarax S, Alauddin MM, Mourtada F, Ariga H, Raju U, Mawlawi O, et al. Early detection of chemoradioresponse in esophageal carcinoma by 3'-deoxy-3'-³H-fluorothymidine using preclinical tumor models. *Clin Cancer Res.* 2006 Aug;12(15):4590–7.
225. Shoghi KI. Quantitative small animal PET. *Q J Nucl Med Mol Imaging.* 2009 Aug;53(4):365–73.
226. Thackeray JT, Bankstahl JP, Bengel FM. Impact of Image-Derived Input Function and Fit Time Intervals on Patlak Quantification of Myocardial Glucose Uptake in Mice. *J Nucl Med.* 2015 Oct;56(10):1615–21.
227. Boellaard R, Krak NC, Hoekstra OS, Lammertsma AA. Effects of noise, image resolution, and ROI definition on the accuracy of standard uptake values: a simulation study. *J Nucl Med.* 2004 Oct;45(9):1519–27.
228. Erdi YE, Nehmeh SA, Pan T, Pevsner A, Rosenzweig KE, Mageras G, et al. The CT motion quantitation of lung lesions and its impact on PET-measured SUVs. *J Nucl Med.* 2004 Aug;45(8):1287–92.